uOttawa

L'Université canadienne
Canada's university

FACULTÉ DES ÉTUDES SUPÉRIEURES ET POSTOCTORALES

uOttawa

L'Université canadienne
Canada's university

FACULTY OF GRADUATE AND POSDOCTORAL STUDIES

Geneviève Leblanc
AUTEUR DE LA THÈSE / AUTHOR OF THESIS

Ms.C. (Earth Sciences)
GRADE / DEGREE

Department of Earth Sciences
FACULTÉ, ÉCOLE, DÉPARTEMENT / FACULTY, SCHOOL, DEPARTMENT

Geology and Mineralization in the Big Four Lake Area, Shining Tree, Abitibi Greenstone Belt, Ontario.

TITRE DE LA THÈSE / TITLE OF THESIS

Dr. A. Fowler/ Dr. J. Ayer
DIRECTEUR (DIRECTRICE) DE LA THÈSE / THESIS SUPERVISOR

CO-DIRECTEUR (CO-DIRECTRICE) DE LA THÈSE / THESIS CO-SUPERVISOR

EXAMINATEURS (EXAMINATRICES) DE LA THÈSE / THESIS EXAMINERS

Dr. André Lalonde

Dr. R. Taylor

Gary W. Slater
Le Doyen de la Faculté des études supérieures et postdoctorales / Dean of the Faculty of Graduate and Postdoctoral Studies

GEOLOGY AND MINERALIZATION IN THE BIG FOUR LAKE AREA, SHINING TREE, ABITIBI GREENSTONE BELT, ONTARIO

by

Geneviève Leblanc

A thesis submitted to the Faculty of Graduate and Postdoctorate Studies
In partial fulfillment of the requirements
for the degree of M. Sc. In Earth Sciences.

OTTAWA-CARLETON GEOSCIENCE CENTRE
UNIVERSITY OF OTTAWA

Your file Votre référence
ISBN: 978-0-494-48469-2
Our file Notre référence
ISBN: 978-0-494-48469-2

ABSTRACT

The purpose of the research work (in partnership with the Ontario Geological Survey (OGS) and International KRL Resources Corp. (KRL)) was to better define the geology and mineralization of the Big Four Lake area, close to Shining Tree in Ontario, part of the southwesthern Abitibi greenstone belt. Rocks of the area belong to the Deloro assemblage a suite of calc-alkaline mafic to felsic metavolcanic rocks, tholeiitic mafic to intermediate metavolcanic rocks, iron formation plus komatiites of the Kidd-Munro and Pacaud assemblages, all cut by later intrusions. The rocks are metamorphosed to the greenschist facies and for the most part are only slightly deformed.

A 1: 10,000 scale geological map was produced in order to characterize the distribution of Deloro assemblage rocks and the Proterozoic intrusions. Seven different units were defined: 1) Mafic to intermediate metavolcanic rocks, 2) South rhyolite, 3) Volcanoclastic rocks, 4) Red Dome rhyolite, 5) Sulfide–rich chemical metasedimentary rocks, 6) Matachewan dike swarm, and 7) Nipissing gabbro. Major and trace element geochemistry shows that unit 1 rocks are tholeiitic whereas units 2 and 4 are calc-alkaline. Accordingly the Deloro assemblage rocks (units 1 to 5) are interpreted to have formed in a back-arc setting. The mafic to intermediate metavolcanic rocks have affinities with N-type MORB and a volcanic-arc environment.

In the field, the Red Dome rhyolite has a characteristic hematization whereas the South rhyolite is strongly sericitized and has conspicuous alkali feldspar phenocrysts. Based on the presence of columnar jointing, autoclastic facies, and its massive form, the Red Dome rhyolite is interpreted to be a dome. The South rhyolite was earlier interpreted to be pyroclastic because of the presence of pumice fragments in a breccia that surrounds massive facies. However, there is no evidence of explosive and hot emplacement, and there are red chert clasts within the breccia which is itself located close to a conglomerate containing fragments of the South rhyolite. Because these two facies surround massive rhyolite, the South rhyolite is also interpreted to be a dome.

Mineralization is characterized by pyrite, chalcopyrite, magnetite, hematite, malachite in quartz and carbonate veins that cut the Red Dome rhyolite. Exploration in the area focused on this mineralization because it was thought to be a VMS environment. The chlorite mineral chemistry is relatively iron-rich consistent with a metamorphic rather than hydrothermal origin and the rhyolites are not the FIII type typical of VMS.

It is concluded that the mineralization may have been hydrothermal, possibly from a small, or aborted, VMS system, or related to later regional felsic intrusions or even the Proterozoic intrusions, which may have provided heat to remobilize metals.

SOMMAIRE

Le but de ce travail de recherche (réalisé en collaboration avec la Commission Géologique de l'Ontario (OGS) et International KRL Resources Corp. (KRL)) était de mieux définir la géologie et la minéralisation de la région de Big Four Lake, située près de Shining Tree, en Ontario. Les roches des cette régions sont incluses dans la partie sud-ouest de la ceinture de roches vertes de l'Abitibi et également incluses dans l'assemblage de Deloro. La région, est caractérisé par l'assemblage de Deloro incluant une suite mafique à felsique de roches méta-volcaniques calc-alcalines, des roches mafiques à intermédiaires méta-volcaniques tholéiitiques et des formations de fer. Des komatiites incluses dans les assemblages de Kidd-Munro et Pacaud y sont aussi présentent. Tous ces assemblages sont recoupés par des intrusions datant du Protérozoïque. Les roches de la région de Big Four Lake sont métamorphisées au faciès schiste vert et ne présentent pas d'évidence de déformation importante.

Une carte géologique à l'échelle de 1 : 10 000 fut produite afin de caractériser les roches de l'assemblage de Deloro et les intrusions protérozoïques. Un total de sept différentes unités sont définies : 1) roches méta-volcaniques mafiques à intermédiaires, 2) rhyolite du Sud ("South rhyolite"), 3) roches volcaniclastiques, 4) rhyolite du Dôme Rouge ("Red Dome rhyolite"), 5) méta-sédiments chimiques enrichis en sulfures, 6) dykes de Matachewan et 7) gabbro de Nipissing. La géochimie des éléments majeurs et traces démontre que l'unité 1 est tholéiitique alors que les unités 2 et 4 sont calco-alcalines. De cette observation, les roches de l'assemblage de Deloro sont interprétées comme s'étant formées dans un environnement de bassin d'arc volcanique. Les roches méta-volcaniques mafiques à intermédiaires présentent des affinités avec des environnements de MORB du type N et d'arc volcanique.

Sur le terrain, la rhyolite Dôme Rouge présente une hématisation caractéristique tandis que la rhyolite du Sud est intensément séricitisée et contient des phénocristaux de feldspath alcalin. Dû à la présence de joints columnaires et de faciès autoclastiques et également dû à sa nature massive, la rhyolite Dôme Rouge est interprétée comme étant un dôme. L'origine de la rhyolite du Sud était auparavant interprétée comme pyroclastique dû à la présence de fragments de pierre ponce dans une brèche entourée de faciès massifs de cette même rhyolite. Cependant, il n'y a aucune évidence d'emplacement à haute température, cette brèche contient des fragments de chert rouge et de plus, cette unité est située à proximité d'un conglomérat contenant des fragments de la rhyolite du Sud. Étant donné que ces deux faciès sont entourés par des faciès massifs de cette même rhyolite, la rhyolite du Sud est aussi interprétée comme étant un dôme.

La minéralisation de la rhyolite Dôme Rouge est caractérisé par de la pyrite, chalcopyrite, magnétite, hématite et malachite dans des veines de quartz et carbonate. Parce que cette minéralisation était interprétée d'origine

hydrothermale associée à un environnement de "VMS", l'exploration dans cette région y était plus accentuée. La composition de la chlorite est relativement enrichie en fer, ce qui concorde avec un environnement métamorphique plutôt qu'hydrothermal et également dû fait que la rhyolite Dôme Rouge n'est pas du type FIII qui caractérise les environnements "VMS".

Ces observations concluent que la minéralisation est probablement d'origine hydrothermale, possiblement d'un petit système "VMS", ou d'un système "VMS" interrompu, ou reliée au intrusions felsiques régionales ou même aux intrusions protérozoïques, qui ont peut-être générées la chaleur nécessaire à la remobilisation des métaux.

TABLE OF CONTENTS

LIST OF TABLES

LIST OF FIGURES

LIST OF PLATES

LIST OF APPENDICES

LIST OF MAPS

CHAPTER ONE: INTRODUCTION

The general objective of this thesis is to characterize the Deloro assemblage and its copper mineralization within the Red Dome rhyolite of the Shining Tree area, Ontario. This project is in collaboration with the University of Ottawa, the Ontario Geological Survey (OGS) and with the junior exploration company, International KRL Resources Corporation (KRL), based in Vancouver, BC. The objectives and the methodology are described in detail in this chapter.

1.1 LOCATION AND ACCESS

The study area is approximately mid-way between Sudbury and Timmins (Figure 1.1). The village of Shining Tree is approximately 100 km south of Timmins and approximately 120 km north of Sudbury and is easily accessed by Highway 560 from Highway 144 that connects Timmins and Sudbury. Several secondary forestry and drill roads, such as the Grassy road extending north of Highway 560 and the Bay Lumber road extending to the south, make the field access easy.

The map area is located in the western part of Macmurchy Township, District of Timiskaming. The precise geographic coordinates at the four corners of the parallelogram-shaped area (Figures 1.2), are 47° 37' 45"N and 81° 10' 26"W (SW corner), 47° 36' 37"N and 81° 08' 07"W (SE corner), 47° 38' 53"N and 81° 11' 13"W (NW corner) and are 47° 37' 35"N and 81° 07' 20"W (NE corner). In this thesis, the area will be referred as Big Four Lake.

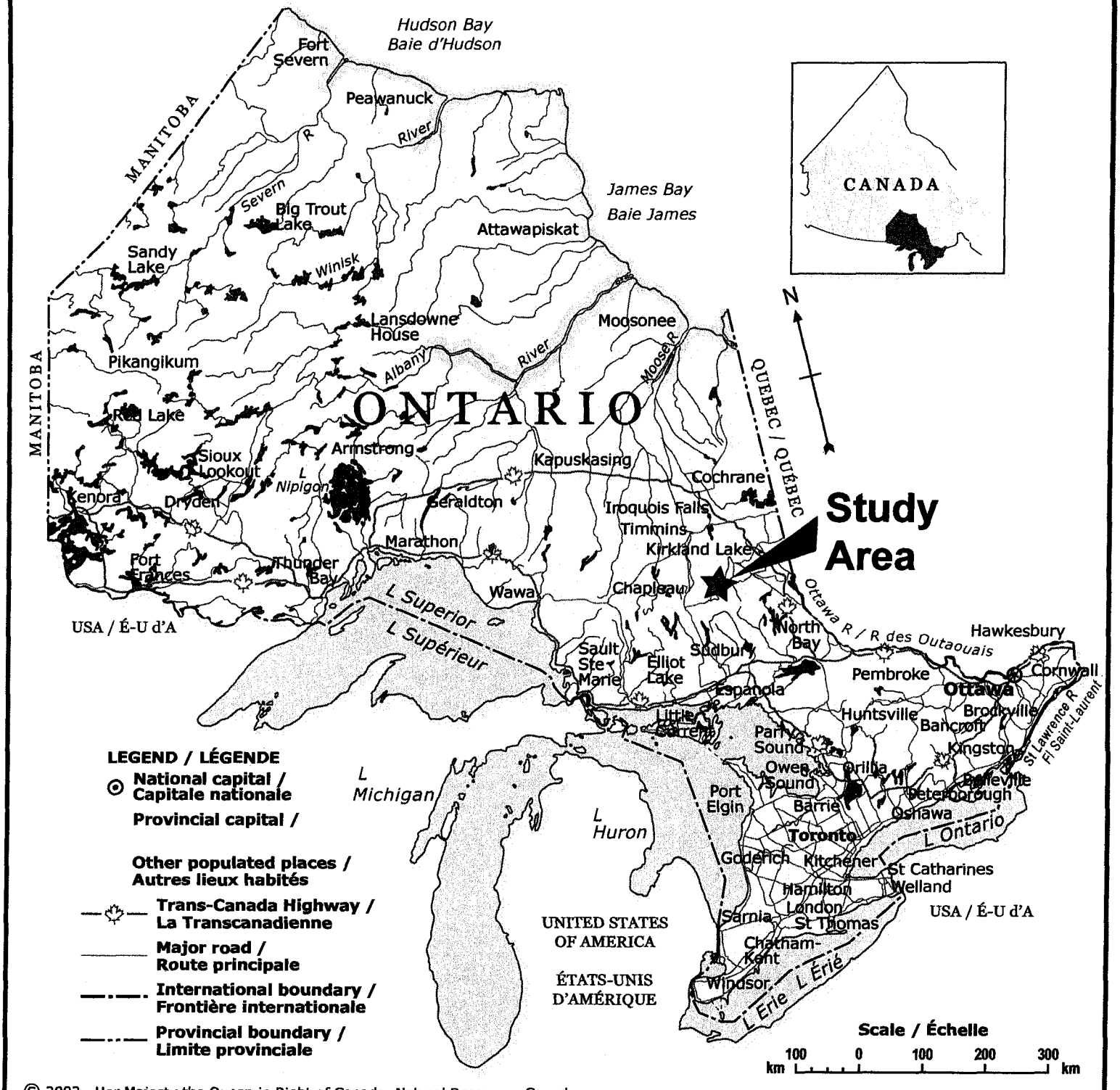

Figure 1.1: Regional location map (modifed *from* Caldbick, 2004)

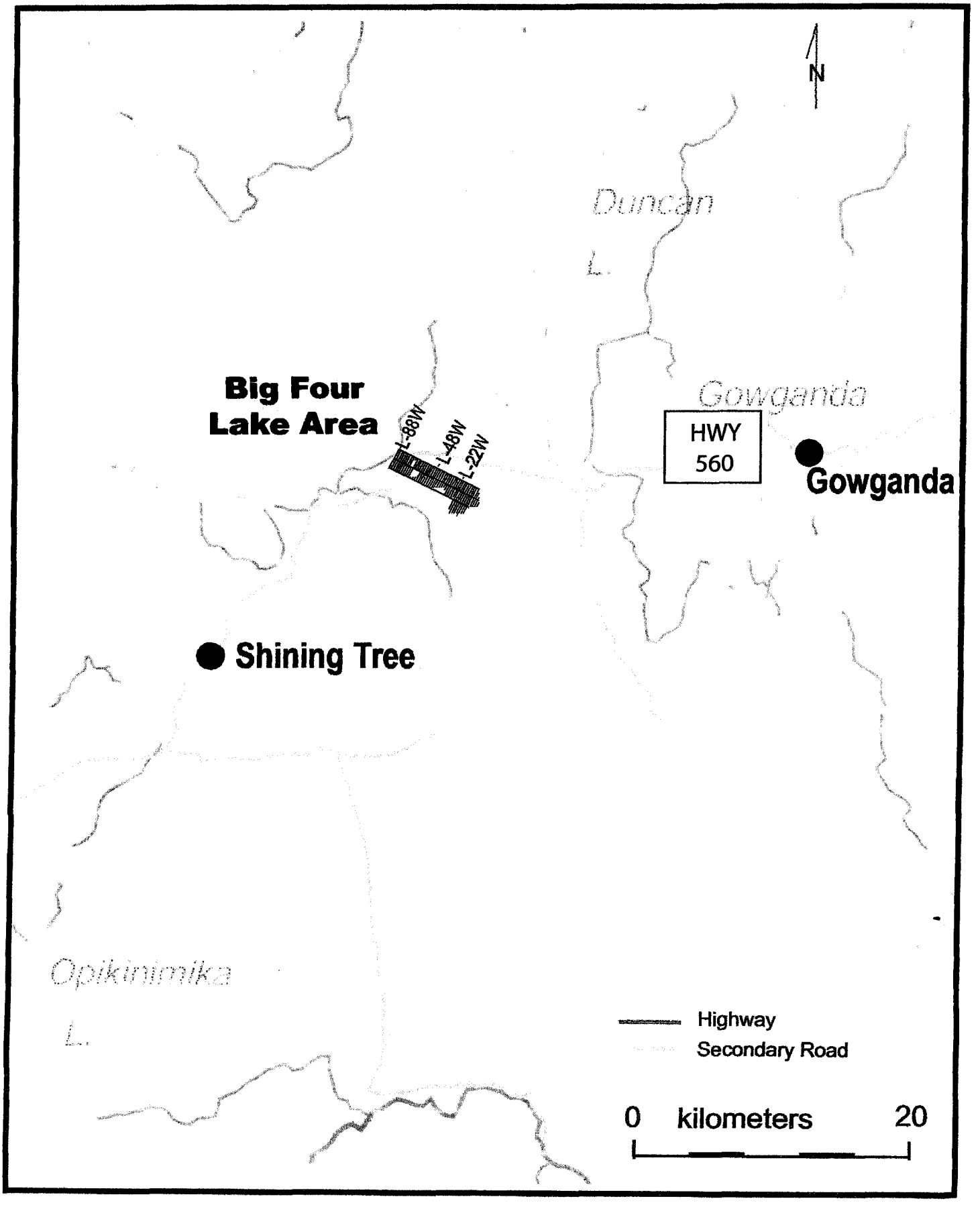

Figure 1.2: Big Four Lake area (modified *from* Caldbick, 2004)

1.2 REGIONAL GEOLOGY

The Shining Tree area is in the south-west part of the Abitibi sub-province (Figure 1.3) and is part of the Abitibi greenstone belt (Ayer *et al.*, 2002).

Figure 1.4: Hierarchical scheme of the geological divisions used in the thesis

Superior province

⇓

Abitibi sub-province

⇓

Southern Abitibi greenstone belt

⇓

Shining Tree area

⇓

Big Four Lake area

The Abitibi sub-province is composed of approximately 60% granitic rocks and approximately 40% greenstone rocks of Neoarchean age (Card and Poulsen, 1998). It was developed between 2.8 and 2.6 Ga (Jackson and Fyon, 1991). The granitic rocks are generally represented by large batholiths. The metavolcanic and metasedimentary rocks are concentrated in the Abitibi greenstone belt delimited on its western boundary by the Kapuskasing tectonic zone, a Neoarchean-Paleoproterozoic intra-cratonic region characterized by thrusting and strike-slip faulting (Percival and Card, 1983). To the south-east the Abitibi sub-province is in tectonic contact with the Neoarchean rocks of the Pontiac sub- province and the

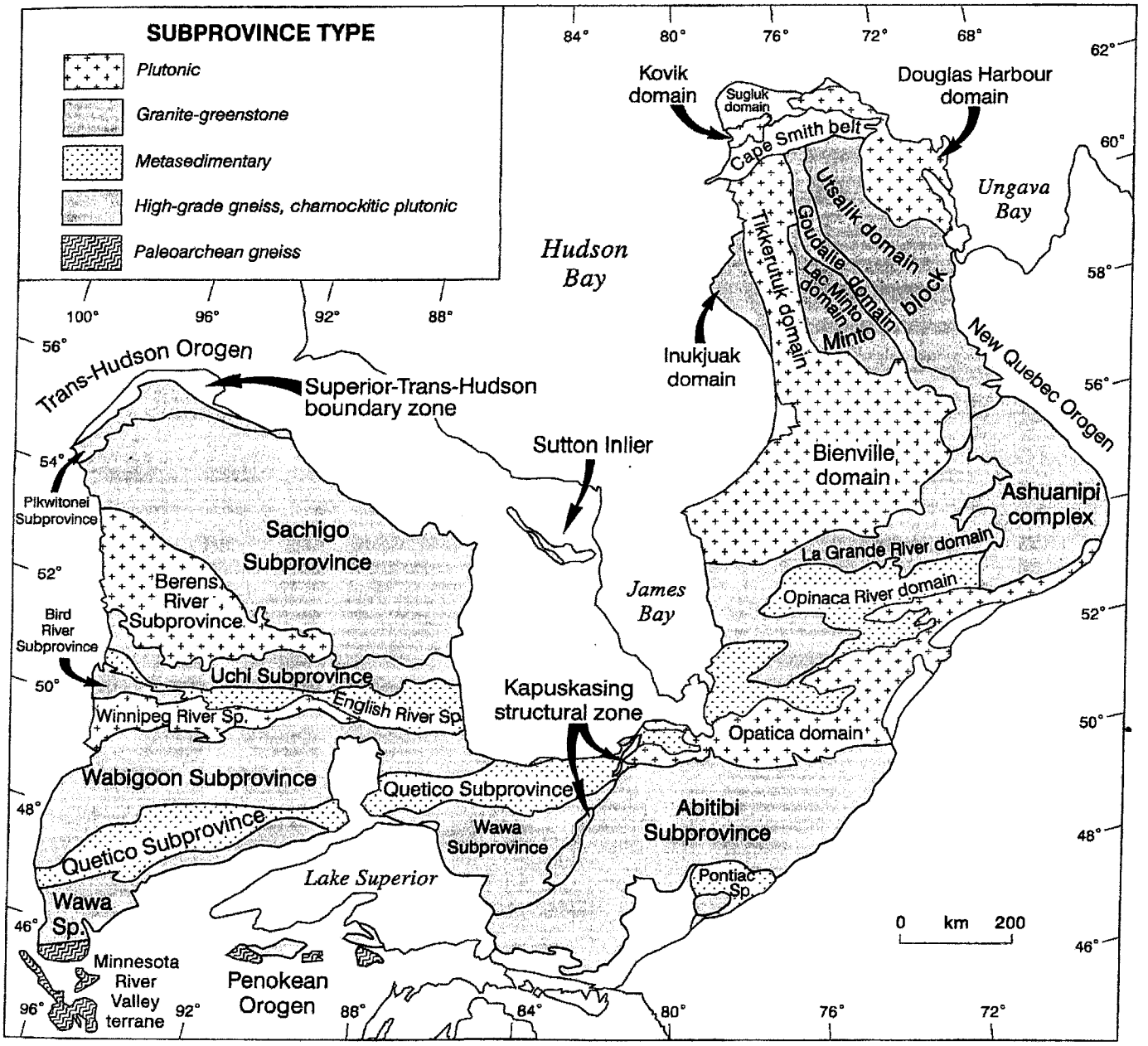

Figure 1.3: Geological map of the sub-provinces of the Superior province (modified *from* Card, 1990)

high-grade gneisses of the Mesoproterozoic Grenville (Card and Poulsen, 1998). To the south, the rocks of the Abitibi sub-province are unconformbly overlain by the Paleoproterozoic sequence of passive rift margin metasedimentary rocks of the Huronian supergroup (Card and Poulsen, 1998). To its north, the Abitibi sub-province is limited by Archean gneiss and plutonic rocks of the Opatica plutonic belt of the James Bay area (Card and Poulsen, 1998).

The Abitibi greenstone belt is composed of a large number of Neoarchean volcano-sedimentary sequences and intrusive rocks ranging from ultramafic complexes to post-tectonic granites. It is one of the largest continuous areas of well-preserved, Archean, low-grade, metamorphic volcanic and sedimentary rocks in the world. It is also one of the richest mining areas in the world, with important quantities of gold, copper, zinc, silver and iron having been extracted from the Abitibi. Because of its economic and geologic importance, and its easy access, the exploration and the study of these rocks was and will remain important (Card and Poulsen, 1998).

The geology of the entire Abitibi will not be reviewed because the study area only represents a small portion of the south-west Abitibi greenstone belt. Rather, the emphasis is put on the south-west part of the Abitibi greenstone belt.

New mapping and U-Pb zircon geochronological results in the southern Abitibi greenstone belt support an autochthonous regional stratigraphy comprised of nine supracrustral assemblages, rather than the collage of allochthonous terranes proposed in recent publications. "Previous tectonic models ranged from dominantly vertical tectonics with development of a belt-wide geosynclinal basin formed in

response to rifting, crustal subsidence and cyclical volcanic and sedimentary infill (Goodwin, 1977; Jensen and Langford, 1985) to mobilist models with greenstone belt development occurring at convergent plate margins (Dimroth *et al.*, 1983a; Ludden *et al.*, 1986; Jackson *et al.*, 1994)" (Ayer *et al.,* 2002).

Ayer *et al.* (1998) divided the southern part of the Abitibi greenstone belt into nine distinct supracrustal assemblages. Their work stems from the earlier interpretations of Jackson and Fyon (1991), who divided the area into 55 different supracrustal assemblages, based on lithologic, structural, geochemical and geophysical data, together with new geochronological U-Pb zircon data. Importantly, Ayer *et al.* (2002) wrote, "The numerous stratigraphic correlations, inheritated ages and continuity of lithology support the development of an autochtonous terrain rather than an allochtonous tectonic development prior to the regional deformation". Because the supracrustal assemblages include the Swayze, Shining Tree and Montcalm greenstone belts and, because they are separated by granitic intrusions or covered by Proterozoic sediments, Ayer *et al.* (2002) think they are part of one extensive greenstone belt.

Folowing is a brief description of each assemblage of Ayer *et al.* (2002 and 2005), starting with the older ones (Figures 1.5, 1.6 and 1.7):

1) The Pacaud assemblage is dated between 2750 and 2735 Ma. This assemblage is primarily composed of mafic, tholeiitic volcanic rocks with sparse aluminum-enriched komatiitic rocks and a few intermediate to felsic calc-alkaline rocks. These tholeiitic and calc-alkaline rocks were interpreted

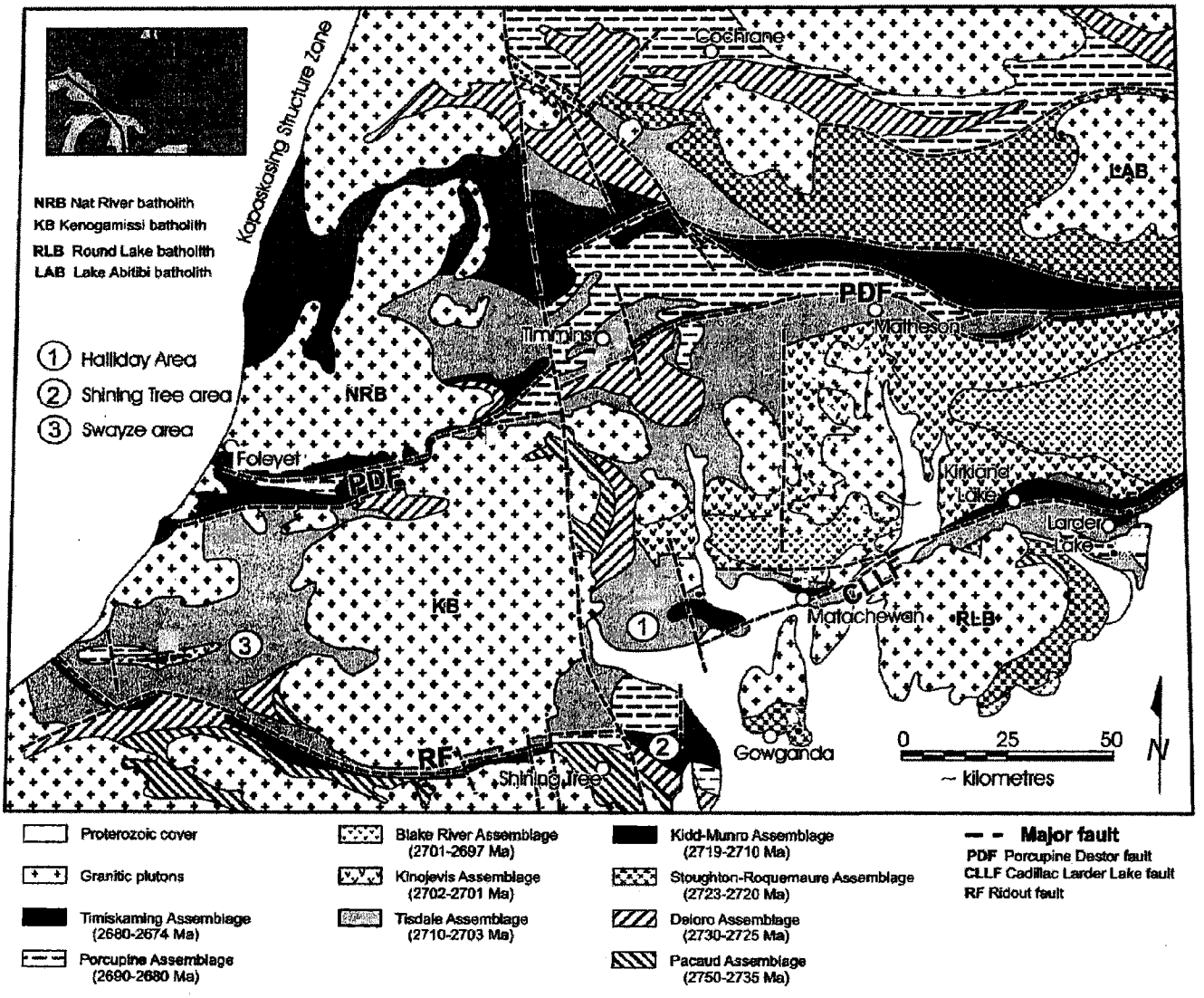

Figure 1.5: Map of the assemblages for the south-western part of the Abitibi greenstone belt (modified *from* Ayer *et al.*, 2002a)

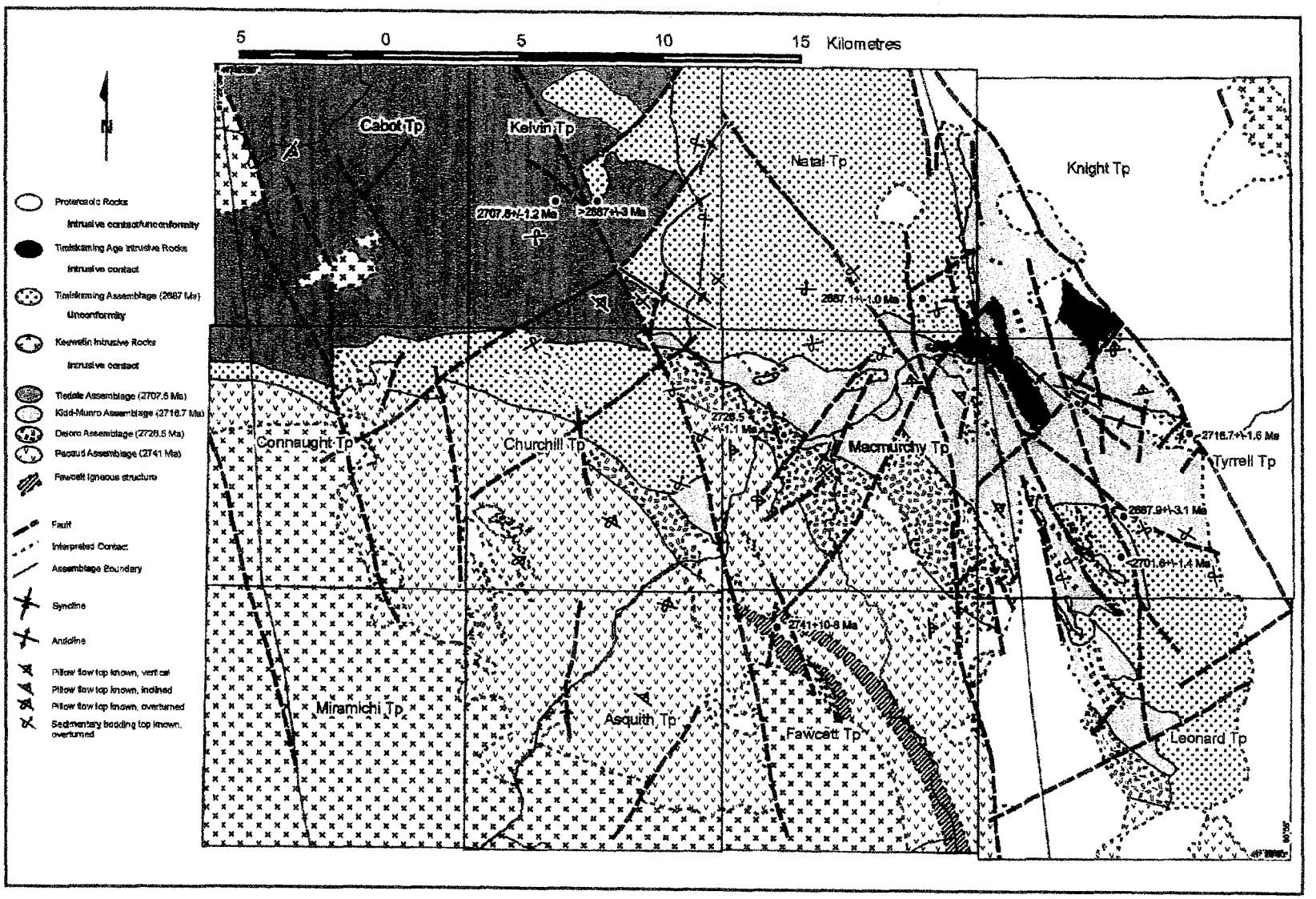

Figure 1.6: Lithostratigraphic assemblages of the Shining Tree area (modified *from* Oliver *et al.*, 1999)

Assemblage Name (Age in Ma)	Includes Previously Identified Formations and Groups Within Study Area	Basal Contact Relationships	Dominant Rock Types	Volcanic Chemical Affinity
Timiskaming (2676–2670)	Timiskaming, Dome, Three Nations, Hearst	Angular unconformity	Conglomerate, sandstone, mafic to intermediate volcanic	Alkalic to calc-alkalic
Porcupine (2690–2685)	Porcupine, Krist, Beatty, Hoyle, Whitney, Hearst	Angular unconformity	Turbidite, minor conglomerate and iron formation	Calc-alkalic
Upper Blake River (2701–2696)	Blake River, Kamiskotia, Skead	Conformable	Mafic to felsic volcanic	Tholeiitic and calc-alkalic
Lower Blake River (2704–2701)	Kamiskotia, Kinojevis, Garrison	Conformable	Mafic and minor felsic volcanic	Tholeiitic
Upper Tisdale (2706–2704)	Tisdale, Marker Horizon, Duff, Coulson, Gauthier	Conformable to unconformable	Intermediate to felsic volcanic	Calc-alkalic
Lower Tisdale (2710–2707)	Tisdale, Bowman, Larder Lake	Conformable to unconformable	Ultramafic, mafic, felsic volcanic and iron formation	Komatiitic, tholeiitic and calc-alkalic
Upper Kidd–Munro (2717–2711)	Munro	Conformable to unconformable	Ultramafic, mafic, felsic volcanic and iron formation	Komatiitic, tholeiitic
Lower Kidd–Munro (2719–2717)	Munro, Coulson, Rand	Conformable to unconformable	Intermediate to felsic volcanic	Calc-alkalic
Stoughton–Roquemaure (2723–2720)	Stoughton–Roquemaure, Kinojevis, Wabewawa, Catherine	Conformable to unconformable	Ultramafic, mafic, intermediate and felsic volcanic	Komatiitc, tholeiitic and calc-alkalic
Deloro (2730–2724)	Upper Deloro, Redstone River	Unconformable	Mafic, intermediate and felsic volcanic and iron formation	Tholeiitic and calc-alkalic
Pacaud (2750–2735)	Pacaud, lower Deloro	Unknown – removed by intrusions	Ultramafic, mafic and felsic volcanic	Komatiitic, tholeiitic and calc-alkalic

Figure 1.7: Summary of the southern Abitibi greenstone belt supracrustal assemblage names, ages, basal contacts, rock types and chemical affinities (modified *from* Ayer *et al.*, 2005)

by Ayer *et al.* (2002) to have formed in an ensimatic ocean basin and arc environment;

2) The Deloro assemblage is dated between 2730 and 2724 Ma. Mafic to felsic calc-alkaline volcanic rocks dominate this assemblage, locally with mafic tholeiitic volcanic rocks. Extensive iron formation units, composed mainly of oxide minerals, are generally situated at the top of this assemblage. This assemblage was interpreted to have formed in an oceanic arc environment;
3) The Stoughton-Roquemaure assemblage is dated between 2723 and 2720 Ma and is composed mainly of basaltic tholeiitic volcanic rocks, locally with komatiitic rocks and felsic calc-alkaline volcanic rocks. It is interpreted to have formed in a plume geological environment;
4) The Lower Kidd-Munro assemblage is dated between 2719 and 2717 Ma. This assemblage is composed of calc-alkalic intermediate to felsic volcanic rocks;
5) The Upper Kidd-Munro assemblage is date between 2717-2711 Ma. This assemblage is composed of ultramafic, mafic and felsic volcanic rocks and iron formation. The volcanic rocks have komatiitic and tholeiitic affinities. Ayer *et al.* (2002) interpreted that the Kidd-Munro assemblage to have formed in plume and island-arc environments;
6) The Lower Tisdale assemblage is dated between 2710 and 2707 Ma. This assemblage is composed of basaltic to rhyolitic tholeiitic volcanic rocks, aluminum-depleted komatiites, felsic calc-alkaline volcanic rocks and iron formation.
7) The Upper Tisdale assemblage is dated between 2706 and 2704 Ma. This assemblage is composed of calc-alkalic intermediate to felsic rocks. The

Tisdale assemblage is also interpreted to have formed in plume and island-arc environment (Ayer *et al.,* 2002);

8) The former Kinojévis assemblage was dated between 2703 and 2701 Ma and is now included within the Blake River (see below) as the Lower Blake River assemblage. It is mainly composed of mafic tholeiitic volcanic rocks with minor tholeiitic felsic volcanic rocks; The former Kinojévis assemblage has been interpreted to have formed in a plume environment (Ayer *et al.,* 2002).

9) The Upper Blake River is dated between 2701-2696 Ma. It is composed of tholeiitic and calc-alkalic mafic to felsic volcanic rocks. The upper Blake River assemblage is interpreted to have formed in rifted, island-arc environment; (Ayer *et al.*, 2002)

10) The Porcupine assemblage is dated between 2690 and 2685 Ma. This assemblage is mainly composed of sandstones, siltstones and shales, comprising part of a turbiditic sequence (Born, 1995). This assemblage unconformably overlies the previous volcanic assemblages all of which were deposited in a submarine environment. Locally, minors units of conglomerate and iron formation are present. There are no volcanic rocks in this assemblage;

11) The Timiskaming assemblage is dated between 2676 and 2670 Ma. This assemblage unconformably overlies the Porcupine assemblage. It is mainly composed of sedimentary rocks such as subaerially-deposited polymictic conglomerates and fluviatile sandstones, together with alkalic to calc-alkalic mafic to intermediate volcanic rocks.

According to Ayer (2002): "The older seven assemblages correspond to a relatively continuous volcanism between 2750 and 2696 Ma. The chemical and isotopic signatures of the volcanic rocks during this interval suggest repetitive extraction from a plume and/or from the mantle via a subduction zone, both of which have long-term Nd and Hf isotopic depletion signatures with no evidence of contamination by enriched material. Intimate intermingling of the different magma clans occurs throughout much of the stratigraphic section. Regional fault control on the distribution of the volcanic assemblages provides evidence for early dip-slip movement associated with volcanic extension dating back to at least 2725 Ma (Ayer *et al.*, 2002).

The two youngest assemblages described by Ayer *et al.* (2002) unconformably overly the volcanic assemblages and are generally proximal to the regional faults (Ayer *et al.*, 2002). These two assemblages are in general broadly contemporaneous with the syntectonic granitic plutons, the regional folding and with the reactivation of the movement of the regional faults associated with the accretion of the Abitibi with the Superior province craton. The presence of similar age assemblages on both sides of the Porcupine-Destor, Cadillac-Larder Lake and Ridout faults shows they are not paleosuture zones as previously thought (Ayer *et al.*, 2002).

Autochthonous repetition of different geodynamic environments over 50 million years of volcanic activity with five dominantly tholeiitic ± komatiitic assemblages and two dominantly by calc-alkaline assemblages, as well as the extensive intermingling of these different magma clans in a number of these assemblages, appears to be unique in the Archean. It suggests complex, large-scale and long-lived interaction between mantle plumes and subduction zone magmas. The Nd isotope data indicate a derivation of the diverse volcanic magmas from homogeneously depleted sources with $\varepsilon_{Nd}=2.5\pm0.5$ demonstrating a lack of contamination by ancient enriched components (Ayer *et al.* 2002)."

Based on the work of Ayer *et al.* (2002), the intrusions of the Abitibi greenstone belt have been defined and classified in more detail from Chown *et al.* (1992), Sutcliffe *et al.* (1993) and Heather (1998). Plutonic rocks of the southern part of the Abitibi greenstone belt can be classified into three distinct suites:

1) synvolcanic, 2) syntectonic and 3) post-tectonic.

The synvolcanic intrusions are dated between 2740 and 2696 Ma (Corfu, 1993; Heather, 1998; Mortensen, 1993a, b; Ayer *et al.*, 2005). They are typically sills, often stratified with magma mingling textures and are massive to very foliated (Heather, 1998). They have similar ages and composition to the assemblages described above.

The syntectonic intrusions are dated between 2695 and 2670 Ma and are widespread throughout the Abitibi greenstone belt (Chown *et al.*, 1992; Corfu, 1993; Mortensen, 1993a, b; Heather, 1998; Davis *et al.*, 2000; Ayer *et al.*, 2005). They are massive or foliated and dispersed as small intrusions into supracrustal rocks or as batholiths. The youngest syntectonic intrusions are composed of tonalites and granodiorites and form the major part of the batholithic complexes. The latest intrusions are more potassic in composition; they are mainly composed of granites, monzonites and syenites with mafic phases defined by diorites, gabbros, clinopyroxenites, hornblendites and associated lamprophyres (Ayer *et al.*, 2002).

The post-tectonic intrusions are dated between 2670 and 2660 Ma and are mainly located in the southern part of the Abitibi greenstone belt (Heather, 1998; Davis *et al.*, 2000; Ayer *et al.,* 2005). They are massive and are generally part of the batholithic complexes. They are composed of "Algoman" type biotite granite, pegmatites and "S" type biotite and muscovite granites (Ayer *et al.*, 2002).

The metamorphic facies of the southern part of the Abitibi greenstone belt varies between lower to middle greenschist facies, with local amphibolite facies (Jolly, 1980; Dimroth *et al.*, 1983b; Powell *et al.*, 1995). The amphibolite facies is generally in close proximity to the batholiths and is interpreted as being the metamorphic contact aureole associated with them (Card and Poulsen, 1998). Amphibolite facies rocks are present close to major fault zones where fluids were circulated (Ayer *et al.,* 2002). The peak of metamorphism is dated between 2677 and 2643 Ma and does not appear to have been associated with the burial metamorphism because it is after the

supracrustal accumulation phase (Powell *et al.*, 1995). From Ayer *et al.* (2005) the regional metamorphism occurs from approximately 2690 and 2640 Ma in the Abitibi greenstone belt area.

1.3 Previous work

Previous work prior to 1977 was documented by M.W. Carter (1977).

The first geological mapping work published about the Shining Tree area was in 1896 by Burnwash (1897). His goal was to study in detail the western limit of the Macmurchy Township. Later in 1900, Coleman (1901) studied the iron formation in the area. Between 1909 and 1913, Collins mapped the Onaping area situated on the southern part of the Macmurchy Township (Collins 1911, 1912, 1917). In 1911 and 1912, Stewart (1912, 1913) mapped the "West Shining Tree gold area" situated on Macmurchy Township. Between the years of 1912 and 1923, a few articles on the geology of "West Shining Tree gold area" were published in several mining journals (Hodge, 1912; Hore, 1918, 1919a, b, c, d; Goodwin, 1919; Weed, 1923). In 1919, Hopkins (1920a) started a preliminary geological study of the deposits of the "West Shining Tree gold area". This work (Hopkins, 1920b) was published prior to the deposits being described again (Hopkins, 1922). In 1925, Finley (1926) mapped the Wasapika profile situated in the south-western part of Macmurchy Township. He also mapped the north-east zone of the township the same year. This report written by Gledhill (1926), after the untimely death of Finley, is under "Notes on the South Part of the Grassy River Area".

In 1926, Langford (1927) examined also the Wasapika profile and mapped the intrusions and the veins associated with the gold deposits. In 1931, Graham (1932) mapped the east part of Macmurchy Township, Tyrrell and Knight Townships.
In 1934, Laird (1935) visited the Wasapika profile of the "West Shining Tree gold area", located on the south-western part of the Macmurchy Township and wrote a report on the new development of the "West Shining Tree gold area". Between 1927 and 1990, most of the Shining Tree area was included in the Temagami Native Land Caution and placed off limits to mineral exploration and staking.

The area of Shining Tree was mapped again by the Ontario Geological Survey by Carter at the beginning of the seventies. A report on Macmurchy and Tyrell Township were published by him in 1977 (Carter, 1977). During these years, geological maps and reports on specific townships were published to produce a final 1: 50,000 geological map and a cumulative report on Shining Tree area, (Carter, 1987).

In 1990, the Ontario Geological Survey established a township-wide airborne magnetometer and electromagnetic survey.

Later in 1996, Johns from the Ontario Geological Survey, started a new study of the same area to re-evaluate the geology and the mineral potential of this part of the Abitibi greenstone belt. Two 1: 30,000 geological maps were published, one in 1999 for the east half (Johns, 1999a) of Shining Tree area and one in 2000 for the west half (Johns, 2000) of the Shining Tree area. A final 1: 50,000 geological map on the Shining Tree area was also published by Johns in 2003.

BRIEF HISTORY OF THE PREVIOUS WORK ON THE COPPER HILL PROPERTY

The Copper Hill property, where the Brunet Copper occurrence is located and where the detailed mapping for this thesis was done, has been owned until recently by KRL since the 1990's, it is now owned by Golden Harp Resources Inc.

Mining exploration was done since the 1960's by several companies. In 1964 and 1965, Mokta (Canada) Limited had an option on the property. The interest on the property was stimulated by a copper occurrence characterized by a quartz-carbonate vein trending north-north-east, with a steep dip of 75° E within a brecciated, red rhyolite. This vein is 1.5 m wide and is exposed over at least, 45 meters. A hand sample taken by G. Willars, for the company Raylloyd Mines and Exploration Limited, yielded Cu concentration values of 5.91% over 122 cm (assessment files from resident geologist of the Ministry of Natural Resources of Ontario in Kirkland Lake). The metallic minerals found were chalcopyrite, bornite and specularite. During this period, drilling, geophysics (magnetometer and induced and electromagnetic polarization) and geological mapping were completed. After the recognition of several geophysical anomalies, a second drilling program was started. Fifteen drill holes, totaling 1488 meters were drilled. Only minor quantities of copper were detected. The option was abandoned by Mokta (Canada) Limited. In 1967, Raylloyd Mines and Exploration Limited optioned the property and drilled another 150 meters after new geological observations, to verify the extension, at depth, of the vein. No further work was done by Raylloyd Mines and Exploration Limited. The geological

mapping was continued by C.W. Brunet. In 1971, Brunet had a total of seven claims, all situated in the center of Macmurchy township. A "manual" copper extraction was done by him in 1972. In 1977, Brunet converted the claims to a mineral lease. In 1976, Getty minerals drilled one hole east of Bay Lumber road, unfortunately the results are unknown (Caldbick, 2004).

The following section refers to historical work in the Shining Tree area, specifically on Brunet Copper occurrence done by KRL. This summary was compiled by Watkins (2000).

- May 1995

  - KRL acquired the Brunet mineral lease.

- September 1998 – KRL

  - A high sensitivity magnetic and spectrometer airborne survey was flown over a 4 by 4 km area centered on the Brunet Copper occurrence.

- February 1999 – KRL

  - 24 kilometers of grid cut with 100 meter spaced lines centered on a set of airborne anomalies. 24 line km of magnetic and VLF-EM are initiated as well as 4 line km of pulse electromagnetic (PEM) survey on 4 lines; 5600-5900W (Figure 1.8).

- May and June 1999 – KRL

- Two diamond drill holes; CH99-01 and 02 are drilled totaling 867 meters. 264 core samples are analyzed for multi-elements. The drill holes are further surveyed with down hole geophysics. A program of 15 line km of surface geology and prospecting occurs with reconnaissance geology over the claim group.

- October and November 1999 – KRL

  - 70 km grid cut with 200 meter spaced lines; 2400-8800W. 40 km of surface geology performed on the grid lines. 699 soil samples are retrieved from lines 2400W to 6900W.

- December 1999 – KRL

  - 70 line km of magnetic and VLF-EM are surveyed on the Brunet Copper area.

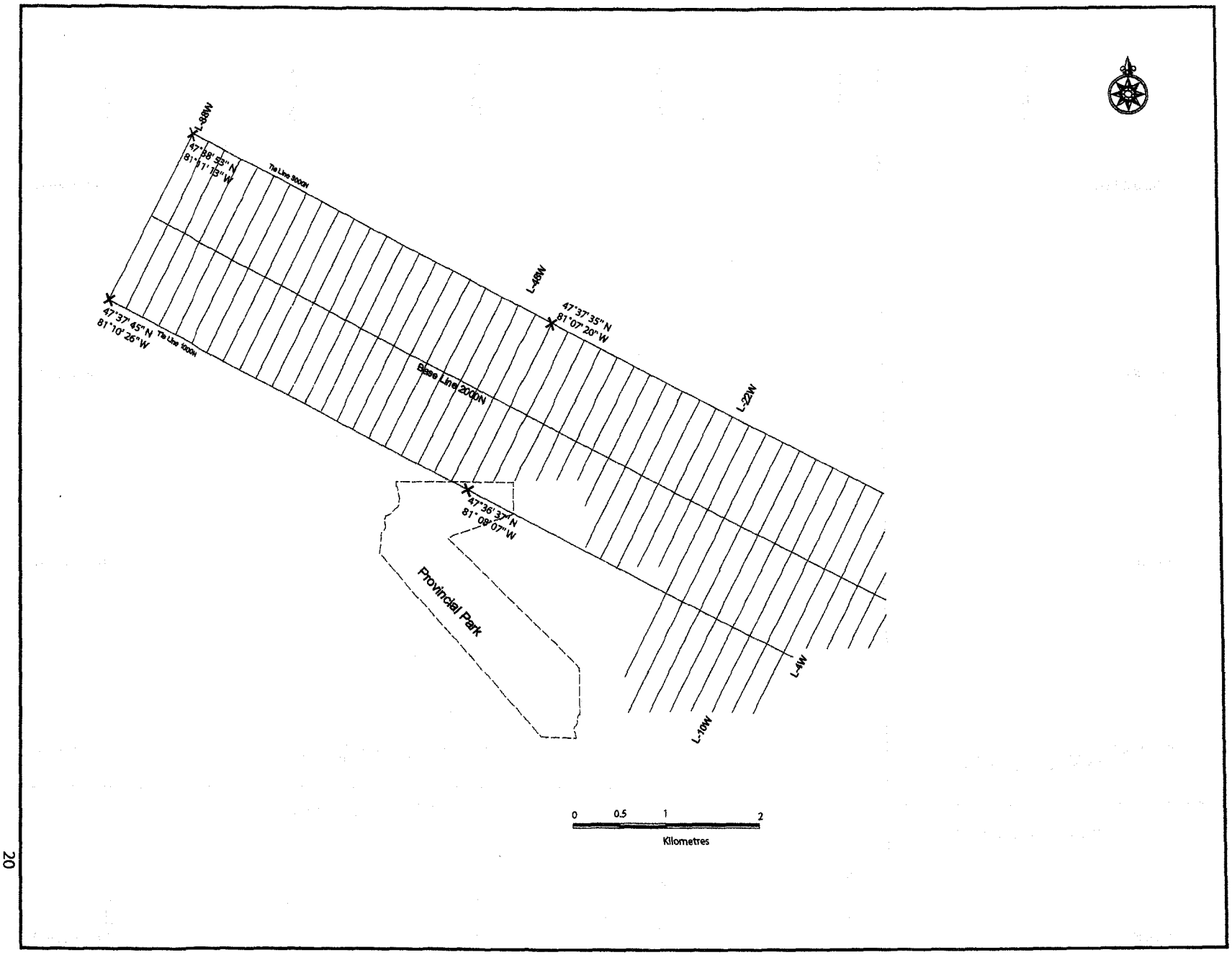

Figure 1.8: KRL grid

- March 2000 – KRL

  - A drill program totaling 2156 meters in 7 holes from CH00-03 to 09 is completed with 450 samples analyzed. Down hole geophysics is done in holes CH00-03, 05 and 07.

- April 2000 – KRL

  - The grid is expanded to the southeast on 200 m spaced lines, 2400 to 8800W and surveyed with magnetic and VLF-EM.

- June and July 2000 – KRL

  - 1,028 meters cored in drill holes CH00-10 to 13. Geological mapping of the west end of the Copper Hill grid. Gold is discovered in the Golden Sylvia iron formation. Gold is also discovered 3 km north of the Golden Sylvia iron formation (lines 30 and 31W area). After this date most of KRL's emphasis was on the Golden Sylvia area except for prospecting, mapping the overall claim property. An airborne magnometer and electromagnetic geophysical survey was flown in 2004 on the entire property.

1.4 METHODOLOGY

A detailed geological map at 1: 10,000 was completed in the summer 2000 over an area of approximately 9 km^2. A total of 11 weeks were spent in the field.

The observations were made from roads (Highway 560, Bay Lumber road and secondary trails) but mostly from the KRL Brunet Copper occurrence grid over part of the Copper Hill property. The mapping was done on each line situated between the lines 44W and 88W (Figure 1.8). These lines were 2 km long; spaced 200 m apart and strike almost north-south (027-207°N).

The geological map was produced from the data taken in the field and from the compilation of the work done by M.W. Carter and G.W. Johns from the Ontario Geological Survey and from J. J. Watkins from KRL. The majority of the geological contacts were interpreted from the outcrop distribution (Appendix B). The structural geology was also interpreted from the geological contacts and geophysical data.

During the mapping, more than 270 outcrops were observed. From the collaboration of KRL, five drill holes, for a total of almost 1590 m were also studied and sampled. From all the samples taken in summer 2000, 40 were selected for geochemical analyses of the major and trace elements. The analyses were done by the laboratories of the Ontario Geological Survey; Geoscience Laboratories (Geo Labs), based in Sudbury.

The entire set of geochemical samples were first split; one half was kept for hand specimen reference, and the other half was used for thin sectioning and geochemical analysis. The type of microscope used to observe the thin sections was an Olympus BH-2. In addition to these geochemical samples, 26 polished thin sections and 15 extra thin sections were also studied.

All the samples were sent to Geoscience Laboratories of the OGS. The laboratory took care of the preparation (crushing) of the sample for the geochemical analysis. Geo Labs did all the geochemistry; whole rock, trace element, gold and silver, arsenic, ferrous iron and water (moisture and crystalline) analysis. Major elements were analyzed by XRF from fused discs, and trace elements were analyzed by ICP AES or ICP MS. Ferrous iron (Wilson, 1960) was determined by titration and Au plus Ag were analyzed by fire assay. Typically errors are on the order of less than 5% of total abundance for the major oxides, less than 4% of total abundance for the rare earth elements and around 1% for FeO (Saumur, 2005). All the geochemical results are presented in APPENDIX A.

A total of 13 thin sections representing all the lithological units were used for electron microprobe (EMP) analysis. Over 100 analyses were done, at Carleton University, to determine or verify the chemistry of the minerals.

Quantitative analyses were made on an automated 4 spectrometer Camebax MBX electron probe using the wavelength dispersive X-ray analysis method (WDX). Operating conditions were: 15 kv accelerating potential and a beam current of 20 nanoamperes (nA) for silicates and oxides. Peak counting times for each analyzed element were : 15-40 seconds or 40,000 accumulated counts. Background measurements were made at 50% peak counting time on each side of the analyzed peak Raw X-ray data were converted to elemental weight % by the Cameca PAP matrix correction program. A suite of well characterized natural and synthetic minerals and compounds were used as calibration standards. Analyses are accurate

to 1-2 % relative for major elements, 3-5 % relative for minor elements (< 1 wt %) (Peter Jones, personal communication)

Digital BSE (back-scattered electron) images were collected at 512 x 512 resolution with a Lamont 4 element solid state BSE detector and BSE Quad Summing Amplifier interfaced to a 4Pi Analysis Inc. digital imaging system and Power Macintosh computer (Peter Jones, personal communication).

1.5 Nomenclature

1.5.1 Pyroclastic vs Epiclastic rocks

Pyroclastic rocks originate from explosive eruptions and are deposited hot. Pyroclastic debris consists of pumice, scoria, glass shards, crystals and accessory lithic fragments. Epiclastic rocks result from the weathering of volcanic rocks and the proximal sedimentation of the volcanic detritus (Lajoie and Stix, 1992). In Archean terranes it can be very difficult to distinguish the two because of post-magmatic alteration and deformation; hence, the term volcaniclastic is used where there is no clear evidence of hot deposition (e.g. columnar joints, welding) or sedimentary deposition (e.g. mud beds, rounding)

Figure 1.9: Differences between pyroclastic and epiclastic deposits (modified *from* Lajoie and Stix, 1992).

	Epiclastic	Pyroclastic
Texture	Rounded grains of volcanic rocks and crystals. Depending on environment of deposition, sorting may be excellent to poor.	Angular to subrounded pumice, scoria, shards, accretionary and armoured lapilli that maybe deformed or welded. Sorting is poor to very poor.
Composition	Volcanic rock fragments which tend to be polygenetic, with common incompatible phases such as quartz and basalt.	Mostly felsic to intermediate fragments which tend to be monogenetic.
Structure	Normal sedimentary structures.	Common presence of normal or reverse grading, of thick diffuse strata, low angle laminae, and bomb sags.

1.5.2 VOLCANOGENIC MASSIVE SULFIDE -TYPE MINERALIZATION (VMS)

Because the Brunet copper occurrence is hosted in rhyolites, as veins with a characteristic alteration, it has been considered (Glen Johns, personal communication) as being a product of VMS. There are numerous VMS deposits within the Abitibi greenstone belt, examples includes the Noranda, Cyprus, Kidd-Creek and Mattabi deposits (Franklin, 1996).

Volcanic massive sulphide deposits are characterized by the abundance of submarine volcanic rocks and epiclastic rocks. Generally they are lenticular-shaped, stratified ore bodies that formed on or close to the ocean floor and are typically composed of chalcopyrite, pyrrhotite, pyrite and sphalerite. Underlying the orebody there is a silica –rich stockwork zone also rich in sulfide minerals such as pyrite and chalcopyrite. Usually this zone is associated with chloritization and it is called the alteration pipe. The VMS ore deposit systems have a typical hydrothermal alteration pattern. Sericite abundance

gradationally increases whereas the chlorite abundance gradationally decreases going away from the hydrothermal alteration pipe. Usually an exhalite horizon caps the system and serves as a seal. The effects of hydrothermal alteration can be observed up to about 10 km away from the orebody, which is usually never bigger than 2 km in width (Franklin, 1996). The hydrothermal alteration will discuss further in chapter 3.

VMS deposits have been interpreted to have formed from remobilization and concentration of metal by fluids. This hydrothermal activity is widely interpreted to be caused by the heat of the magma underneath a spreading system which drives convection of sea water (Franklin, 1996).

1.6 Objectives

As mentioned above, the general objective of this master thesis is to characterize and describe the Deloro assemblage of the area from a petrologic and geochemical point of view. Furthermore, because the Brunet occurrence has many of the hallmarks of VMS type mineralization another goal is to describe and characterize the copper mineralization in order to determine its type and potential for economic mineralization.

The first objective was to map, in the field, in detail the Big Four Lake area in order to document the geological units comprising the Deloro assemblage locally and so as to gain an understanding of the lithological and structural relations between them. The observation of thin sections and the interpretation of lithogeochemistry data helped to

establish the distribution of the facies, the textures and the mineral petrogenesis. The description of the mineralization and the alteration revealed the time relations between the different events.

1.7 Acknowledgments

This study was made possible by the collaboration of the University of Ottawa, the Ontario Geological Survey and KRL. Foremost, I would like to thank my supervisor Dr. Tony Fowler, who made this project a precious experience by his excellent supervision. Thanks to the OGS who made the project possible, especially to John Ayer for his assistance, support and co-supervision of the thesis and thanks to Glen W. Johns (deceased) who provided supervision in the field. I also want to thank Dr. André Lalonde (Mineralogy professor, University of Ottawa) for his assistance. I also would like to thank Seamus Young and John J. Watkins from International KRL Resources Corp. for their trust and support. And also a big thank you to Martin Lapointe of Aur Resources Inc. for his good insights. I would also like to thank the Faculty of Graduate and Postdoctorate Studies and Dr. André Desrochers (Director of Graduate Studies Earth Sciences) who really understood my unconventional situation. Priceless technical and administrative assistance were provided by Peter Jones (microprobe technician, Carleton University, Ottawa), George Mrazec (preparation of the polished and thin sections, University of Ottawa). Also thanks to Lise Maisonneuve (Graduate studies administrator, University of Ottawa), Ginette Soutard (Graduate studies administrator, University of Ottawa), Nicole Lanthier (Graduate studies administrator, University of Ottawa), Anne Bourbonnais (Graduate studies administrator, University of Ottawa), Margaret Moriarty (Graduate studies

administrator, University of Ottawa), Christine Bourbonnais-Hendley (Graduate studies administrator, University of Ottawa) and Hélène de Gouffe (secretary, Earth Sciences Department, University of Ottawa).

However, the main acknowledgment goes to the ones who never stopped trusting, believing and supporting me, even if I was not always making it easy!

CHAPTER TWO: GEOLOGY OF BIG FOUR LAKE AREA

This chapter describes the macroscopic field and microscopic petrographic observations of Big Four Lake area.

On the 1: 10,000 scale map, seven different units were defined (Figures 2.1 and 2.2, Appendix B and Geology of Big Four Lake area map). Two intrusive rock units, dated as early Proterozoic (Johns, 1996), called the Nipissing gabbro (unit 7) (2219 - 3.5/+3.6 Ma, Corfu and Andrews 1986) and the Matachewan dike swarm (unit 6) (2454±2 Ma, Heaman 1988) cross-cut the units of Deloro assemblage. The Deloro assemblage, dated by Ayer *et al.* (2002), at 2730 and 2724 Ma, includes five volcanogenic units in Big Four Lake area; (1) Mafic to intermediate metavolcanic rocks, (2) South rhyolite, (3) Volcaniclastic rocks, (4) Red Dome rhyolite, and (5) Sulphide -rich chemical metasedimentary rocks

Stratigraphically the Sulphide–rich chemical metasedimentary rocks (unit 5) are the youngest, of the Deloro assemblage, in the area. This unit caps the Deloro assemblage (Ayer *et al.*, 1998) and is at the upper contact of the Red Dome rhyolite (unit 4) in the area (Lebel, 2000). Within the Mafic to intermediate metavolcanic unit a few small horizons, similar to unit 5, of chemical metasedimentary rocks (unit 1a) were observed in the field and in drill core within unit 1. They are interpreted to represents breaks in the volcanism. The Volcaniclastic unit (#3) is situated within the South rhyolite (unit 2) and is mostly composed of rounded clasts similar in composition to the South rhyolite. It is therefore considered younger than it consistent

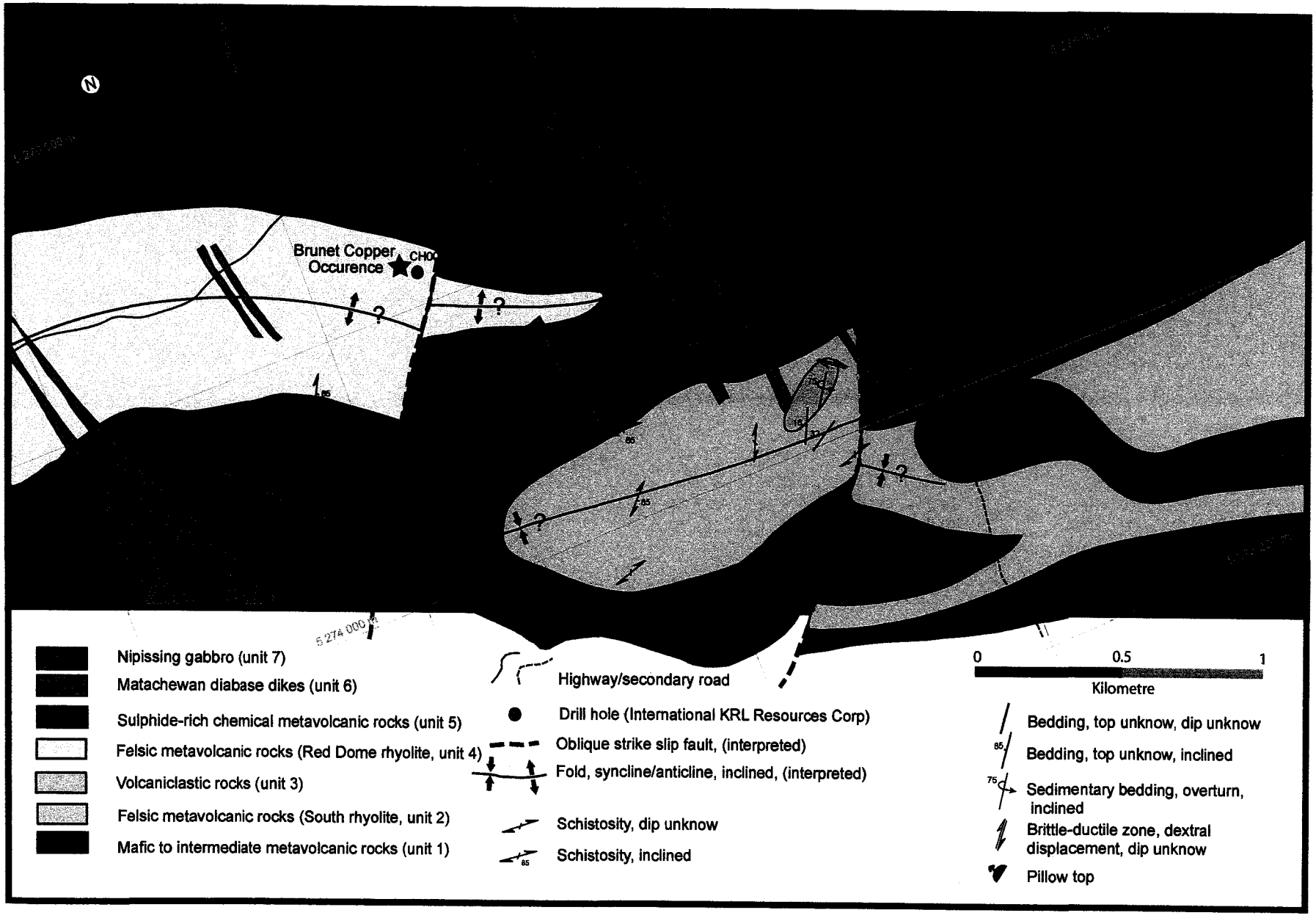

Figure 2.1: Geological map of Big Four Lake area

with the facing direction. In addition a breccia (unit 2a) composed of south rhyolite pumiceous fragments was found in a small outcrop along the Bay Lumber Road.

The oldest felsic metavolcanic unit in the map area is South rhyolite unit, it underlies Red Dome rhyolite (Lebel, 2000). The oldest rocks, in the area, are the Mafic to intermediate metavolcanic rocks (unit 1).

Figure 2.2: Idealized stratigraphic column for Big Four Lake area

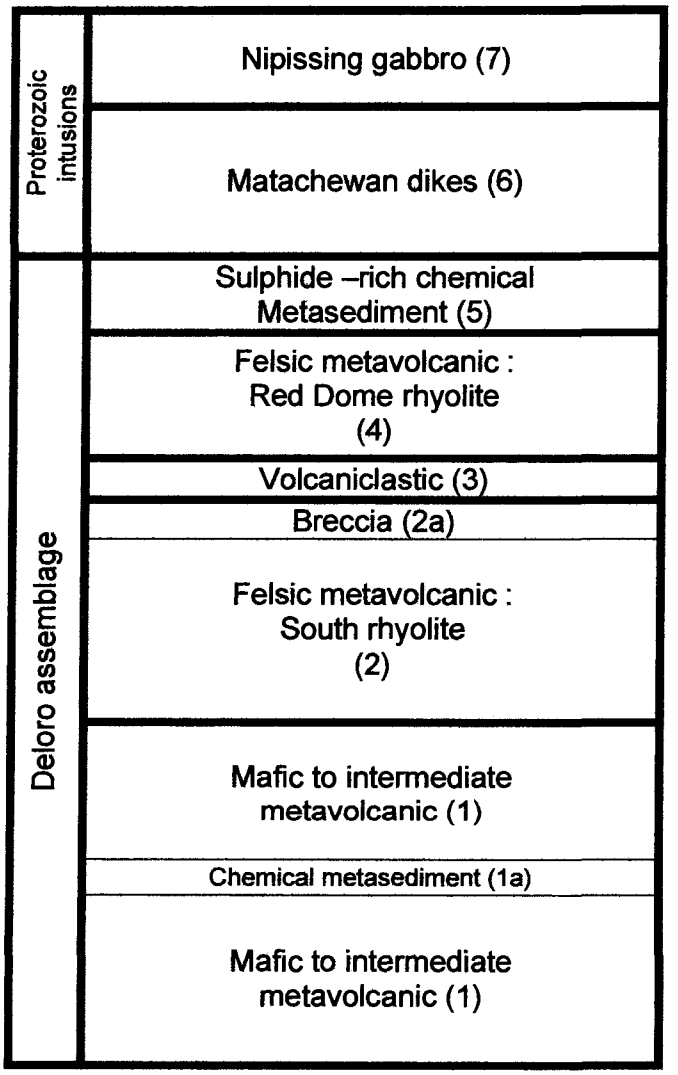

2.1 LITHOLOGICAL UNIT DESCRIPTIONS

In this section, the descriptions of the rock units of Big Four Lake area will follow the stratigraphic column (Figure 2.2), starting by the oldest unit.

2.1.1 MAFIC TO INTERMEDIATE METAVOLCANIC ROCKS (1 AND 1A)

The rocks of this unit are the most abundant in the area mapped. This unit (dark green on Figure 2.1) is composed of both massive and pillowed flows (Plate 1). On the rims of the pillows, vesicles can be visible on some outcrops. Occasional breccia textured outcrops were observed, they were interpreted to be pillow breccia. The rocks are fine-grained, having been altered to chlorite and minor sericite. The fresh surface colour is dark green and the weathered surface colour is typically light brownish tan (typical "bleached basalt" coloured). Millimetre-sized patches of a fine-grained mineral interpreted to originally have been amphibole (after pyroxene) is altered to chlorite. Centimetre-sized chlorite-, calcite- and quartz-filled amygdules are common. Parts of this unit are mineralized, containing minor pyrite, and rarely chalcopyrite in brecciated horizons.

A total of 29 thin sections were taken for further observations (samples 00-GL-08, 00-GL-22, 00-GL-53, 6001, 6006, 6012, 6014, 6016, 6023, 6024, 6026, 6029, 6032, 6039, 6044 to 6047, 6049 to 6054 and 6056 to 6060). Plate 2, shows a typical photomicrograph of this unit. Usually, the rocks composing this

Plate 1

Pillowed (tops ~SE) basalt in Mafic to intermediate metavolcanic rocks (unit 1)
Geochemistry sample #6006 (Outcrop 00-GL-09), Hammer used for scale (~0.5 m)
Secondary road oriented roughly east-west, accessible from Bay Lumber road going west

Plate 2

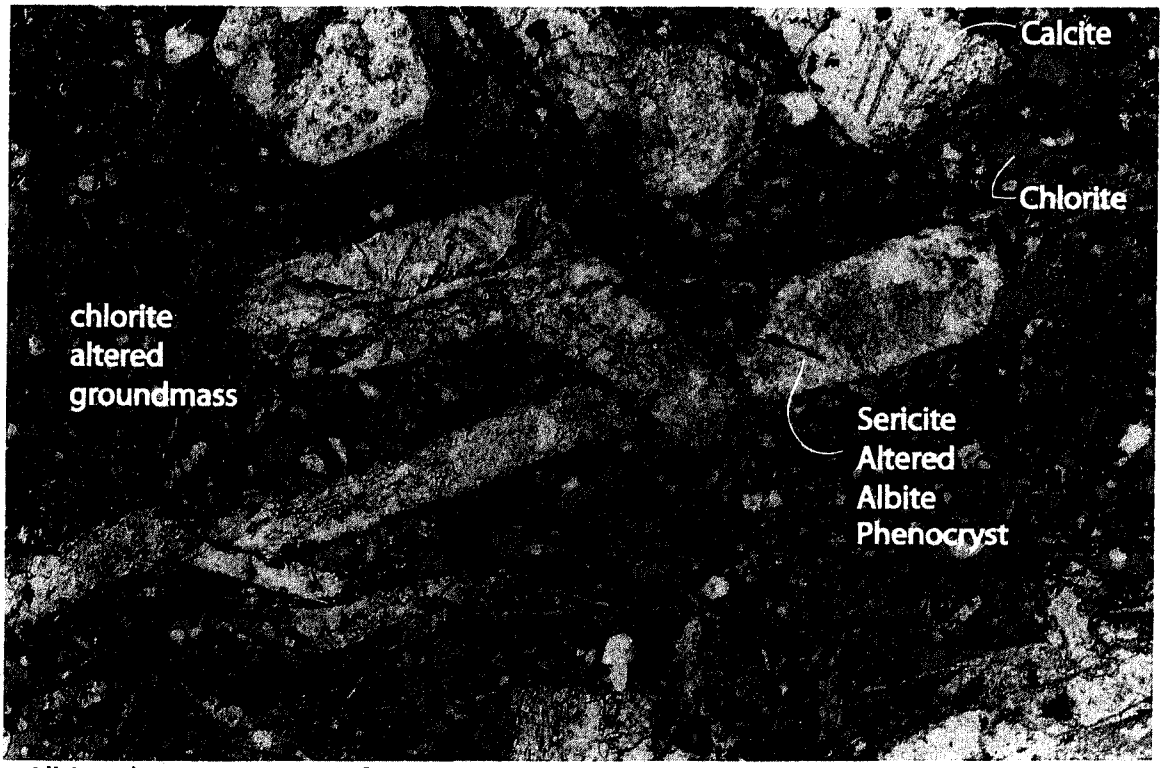

Albite phenocrysts in Mafic to intermediate metavolcanic rocks (unit 1)
Geochemistry sample #6047 (Outcrop 00-GL-28), Transmitted light, (FOV)= 2 mm
South side of Higway 560, close to Grassy road

unit have a moderately to highly-altered groundmass composed of carbonate, chlorite and occasional quartz. Plagioclase phenocrysts are present in most of the samples and they show different degrees of sericite alteration. Rare relics of amphibole, usually highly altered to chlorite, are occasionally observed (sample 00-GL-53, 6032, 6045 and 6046). Relics of pyroxene are rarely observed (samples 00-GL-53 and 6032). Chlorite, carbonate and sericite blebs and veins are quite common. In a few samples, spherulitic textures were observed (outcrops 00-GL-48 and -49). Fine, disseminated pyrite is quite common in these rocks. Iron oxides are present in about 50% of the samples observed; usually hematite is more common than magnetite. Rare chalcopyrite was observed in this unit.

2.1.2 Felsic metavolcanic rocks: South rhyolite (2 and 2a)

This unit (dark yellow on Figure 2.1) is dominantly massive but includes horizons of volcaniclastic rocks (unit 2a) (Johns and Amelin, 1999). It is located on the east end of the map area. The rock is usually light yellowish cream coloured on fresh and weathered surfaces. The majority of the rocks included in this unit are composed of a fine-grained groundmass of mainly sericite with phenocrysts of plagioclase and quartz. One large outcrop of unit 2a (00-GL-35) has subangular pumice fragments in a chlorite- altered matrix (Plate 3). One clast of red chert (≈ 2 cm in size) was found on the same location (outcrop 00-GL-35). This fragment was likely derived from chemical metasedimentary rocks (unit 1a) older than South rhyolite. Compared to the rest of the area, the majority of the rocks of the South rhyolite are deformed,

Plate 3

Volcaniclastic rocks of South rhyolite (unit 2a)
Geochemistry sample #6048 (Outcrop 00-GL-35), Hammer used for scale (~0.5 m)
Bay Lumber road

Plate 4

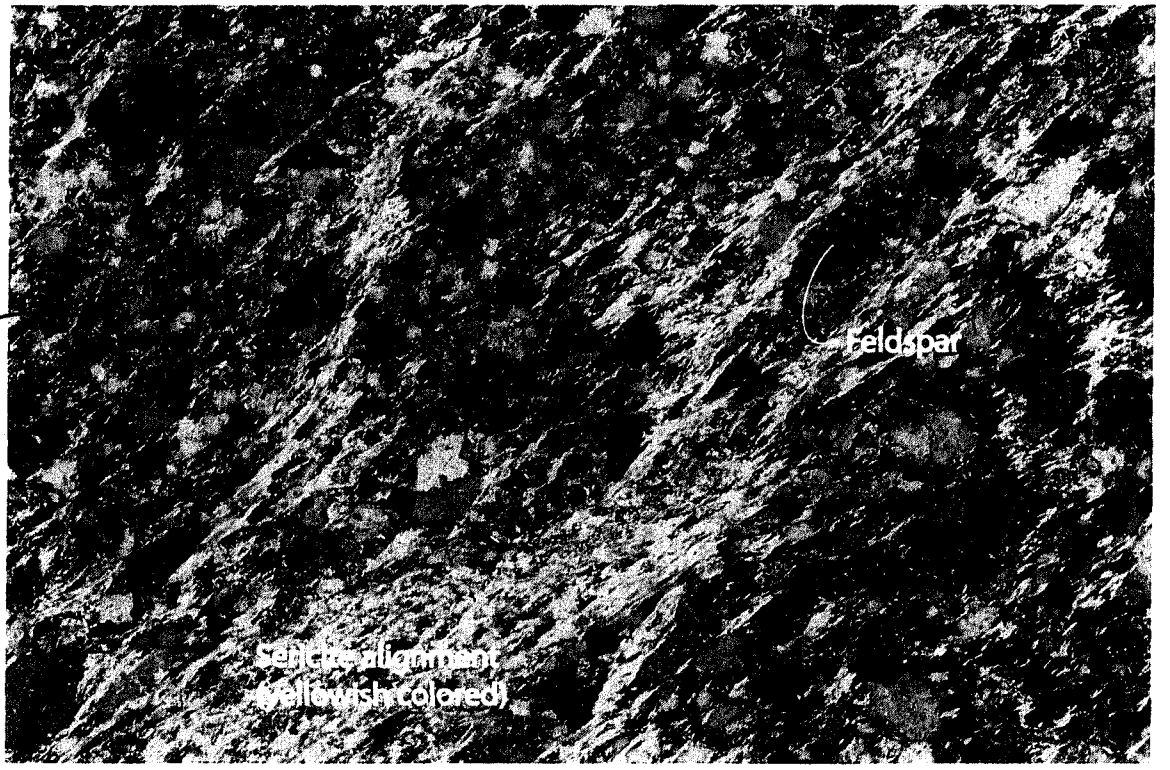

Alignment of sercite in the groundmass of South rhyolite (unit 2)
Geochemistry sample #6036 (outcrop 00-GL-29), Cross nicols, (FOV)=2 mm
Secondary road oriented roughly east-west, accessible from Bay Lumber road going west

Plate 5

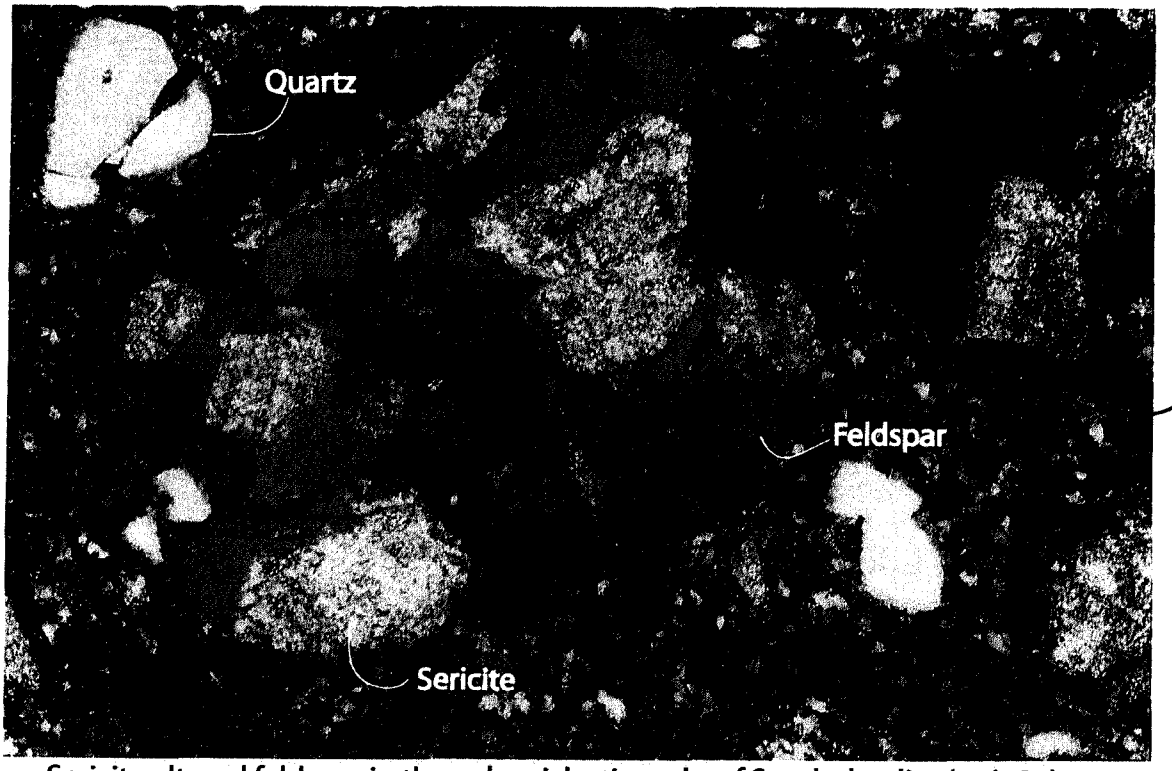

Sericite altered feldspar in the volcaniclastic rocks of South rhyolite (unit 2a)
Geochemistry sample #6048 (outcrop 00-GL-35), Cross nicols, (FOV)=2 mm
Bay Lumber road

as evidenced by a prominent penetrative foliation due to the alignment of sericite in the groundmass (Plate 4).

Only six samples were taken for petrographic observation (samples 6005, 6034, 6036, 6042, 6048 and 6055). Plate 5 shows a typical thin section photomicrograph of the South rhyolite rocks. The quartz phenocrysts have been partially resorbed. The feldspar phenocrysts are variably altered to sericite, broken and sometimes clustered together. Twinning is sometimes seen in plagioclase (albite) phenocrysts when it is less altered to sericite. Rare quartz phenocrysts show "undulatory extinction", evidence of deformation. Poorly-developed perlitic fractures are found within a volcanic breccia outcrop exposed on the Bay Lumber road (00-GL-35). Sericite and quartz veinlets are common. A few samples contain a minor percentage of chlorite and/or calcite amygdules. Traces of pyrite and iron oxides were locally noted.

It is difficult to deduce the nature of the South Rhyolite. It is dominated by a massive facies with subordinate volcaniclastic rocks for which there is no concrete evidence regarding the mode of deposition. It could represent an eroded dome that preserves some breccia fragments (unit 2a) and volcaniclastic material (unit 3)

2.1.3 Volcaniclastic rocks (3)

The rocks of this unit (grey on Figure 2.1) are clastic and mainly composed of felsic volcanic detritus. Two types of volcaniclastic rocks were identified;

Plate 6

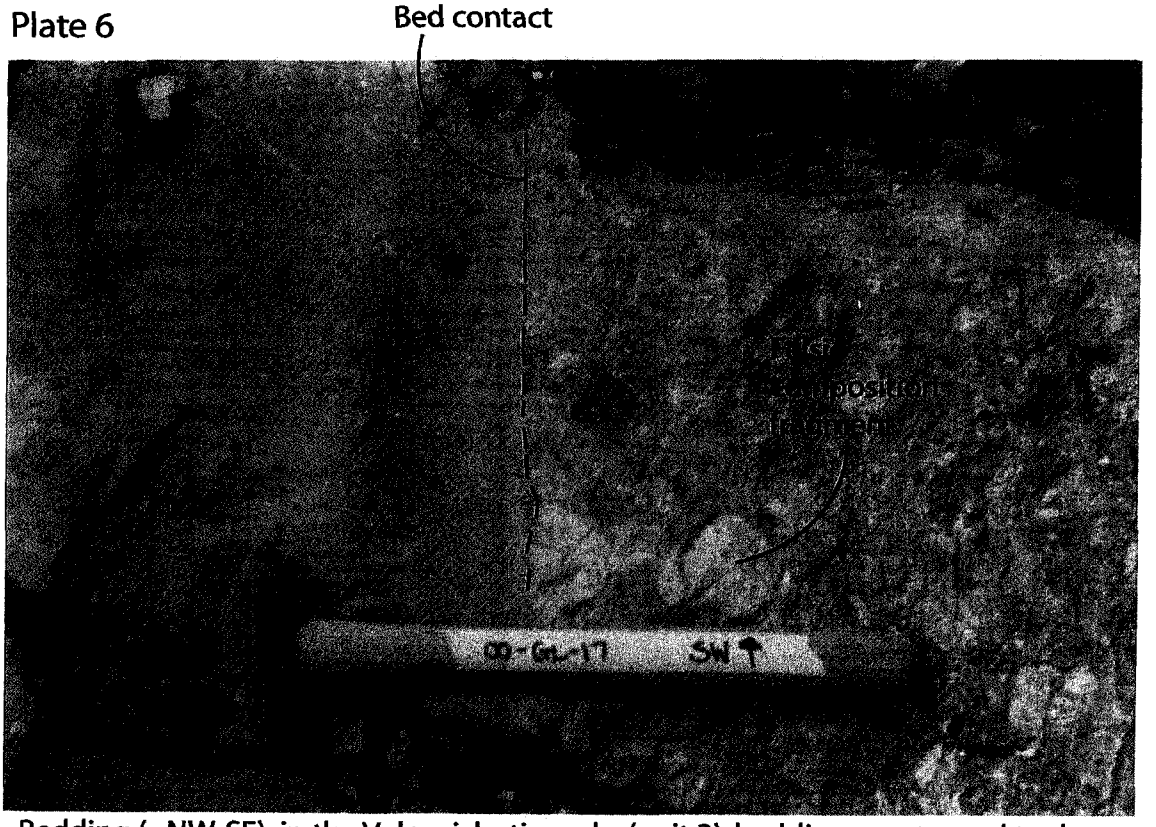

Bedding (~NW-SE) in the Volcaniclastic rocks (unit 3), bedding overturned to the west
Outcrop 00-GL-17, Hammer used for scale (~0.5 m)
Secondary road oriented roughly east-west, accessible from Bay Lumber road going west

volcanic conglomerate and sandstone. In the map area, these rocks were isolated in a small pocket of few hundred meters wide.

In the conglomerate (Plate 6) the clasts range in size from sand (0.02-2 mm) to cobble (64-256 mm) and are generally subangular to subrounded in shape.

Sedimentary structures such as flames in finer-grained beds and grading are preserved in some outcrops (00-GL-17). The flame structures and the grading give a top direction to the east, although the dip of the beds is to the west meaning the beds of the volcaniclastic rock on this outcrop are overturned. Generally, although there are mafic clasts present, most clasts are light coloured and likely felsic in composition. The matrix seems to have the same composition as the clasts and usually the conglomerate is sub-clast supported. The volcaniclastic rocks seem to be an epiclastic deposit resulting from weathering of underlying felsic metavolcanic rocks of the South rhyolite unit. However, locally (south of the mapped area) the clasts in the conglomeratic rocks are elongated and deformed and their composition is more mafic (outcrops 00-GL-18 and 00-GL-19). Chlorite and quartz veins also locally cross-cut this unit. No sample of the conglomerates was taken for microscopic observations.

In the field, the typical volcaniclastic sandstone (outcrop 00-GL-16), is located west of the volcanic conglomerate describe above. Primary bedding is preserved, but is strongly suspected to be deformed because of its sudden change of direction on the actual outcrop. This sandstone is mainly composed

of quartz fragments but also reacts to HCl acid indicating the presence of carbonate cement. The fresh and weathered surface colours alternate between light to dark grey depending of the grain size of the clasts present in the bed. Usually finer grain size beds are darker grey coloured. Under the microscope, the majority of the sub-angular quartz grains show "undulatory extinction" indicating strain. The calcite crystals are aligned sub-parallel to the bedding. The matrix supporting the quartz clasts is only composed of calcite. The calcite matrix is more abundant in the lighter colored beds. Within a specific bed, the crystals of quartz and calcite are equigranular. In the darker-coloured beds, presence of graphite is strongly suspected but, it's impossible to clearly identify due to the ultra-fine grain size. The proportion between the coarser- and finer-grained beds is about 40:60.

2.1.4 Felsic metavolcanic rocks: Red Dome rhyolite (4)

In the new Highway 560 road cut, immediately west of the bridge over the West Montreal river, the Red Dome rhyolite (light yellow on Figure 2.1) consists of series of massive, 5 to 10 meters thick horizons with columnar jointed tops (Lebel, 2000). Columnar joints were observed locally in this unit (Plate 7). This unit also contains some horizons of breccia likely an autoclastic breccia facies, typical of a rhyolitic dome. The radiometric age of this unit is 2726.5 ±1.1 Ma (Johns and Amelin, 1999). New SHRIMP (Sensitive High-Resolution Ion Microprobe) results on additional zircons from this sample indicated the presence of a wide range of less precise ages from 2750.9 ± 16.4 Ma to as young as 2673.2 ± 8.9 Ma (Ayer *et al.*, 2005). Theses younger zircons suggests the rhyolite unit may in fact be a somewhat younger sill-like

Plate 7

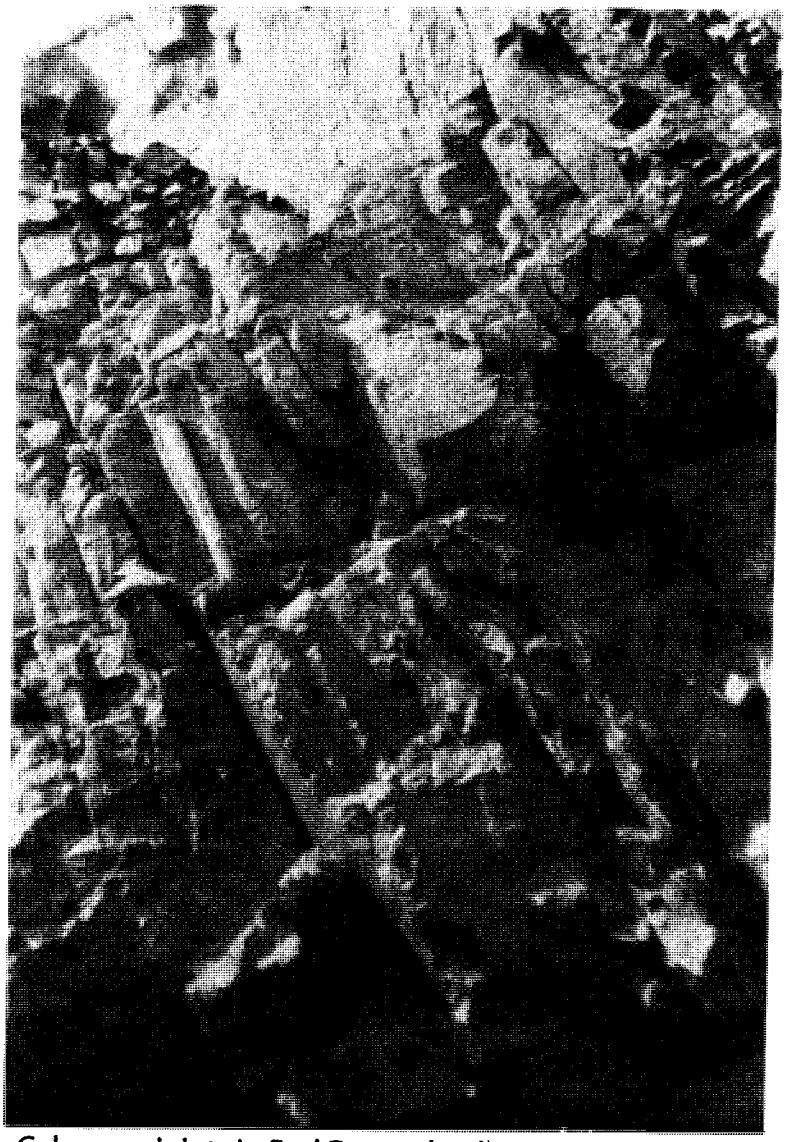

note:
hematite
alteration

Columnar joints in Red Dome rhyolite (unit 4)
Geochemistry sample #6020 (Outcrop 00-GL-27),
Hammer used for scale (~0.5 m)
Highway 560, close to Brunet Copper occurence

intrusion intruding the Deloro assemblage, with the older ages representing inheritance from host volcanics. Rare brecciated dikes containing polymictic clasts and minor chalcopyrite in the matrix were interpreted as diatreme breccia by Glen W. Johns (personal communication, OGS Geoscientist). The rock is composed of millimetric sized, rounded, phenocrysts of quartz and alkali feldspar within a fine-grained quartzo-feldspathic groundmass. Feldspar phenocrysts (often potassic feldspar) are less than a millimetre in size and are generally altered to sericite. This unit also contains copper mineralization (e.g. Brunet copper occurrence) as a chalcopyrite-pyrite-malachite assemblage hosted in quartz±calcite veins. A grab sample taken by KRL returned an assay of 17% copper. Close to the Brunet copper occurrence, the rock has a pronounced red colour due to strong pervasive hematite alteration. Usually the rock is light greenish yellow due to pervasive sericitization. Zones of intense chlorite alteration were also observed on the fresh road cuts on Highway 560. Locally veinlets of quartz, chlorite, sericite and hematite, millimetric range wide, can be observed.

A total of 15 thin sections were produced for microscopic observations (samples GL-26 to GL-32, 00-GL-34, 27C, 6013, 6018, 6019, 6020, 6021 and 6043). Plate 8 shows a typical thin section photomicrograph. The rocks included in this unit are composed of a mixture of plagioclase almost completely altered to sericite and quartz in a proportion of 60:40, on average. In the samples observed, only a few contain plagioclase phenocrysts, in such case they are also completely altered to sericite. Rarely twinning was

Plate 8

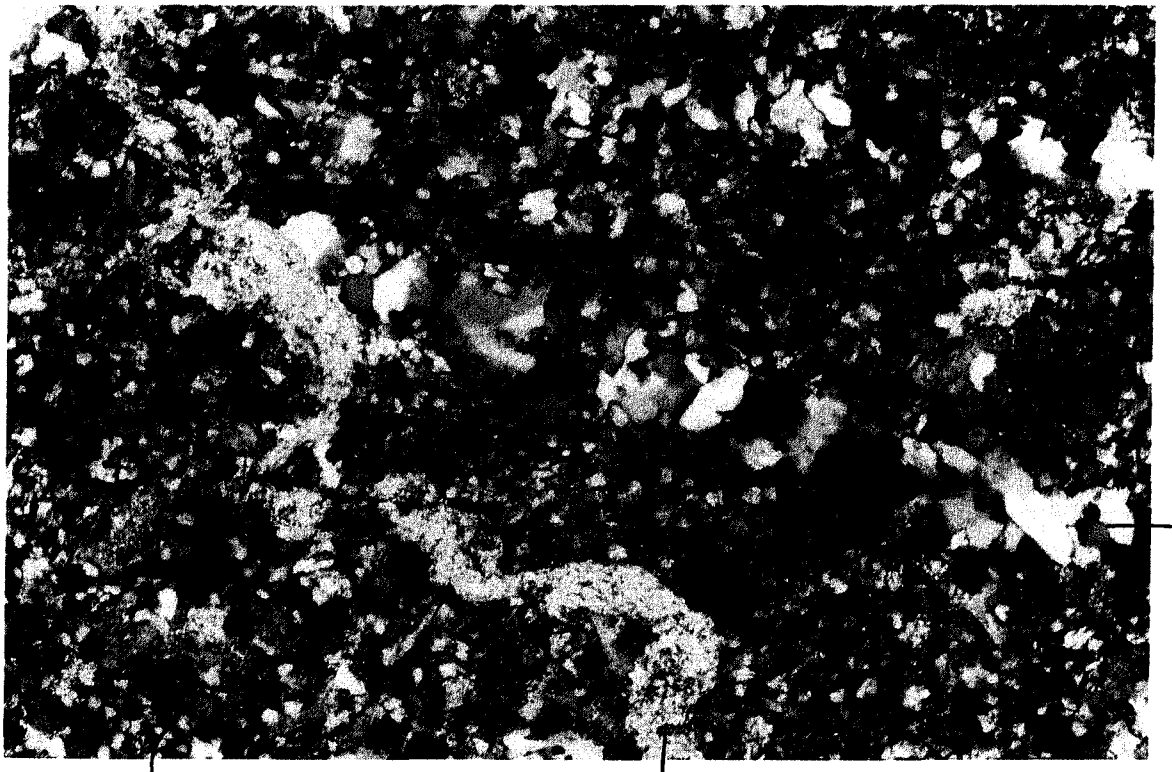

Sericite veinlet cutting a quartz +/- feldspar veinlet in Red Dome rhyolite (unit 4)
Geochemistry sample #6021 (Outcrop 00-GL-27), Cross nicols, (FOV)= 2 mm
Highway 560, close to Brunet Copper occurence

preserved. Calcite is common and always associated with sericite either in the groundmass or in the veins. Traces of epidote are also common. Sericite and quartz veins are present in all samples and rarely quartz+plagioclase veins were observed. Chlorite is often present in some of the thin sections but occurs mainly as blebs and rarely as veins. In some of the samples, the veins are cross-cutting each other and give locally a stockwork texture. Relative timing between the veining events will be discussed later in the paragenesis section of this chapter. Iron oxides, mainly specularite with minor magnetite, were often observed in this unit, either in quartz±carbonate veins or disseminated in the groundmass. In some of the samples, rusty brownish coloured quartz is noted. Traces of pyrite and chalcopyrite were also observed, more often in the samples containing a lot of quartz+carbonate veins.

2.1.5 Sulphide-rich chemical metasedimentary rocks (5)

The Sulphide-rich chemical metasedimentary rocks (black on Figure 2.1) have a lenticular shape in outcrop and are typically about 40 to 60 meters wide, and in places can be traced for up to 1200 meters. These horizons are stratifigraphically situated to the top of Deloro assemblage (Ayer *et al.*, 1998). The chemical sedimentary rocks comprise of thinly-laminated (only seen in drill core), brick red and variable shades of grey colored chert. However, the unit has, most in most places in the field, a brecciated appearance. Locally, rusty-orange-colored weathered surfaces are visible. One outcrop (00-GL-28) has primary bedding striking roughly at 245°. The metasedimentary rocks (about 30 cm thick) are confined between mafic metavolcanic rocks. The chemical

metasedimentary rocks, typically contain decimeter-thick zones having abundant sub-millimetre size pyrite, and locally millimetric grain sized of specularite. On specific outcrops, quartz±carbonates veining, without a specific orientation, is observed. No sample of this unit was taken for microscopic observation.

2.1.6 MATACHEWAN DIKE SWARM (6)

The Matachewan dikes (brown colour on Figure 2.1) cross-cut all the other lithological units of the Deloro assemblage. In the area, these dikes are usually a few hundred meters wide and can be traced for kilometres. This unit is massive and is not as altered as the Archean units of the Deloro assemblage, likely due to its Proterozoic age. Most of the outcrops observed of this unit, were dark-green coloured on fresh surfaces and have a characteristic "elephant skin" -like weathered surface. Commonly the outcrops have a blocky fracture pattern. It is a fine-grained gabbro (often called diabase by the geologists working in the Abitibi Greenstone belt) and in the field area, contains up to 20% epidotized plagioclase phenocrysts, commonly up to 1-2 cm in size (Plate 9). Millimetric epidote±carbonate and chlorite veins are common, having no preferential orientation. The most distinctive characteristics of the unit are its magnetic signature, its altered plagioclase phenocrysts and its north to north-westerly (~330-340°) trend.

Three thin sections were taken for further description (samples 00-GL-70, 00-GL-43 and 6030). Plate 10 shows a typical thin section photomicrograph of the unit. It mainly has a fine-grained (≤1 mm) equigranular groundmass containing

Plate 9

Albite phenocrysts in Matachewan dike (unit 6)
Contact zone beetween unit 6 (Matachewan swarm) and unit 1 (Mafic to intermediate metavolcanic rocks)
Outcrop 00-GL-235, Hammer used for scale (~0.5 m)
Secondary road oriented roughly east-west, accessible from Bay Lumber road going west

Plate 10

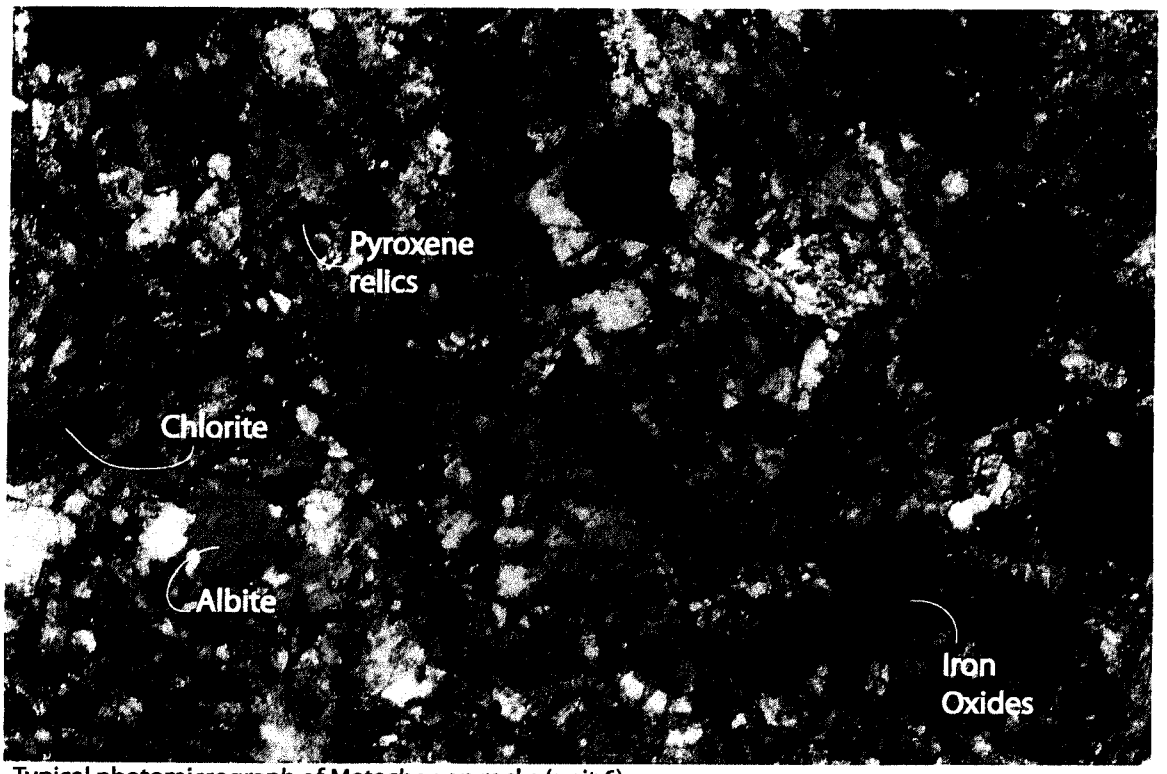

Typical photomicrograph of Matachewan rocks (unit 6)
Geochemistry sample #6030 (Outcrop 00-GL-99), Cross nicols, (FOV)= 2 mm
Ligne 80W, Station 14+05N on KRL grid

30 to 60% relics of amphibole crystals (presumably after clinopyroxene) altered to chlorite. Relics of tabular crystals with twinning barely recognizable are altered to sericite±epidote (presumably after plagioclase). The rocks also contains roughly 10% of opaque iron oxides consisting of fractured subhedral dark-grey-coloured crystals (under reflected light) which were identified as magnetite. The rest of the rock is a mixture of chlorite blebs and veins, sometimes associated with very sparse epidote and quartz. The minor amount of quartz present in the groundmass is generally rusty-brownish coloured likely due to traces of iron. Calcite crystals were rarely observed in these samples and were commonly associated with well developed crystals of clear quartz generally observed in veins. The chlorite, the epidote, the calcite and the clear quartz are interpreted to have been formed late with respect to igneous crystallization.

2.1.7 Nipissing gabbro (7)

In the field this unit (blue on Figure 2.1) is very similar to the Matachewan dikes and is only seen in the east end of the map area. Because of its Proterozoic age, this unit can intrude all the rocks of the Deloro assemblage. Usually, this unit trends north-northeast but, on the map scale this is not visible. However in the area, it intrudes only the South rhyolite and the Mafic to intermediate metavolcanic rocks. The larger intrusion is located in the South rhyolite unit and is about one kilometre long by few hundred meters wide. The smaller one is located in the Mafic to intermediate metavolcanic rocks and is: ~250 square meters in size. It is also described as a massive equigranular gabbro, but usually this unit shows a coarser grain size and a less mafic

composition (about 60:40 ratio of felsic and mafic composition minerals) than the Matachewan (about 80:20) dikes. Usually the fresh surface shows a mixture of dark green and cream colours, the weathered surface colour is generally pretty similar to the fresh surface colour. The gabbro lacks the feldspar phenocrysts and prominent epidotization observed in the Matachewan diabase dikes. It can also be magnetic, but less commonly than the Matachewan dikes. This unit is also not very altered relatively to the units of the Deloro assemblage.

Only one sample was taken for petrographic observation (sample 6017). Plate 11 shows a typical thin section photomicrograph of the gabbro of this unit. The medium grained (~1 mm) gabbro contains about 40% of relics of pyroxene crystals altered to amphibole. The amphibole is usually moderately altered to chlorite. Another 25% of crystals are brown colored under normal transmitted light and are intensely altered likely from pyroxene. Plagioclase are not apparent having been altered mostly to sericite. About 10 to 12% chlorite blebs and veinlets were observed. Two kinds of chlorite are present in this sample; one showing a dark blue colour under polarized light and having a fibrous crystal habit always in association with the amphibole crystals. The other chlorite is present in only a few veinlets in the thin section, this one is grey coloured under polarized light and is not fibrous. Rare epidote is also noted (<1%). Only 10% of quartz is present in this rock and it is either occurring as euhedral crystals in groundmass or in veins. Sparse, and local, iron stained quartz is visible. Traces of euhedral crystals of Ti-rich magnetite, occasionally showing plaid pattern (like kilt patterns), are present in this sample.

2.2 STRUCTURAL GEOLOGY

In Fawcett and Macmurchy townships The Keewatin metavolcanic rocks strike to the north-northwest in the south changing to a westerly strike in the northern Macmurchy Township (Johns and Amelin, 1999). Except for minor top reversals, the sequence youngs to the northeast and north (Johns and Amelin, 1999). The Pacaud, Deloro and Kidd-Munro assemblages (Keewatin metavolcanic) are a homoclinal, overturned sequence with northeast-younging directions (Johns, 1999).

They are two main phases of deformation and associated metamorphism in the Shining Tree area (Oliver *et al.*, 1999a, 1999b). The rocks older than 2.7 Ga (Keewatin metavolcanic rocks, including Deloro assemblage) having undergone two periods of deformation (Oliver *et al.*, 1999).

In fact, the rocks in Big Four Lake area do not show much deformation textures. Only few structural measurements have been taken in the field.

Two poorly developed schistosity orientations, mainly given by the alignment of chloritized ferromagnesian minerals in the Mafic to intermediate metavolcanic rock unit and by the alignment of the sericite in the South rhyolite unit are oriented east-west or southwest-northeast (~070°). The schistosity is more obvious in the South rhyolite unit. It is impossible from the field and petrographic observations to give relative timing between the two orientations because only one deformation was seen at the time on the outcrops or thin sections were never both seen on the same

location. Crenulation textures were identified in the area by Oliver *et al.* (1999) and used to support the concept that two phases of deformation affected the rocks.

Few bedding planes were measured in the volcaniclastic rocks because they are generally not apparent. Their orientation, the trend northeast- southwest, is not concordant with the bedding of the Sulphide -rich chemical sedimentary rock unit oriented parallel to the stratigraphy, almost east-west. The orientation of this chemical metasedimentary rocks correlates with the general orientation of the stratigraphy, all units strike roughly east-west in the area mapped. Johns (1999a) also identified local overturned beds topping southeast in this unit (see explanations in section 2.1.3 of this chapter).

Only one bedding plane, oriented east-west, was measured in the chemical metasedimentary rocks because of the omnipresence of the brecciation on most of the observed outcrops in the field. This outcrop is located just off limit of the map, on the southwest end (outcrop 00-GL-28) and was not the typical rock of this unit (see section 2.1.5 of this chapter).

Only few pillows in the mafic to intermediate metavolcanic rock unit gave top determinations. Two folds were interpreted from the pillow tops and the setting of the lithogeological contacts of the units on the map. No other field evidence is supporting these interpretations. This interpretation is in part made on the assumption that the Mafic to intermediate metavolcanic rocks, located south and north of both of the rhyolite units are the same lithological unit. The trace of the axial plane of the synclinal fold in the Red Dome rhyolite trends east-west and appears to plunge to the

east. The trace of the axial plane of the anticlinal fold, in the South rhyolite, also strikes east-west. The two fold axial planes are probably slightly inclined to the south. In contrast to this interpretation Johns (1999a), based on Carter's map (1977) and geophysical data, put an N-S trending anticlinal fold through the Volcaniclastic unit (unit 3).

Two faults oriented southwest-northeast, interpreted from geophysical data by Johns (1999a), cross-cut the area mapped. The movement along these faults has been interpreted from distribution of lithological units of the maps. John's map area has been disrupted by northwest and northeast –trending faults (Johns and Amelin, 1999).

2.3 ALTERATION AND METAMORPHISM

All the rocks have undergone moderate to extensive degrees of carbonatization, sericitization and saussuritization (Johns and Amelin, 1999). Because the alteration in each unit was described in the lithological unit descriptions section in this chapter and because the emphasis in this thesis is on the economic potential of the Red Dome rhyolite, the focus will be put on the timing of the veining events in the paragenesis section.

It seems that the alteration caused by hydrothermal processes is isolated to the Red Dome rhyolite. All the units of Deloro assemblage are weakly metamorphosed. That means, the hydrothermal alteration is overprinting the metamorphic alteration in Red Dome rhyolite.

The Red Dome rhyolite is hydrothermally altered throughout and a number of alteration facies can be seen in rock exposures, especially along Highway 560 (Lebel, 2000). Pervasive hematite alteration characterizes most of the exposed rhyolite on new Highway 560 road cuts (Lebel, 2000), and is most intense along the edges of the Matachewan dikes. In addition, strong pervasive sericite/pyrite alteration in this rhyolite is present in drill hole CH99-02 (Lebel, 2000). Dark chlorite zones are superimposed on the pervasive stockwork sericite alteration, which turn is superimposed on the pervasive hematite alteration in the Brunet Copper mine and in the new Highway 560 road cuts (Lebel, 2000). The Red Dome rhyolite has also undergone extensive chloritization and silicification (Johns and Amelin, 1999).

The degree of preservation of both macro- and microscopic features and textures indicates that the rocks in the map area have undergone a low degree of metamorphism and selected areas have not been penetratively deformed (Johns and Amelin, 1999). The metamorphic facies throughout most of the Shining Tree area is mid to low greenschist facies (Oliver *et al.*, 1999a, 1999b). Amygdules are filled with chlorite, carbonates or quartz and there is extensive chlorite alteration of feldspars in mafic flows and intrusions (Oliver *et al.,* 1999). Locally, the levels of metamorphism and deformation are low enough to preserve delicate volcanic textures (Johns, 1996). Rare quartz crystals with strained extinction were observed in the Volcaniclastic rocks and in South rhyolite units. Oliver (1999a) also observed this characteristic in the area.

2.4 MINERALIZATION

Chalcopyrite –rich quartz-carbonate veins occurs in and proximal to the Red Dome rhyolite. They are interpreted as late and are mineralized with copper remobilized from the copper –rich Red Dome rhyolite possibly contemporaneous with diabase dike emplacement (Lebel, 2000) or intrusions emplaced regionally (i.e. Johns maps: 1999a, 2000 and 2003). These veins have generally similar strike orientation to the Matachewan swarm dikes. It is interesting to note that the chalcopyrite –rich veins are not only found in Red Dome rhyolite, uncommonly they can be seen in other units, at a smaller scale, mostly in the Mafic to intermediate metavolcanic units, and they always have a north-south trend.

Base-metal mineralization is found at the Brunet copper occurrence, in the Red Dome rhyolite within quartz-chalcopyrite-pyrite-malachite meter-scale veins (Hunter, 1998). The vein system is exposed on surface and typically is a few meters wide and 45 meters long. Centimetre-scale veins of specular hematite are found in altered rhyolite outcrops along Highway 560 near the showing. The Brunet Copper occurrence, where grab samples returned assays of 17% copper have been reported, was developed in one of these veins within the Red Dome rhyolite (Lebel, 2000).

The sulphide-rich, chemical metasedimentary horizons consist of intercalated altered basalt flows, massive syngenetic pyrite –rich bodies, as intersected in drill holes CH99-01 and CH99-02, clastic pyrite bodies, stockwork pyrite zones, chert –rich zones, heterolithic clastic beds possessing epiclasts of Red Dome rhyolite and

bedded graphitic argillite. The metasedimentary rocks contain up to Fe (9.2%), Ag (0.8 ppm), As (48 ppm), Co (59 ppm), Hg (40 ppb), Pb (20 ppm) and Zn (68 ppm) (Lebel, 2000).

Polished-thin-section observations of the occurrence shows that the mineralization is composed mainly of pyrite, and chalcopyrite which were identified in quartz±calcite veins. Minor magnetite and very rare hematite were also observed.

Numerous polished sections were taken from drill core samples of brecciated and often graphitic cherty massive to semi –massive horizons from within the mafic to intermediate metavolcanic rocks. In these sections chalcopyrite, pyrite and magnetite and hematite were also observed.

2.5 PARAGENESIS

The paragenesis of the mineralization is mainly interpreted from both macro- and microscopic observations of Red Dome rhyolite rocks located around the Brunet Copper occurence (Figure 2.3).

At the map scale, the felsic units (units 2 and 4) of Deloro assemblage are mostly altered to sericite and locally to chlorite. Close to the Brunet Copper occurrence alteration visible in outcrop is chiefly composed of an intense hematization and sericitation, with minor silification and chloritization. Alteration of the mafic to intermediate metavolcanic rocks (unit 1) of the Deloro assemblage is characterized by a pervasive chlorite-sericite-carbonate assemblage throughout the groundmass,

and chlorite-carbonate in amygdules. Chlorite-sericite-calcite alteration as well as epidote alteration is evident in the gabbros of the Nipissing and Matachewan dikes in Big Four Lake area.

At the detailed scale, sericite veinlets cut pre-existing early quartz veinlets (Plates 12 and 13). Chlorite appears to have been to develop after sericite (Plate 14). A second generation of quartz veinlets is associated with sufide mineralization wherein pyrite was formed before chalcopyrite and then later hematite and magnetite (Plates 15 to 18). Figure 2.3, summarizes the mineralization events in terms of a paragenetic sequence.

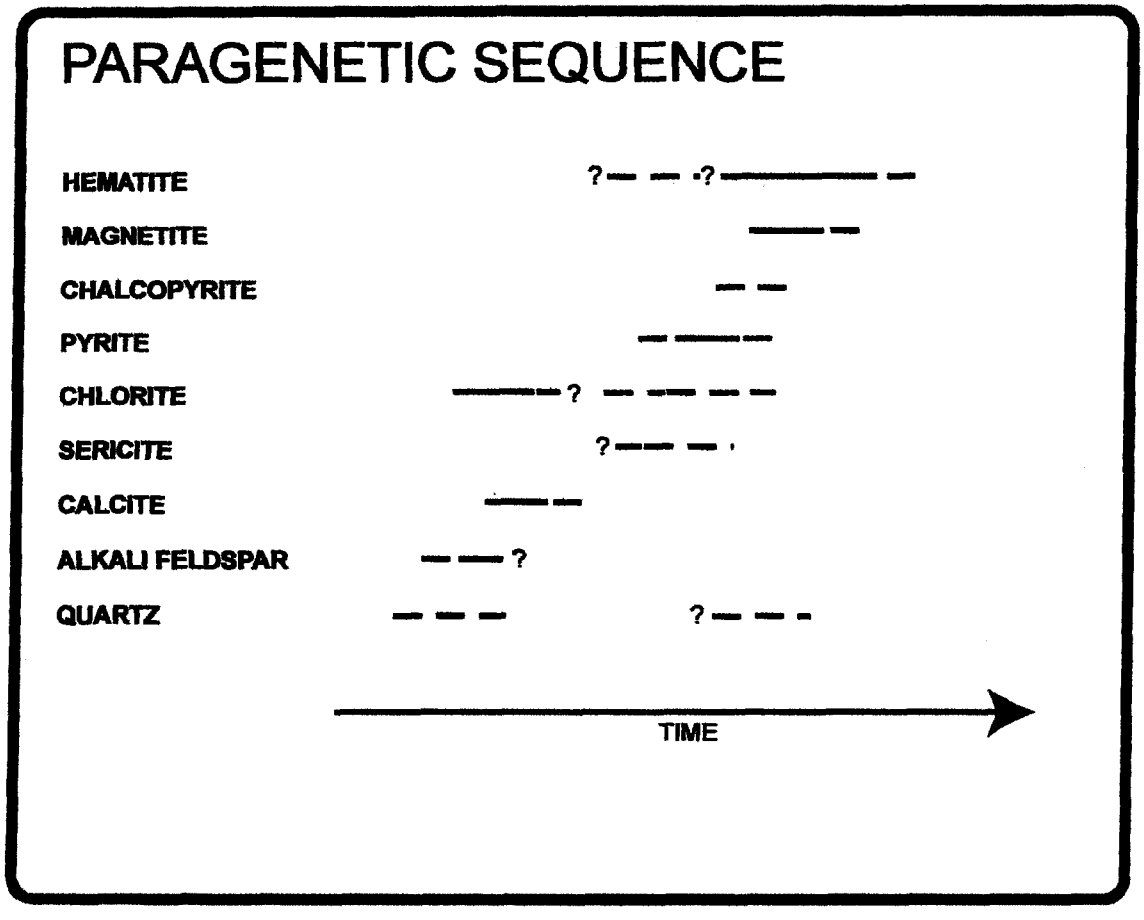

Figure 2.3: Paragenesis of the rocks of Deloro assemblage (focussing on Red Dome rhyolite)

Plate 12

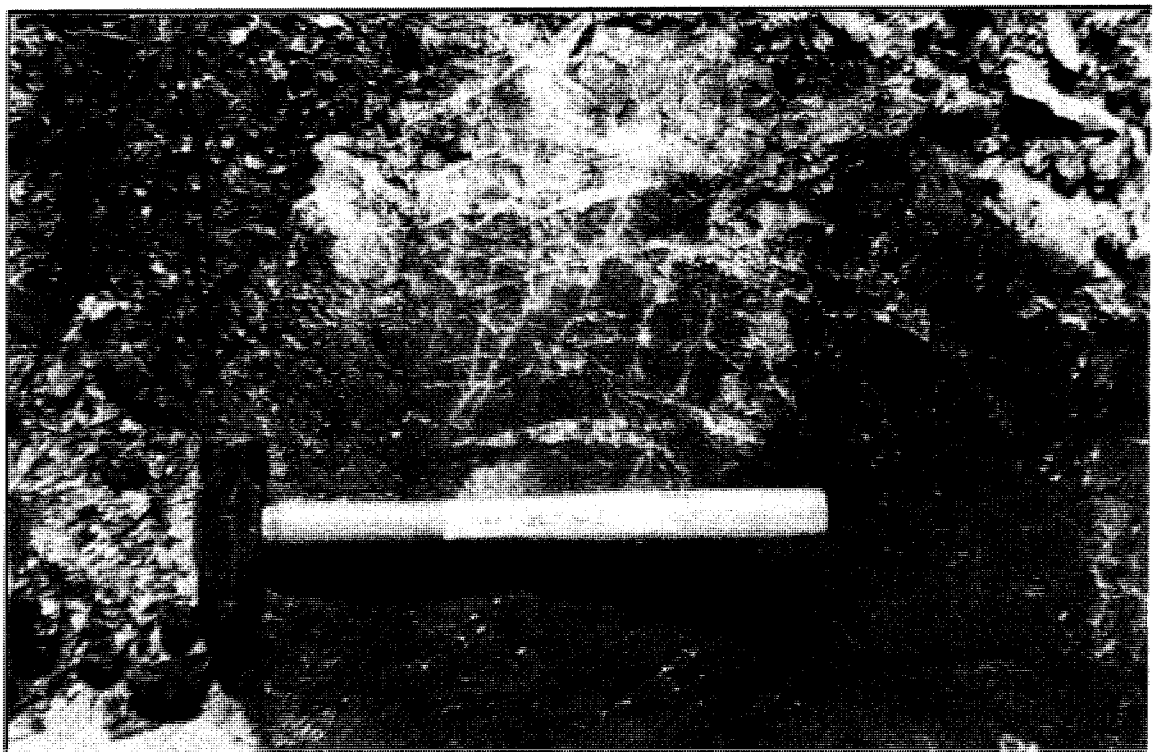

Quartz veinlets (white colored) cutting sericite veinlets (yellow colored) in hematized Red Dome rhyolite (unit 4)
Geochemistry sample #6021 (Outcrop 00-GL-27), Hammer used for scale (~0.5 m)
Highway 560, close to Brunet Copper occurence

Plate 13

Sericite (ser) veinlets cutting both Fe oxides and quartz (qtz) +/- feldspar (feld) veinlets in Red Dome rhyolite (unit 4)
Geochemistry sample #6018 (Outcrop 00-GL-38), Cross nicols, (FOV)= 2 mm
Highway 560, east of Grassy road intersection

Plate 14

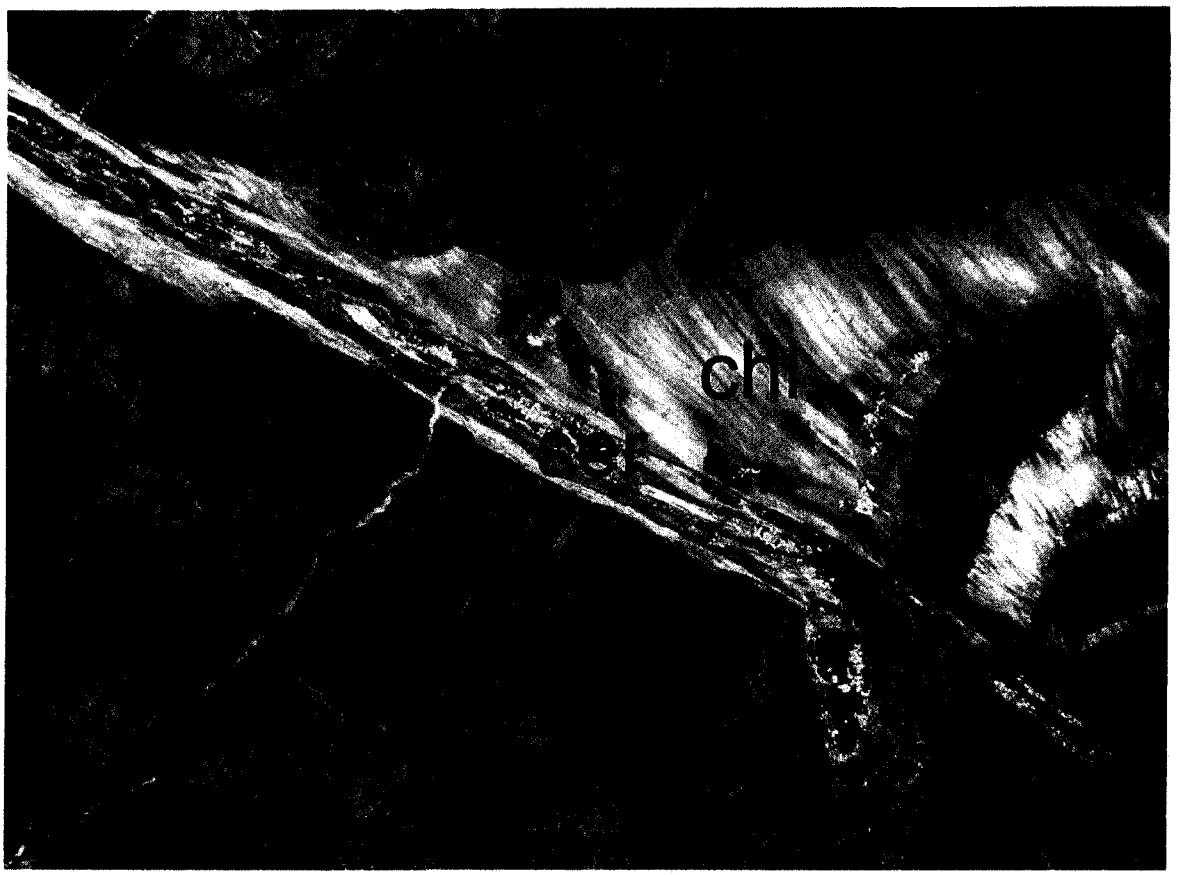

Chlorite (chl) veinlet with sericite (ser) centre in Red Dome rhyolite (unit 4)
Geochemistry sample #6056 (Outcrop 00-GL-27), Cross nicols, (FOV)= 2 mm
Highway 560, near Brunet Copper occurence

Plate 15: Pyrite (py) grains within chalcopyrite (cp) in chlorite altered Mafic to intermediate metavolcanic rocks (unit 1)
Reflective light, (FOV)= 2.5 mm
KRL drill hole CH99-01, depth: 352.00 - 352.50 m

Plate 16: Small grains of chalcopyrite (cp) in silicates between pyrite (py) grains in a semi-massive sulfide breccia horizon within unit 1
Reflective light, (FOV)= 2.5 mm
KRL drill hole CH00-07, depth: 295.62 - 295.70 m

Plate 15

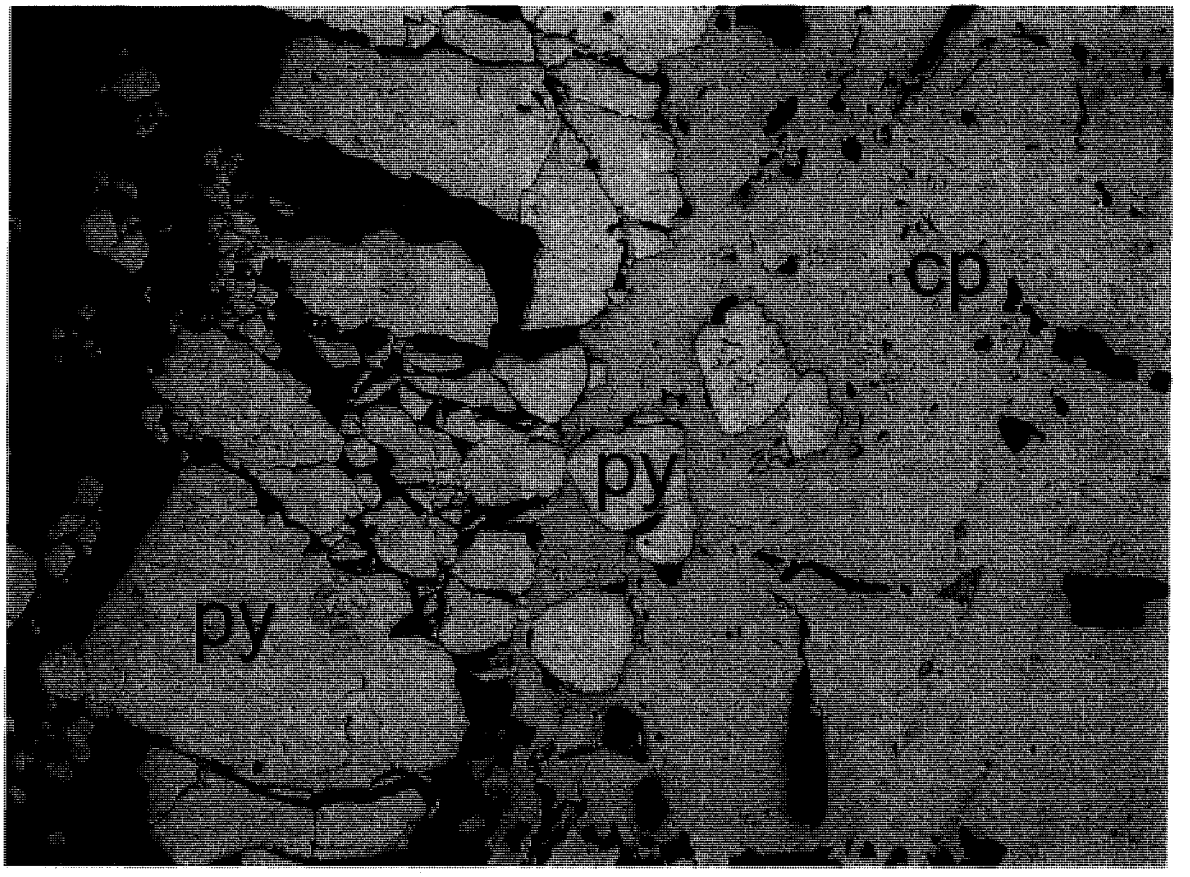

Plate 16

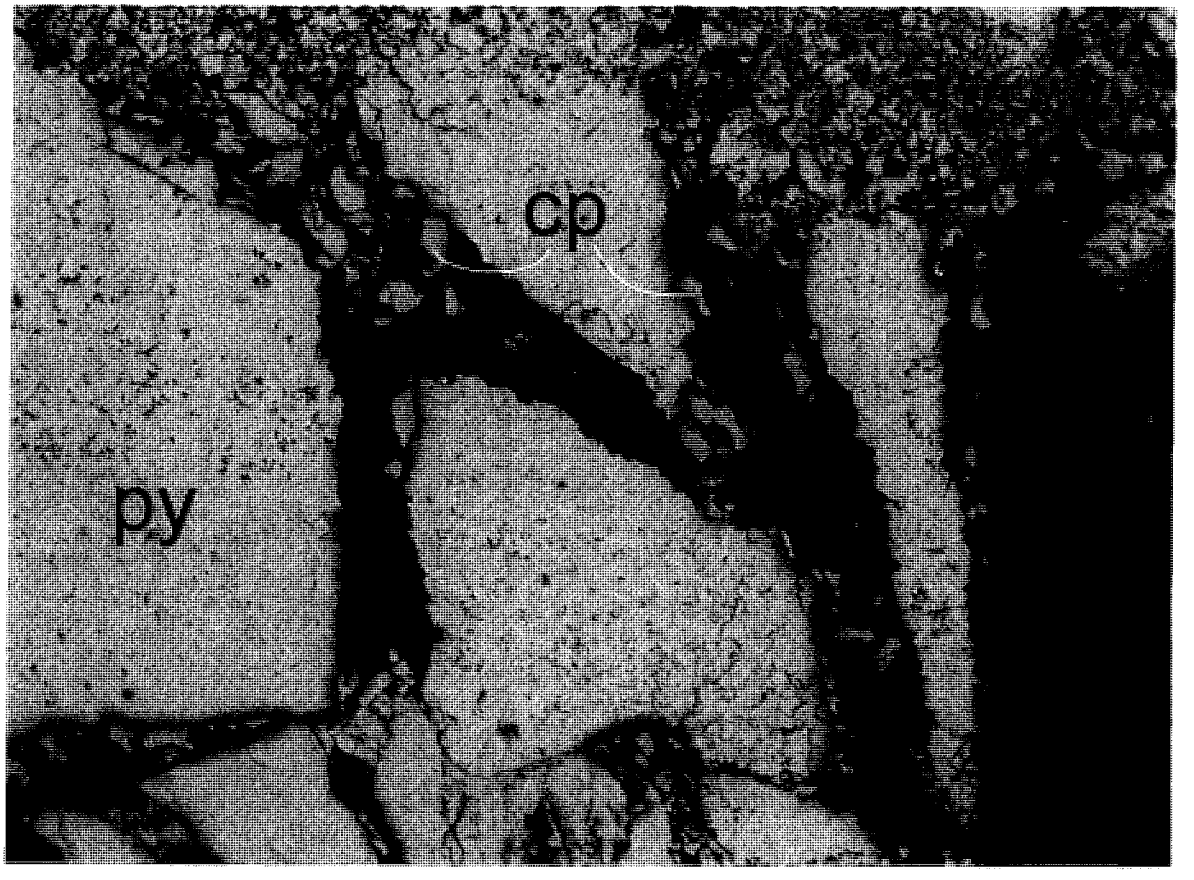

Plate 17: Hematite (hm) in microfractures of chalcopyrite (cp) at Brunet Copper occurrence
Reflective light, (FOV)= 2.5 mm

Plate 18: Hematite (hm) on the edge of magnetite (mg) in brecciated sulfide –rich chert horizon
Reflective light, (FOV)= 2.5 mm
KRL drill hole CH99-01, depth: 388.50 – 388.55 m

Plate 17

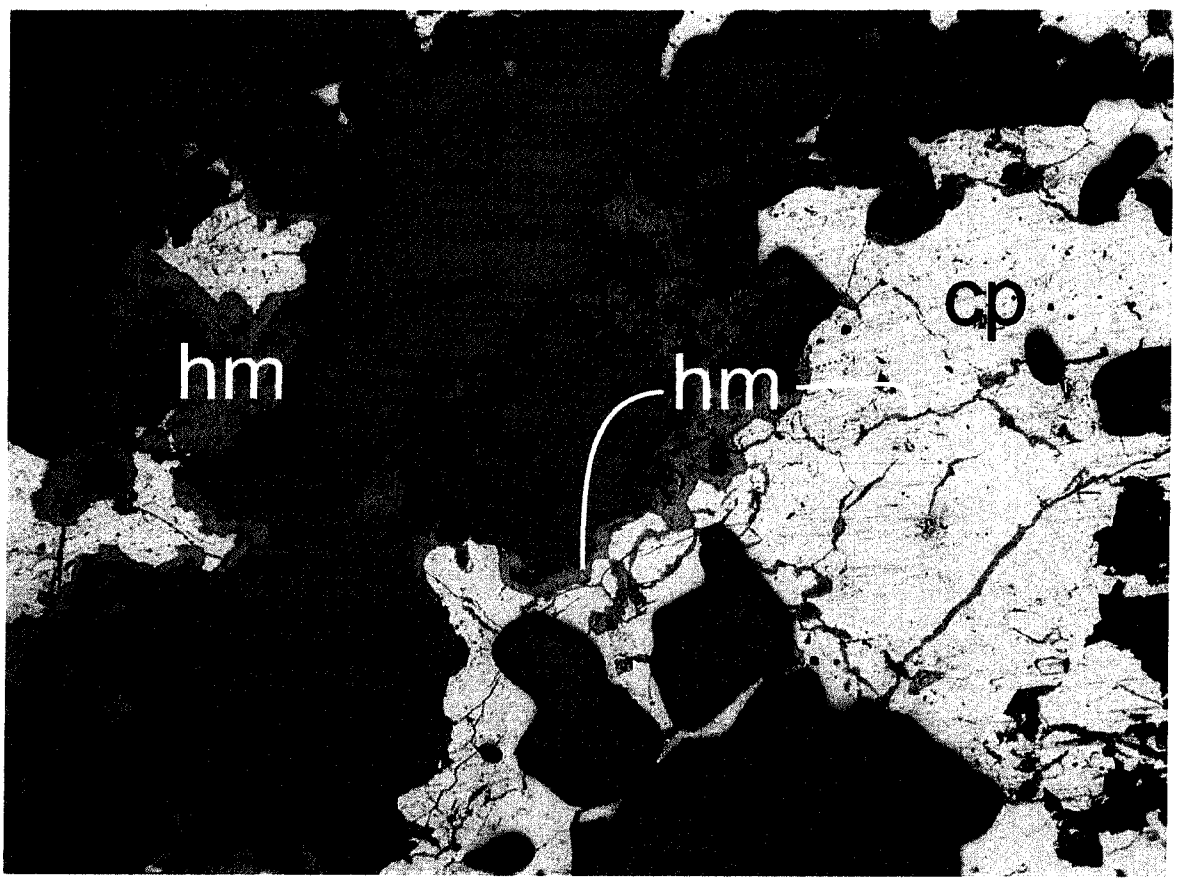

Plate 18

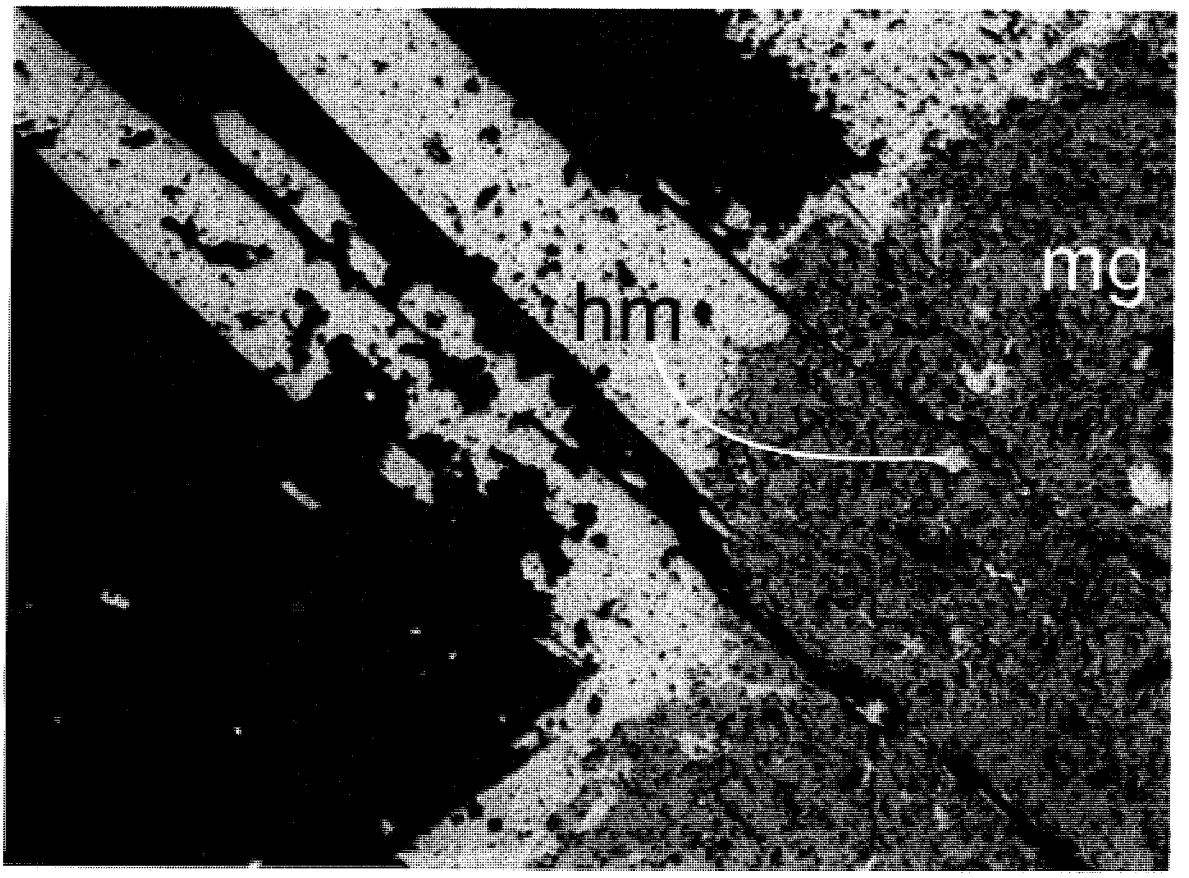

CHAPTER THREE: GEOCHEMISTRY OF BIG FOUR LAKE AREA

The purpose of this chapter is to characterize the rocks in terms of their tectonic affiliation, assemblage and rock type principally using trace element data. In addition, given that the Red Dome rhyolite of the area has potential for VMS mineralization, analyses were done using the methods of Lesher *et al.* (1986), Piché and Jébrak (2004) and Large *et al.* (2001) in order to ascertain its geochemical affinities from an economic perspective.

3.1 REE PLOTS

Rare earth elements (REE) plots are commonly used as empirical evidence to discriminate the tectonic regime under which igneous rocks formed (Rollinson 1993). Geochemical patterns in themselves cannot solve tectonic problems; however the use of geochemical trends can be used to make correlations with modern day rock suites of known tectonic settings. When studying Archean volcanic rocks, it is important to keep in mind that modern tectonic models may not be applicable, and that REE patterns cannot simply be correlated to modern environments. However, REE abundance patterns can be very useful for studying potential tectonic affinities, and for modelling processes that control rock composition such as differentiation.

To be able to make interpretations from REE diagrams it is important to verify that the REE abundances of rocks in this study have not been modified by hydrothermal fluid alteration processes. REE are relatively immobile except under high chlorine concentration conditions (Michard, 1989). The REE abundance patterns for samples from Big Four Lake area display REE profiles which are consistant for different samples from the same unit and therefore they do not appear to have been affected by intense alteration. Since the concentration of REE in hydrothermal fluids is 5 X 10^2 to 10^6 less than the surrounding rock, a very high water/rock ratio is required to modify the REE signature of the host rocks (Michard, 1989). If the rocks had taken on a hydrothermal fluid signature, the REE profile would be light rare earth element (LREE) -enriched and display a positive Eu anomaly.

Oceanic island basalt (OIB) has LREE-enriched profiles, whereas tholeiitic mid-oceanic ridge basalts (MORB) have flat lying REE profiles (Figure 3.1, Sun and McDonough, 1989). Samples from the Mafic to intermediate metavolcanic unit, of Big Four Lake area, have REE patterns that are similar to the MORB field (Figure 3.2).

Several distinct populations of the samples of the Big Four Lake area can be observed on Figure 3.2. The mafic to intermediate metavolcanic rocks of the Deloro assemblage are characterized by generally flat REE patterns and total REE abundances ranging from about 7 to 70 times chondrites. The felsic

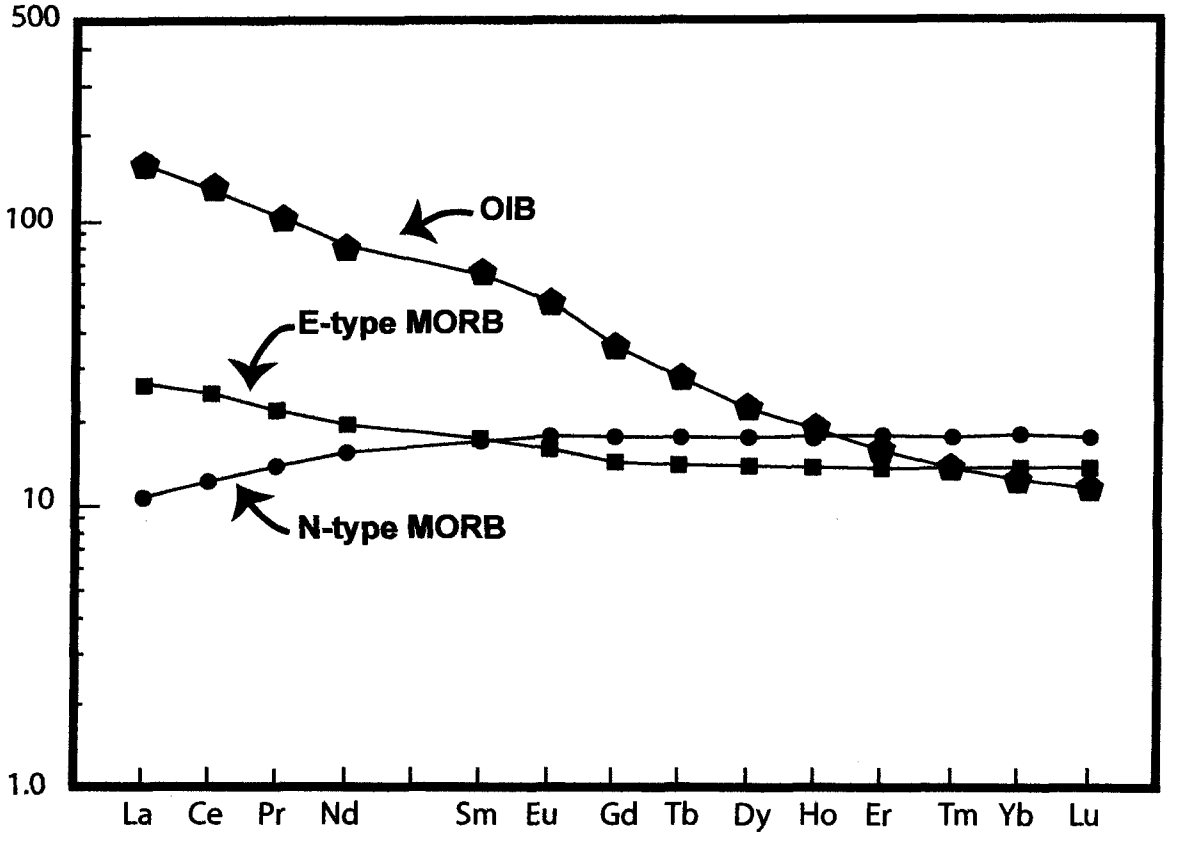

Figure 3.1: Chondrite-normalized REE abundance patterns for average modern MORB and OIB (modified *from* Sun and McDonough, 1989)

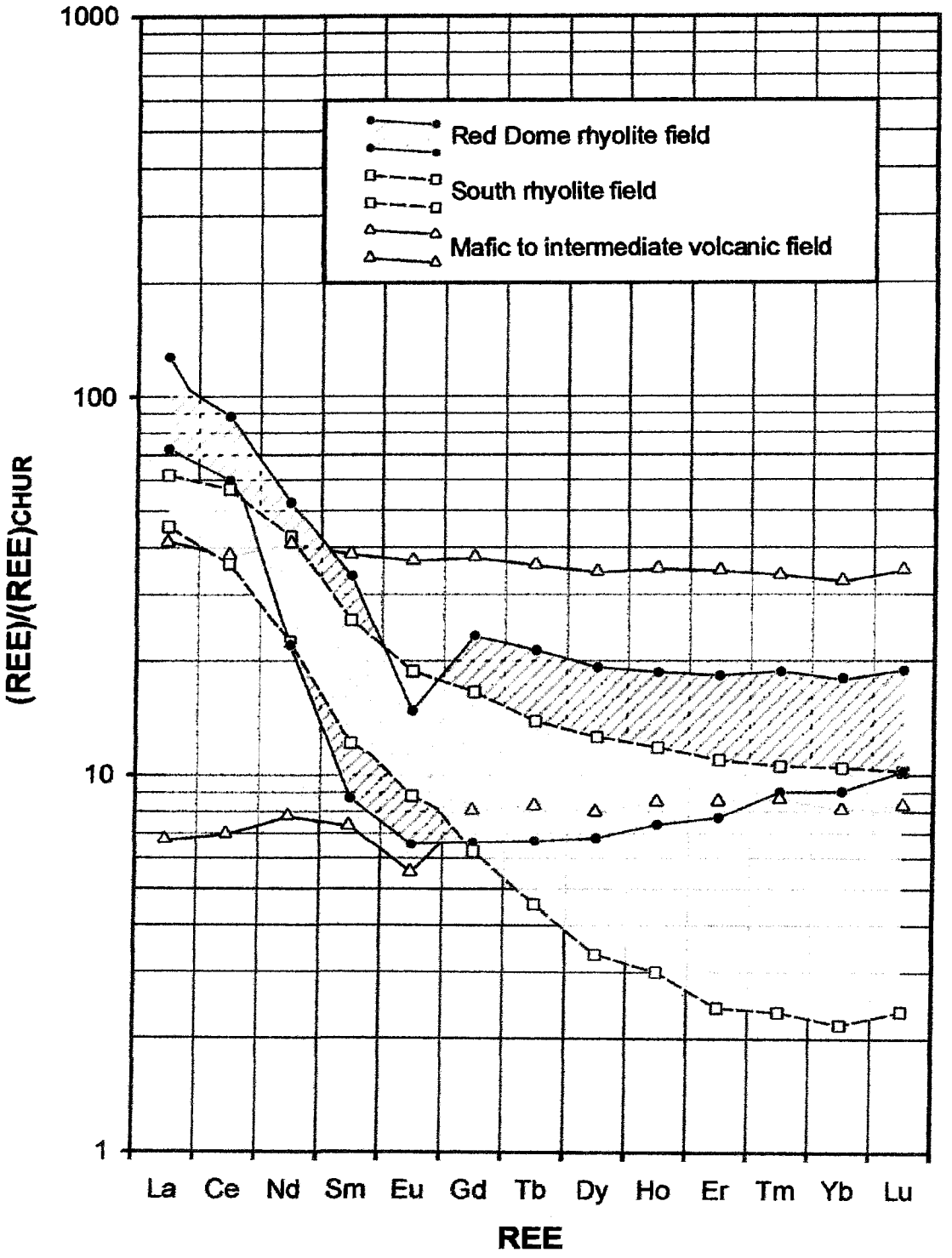

Figure 3.2: REE patterns of the Deloro assemblage rocks. Chondrite abundances used for normalization *from* Sun and McDonough (1989).
Triangles, mafic to intermediate metavolcanic rocks (unit 1);
squares, South rhyolite (unit 2); and circles, Red Dome rhyolite (unit 4)

metavolcanic rocks of the Deloro assemblage commonly have light rare earth elements (LREE) enrichment resulting in steeper REE patterns, that is, $(La/Lu)_{cn} \approx$ 10 for the Red Dome rhyolite, and $(La/Lu)_{cn} \approx 25$ for the South rhyolite.

3.2 JENSEN CLASSIFICATION (1976)

Irvine and Baragar's (1971) chemical classification consists of a ternary diagram (AFM) where the apices are represented by wt% $A=Na_2O+K_2O$, $F=FeO+0.8998Fe_2O_3$ and $M=MgO$. Jensen (1976) modified the diagram to compensate for the mobility of the alkali elements (Na_2O and K_2O) by using Al_2O_3 which is relatively immobile.

The Jensen cation plot is used to classify subalkalic volcanic rocks. It is a ternary plot relating the cation percentages of Al_2O_3, $FeO+Fe_2O_3+TiO_2$ and MgO (Figure 3.3). Jensen selected these apices for his ternary plot because of their relative stability within respect to low-grade alteration of volcanic rocks; and because these cations vary inversely during differentiation. Compared with K, Na (AFM diagram) the element Al is much less susceptible to chemical migration (Jensen, 1976). However, leaching or enriching a rock with small amounts of K_2O, Na_2O, CaO, and SiO_2 does not greatly affect the ratio which is derived from the relative amounts of Al_2O_3, $FeO+Fe_2O_3+TiO_2$ and MgO (Jensen, 1976). Grunsky *et al.* (1992) warns that the Jensen diagram was created to document the composition

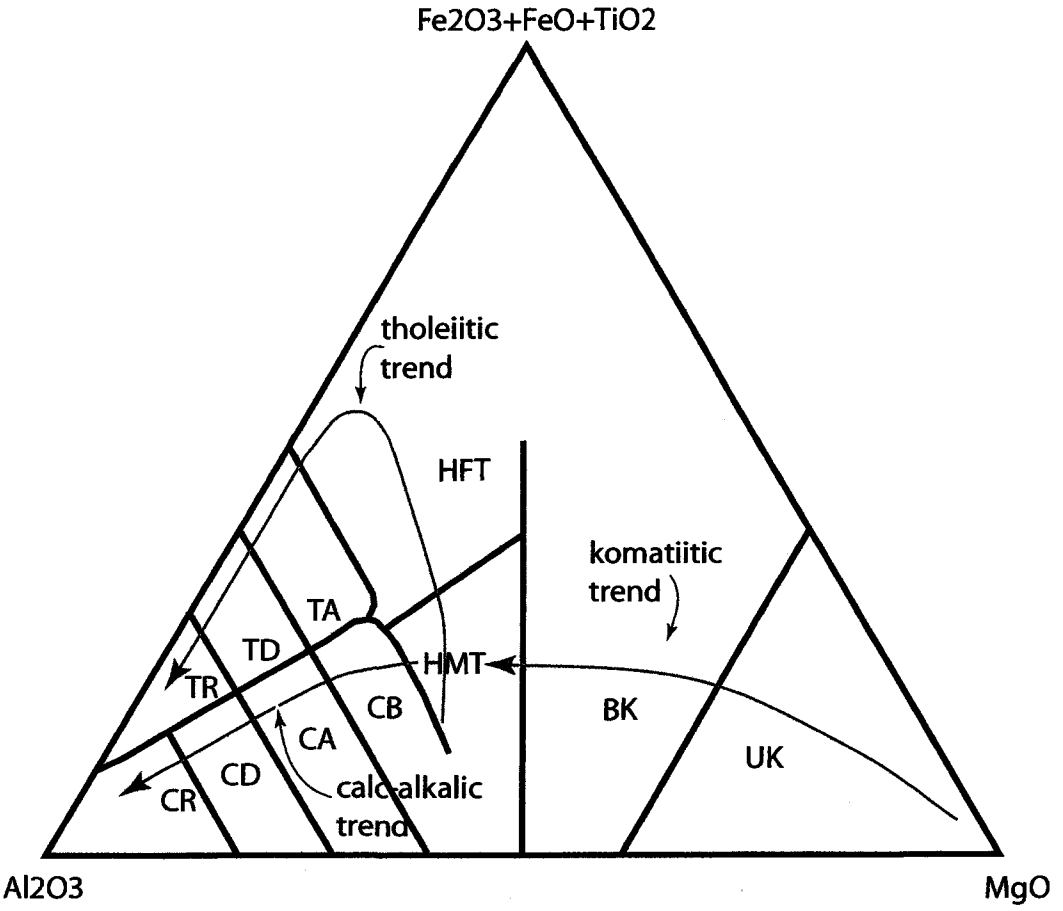

Figure 3.3: Jensen plot showing field descriptors and the Fe-enrichment trend for tholeiitic rocks (modified *from* Jensen, 1976). Green lines represent enrichment trends for tholeiitic, calc-alkalic and komatiitic rocks. UK, ultramafic komatiite; BK, basaltic komatiite; HMT, high Mg-tholeiite; HFT, high Fe-tholeiite; TA, tholeiitic andesite; TD, tholeiitic dacite; TR, tholeiitic rhyolite; CB, calc-alkalic basalt; CA, calc-alkalic andesite; CD, calc-alkalic dacite; CR, calc-alkalic rhyolite.

of rocks from Superior Province Archean greenstone belts and may not be relevant to subalkalic volcanic rocks outside of this environment.

Samples of the South rhyolite are in the field of calc-alkalic rhyolites (Figure 3.4). On figure 3.4, Red Dome rhyolite samples are also in the field of calc-alkalic rhyolites, except for one sample plotting in the field of High Fe-tholeiitic basalt, this sample is the one with pumice fragments in a very highly chloritized altered matrix located on Bay Lumber road (sample 00-GL-35). The Mafic to intermediate metavolcanic rock samples appear to conform to an evolutionary trend from high Fe-tholeiitic basalt to tholeitic dacites (Figure 3.4). However the REE data of these rocks span only a narrow compositional range (~10-30* chondrites) and there is no field evidence of the rocks having dacite composition. For instance quartz phenocrysts, brecciation flow banding were not observed, moreover the rocks are generally pillowed or massive flows typical of basalts in the area. This and the dispersion of the data across the tholeiite calc-alkaline boundary are interpreted as evidence of element mobility. Saumur (2005) has recently shown dispersion in the data of tholeiitic rocks on the Jensen diagram due to Fe mobility.

3.3 MESCHEDE BASALT CLASSIFICATION (1986)

As shown above the mafic to intermediate volcanic rocks of Deloro assemblage have MORB affinities (Figure 3.5). There is more than one type of MORB or

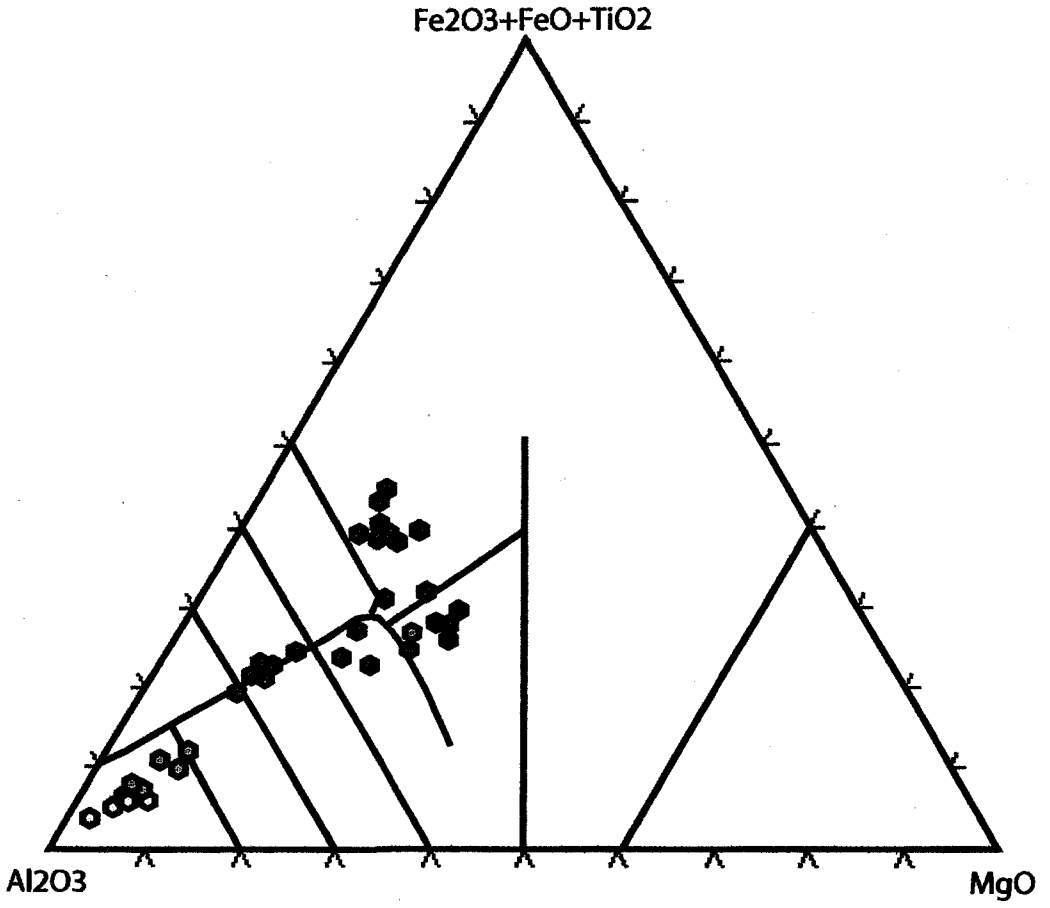

Figure 3.4: Jensen plot of the Deloro assemblage rocks. Green, Mafic to intermediate metavolcanic rocks (unit 1); dark yellow, South rhyolite (unit 2); light yellow, Red Dome rhyolite (unit 4).

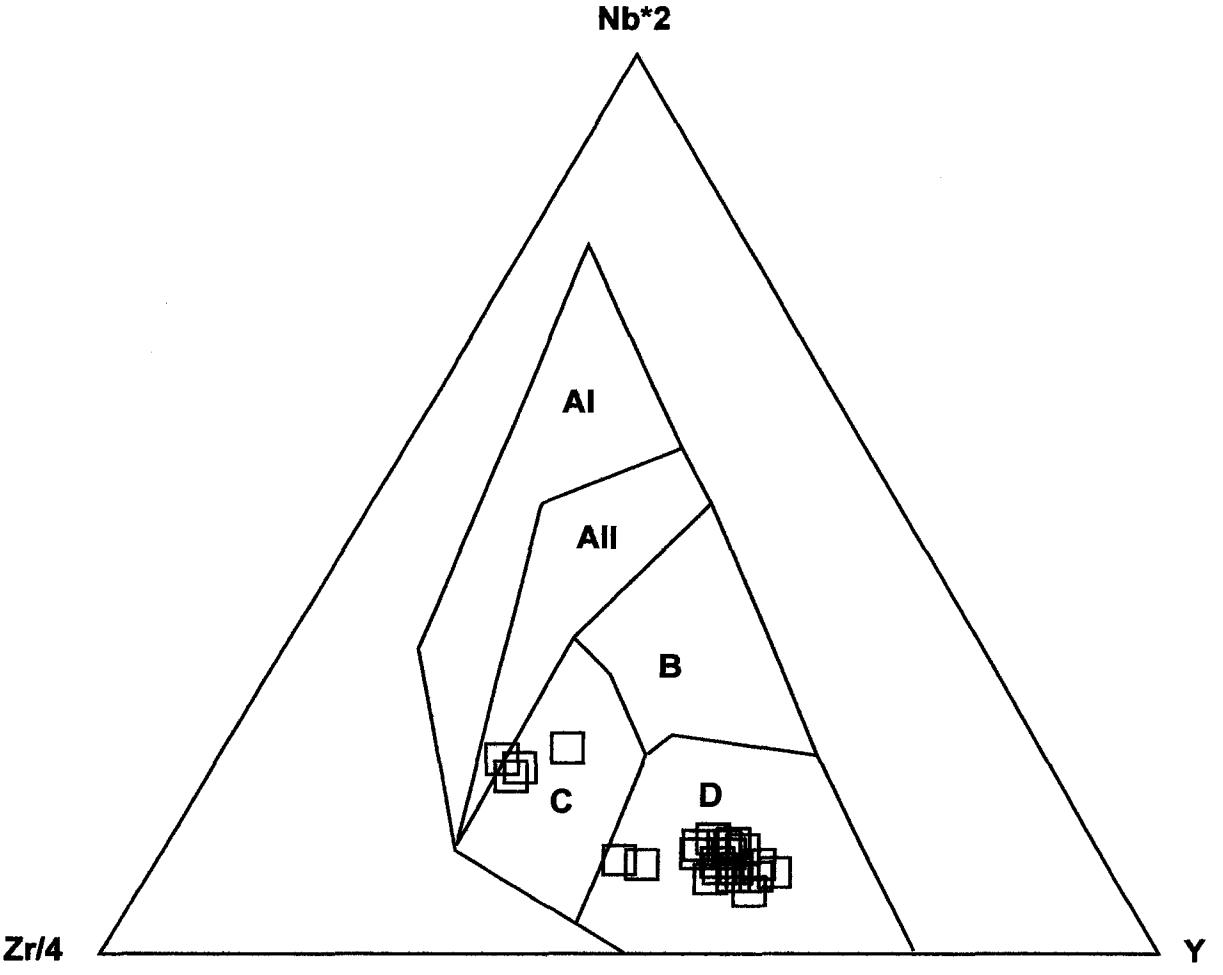

Figure 3.5: Zr-Nb-Y discrimination diagram for the Mafic to intermediate meta-volcanic rocks (unit 1) from the Deloro assemblage. The fields are defined as: AI, within-plate alkali basalts; AII, within-plate alkali basalts and within-plate tholeiites; B, E-type MORB; C, within-plate tholeiites and volcanic-arc basalts; D, N-type MORB and volcanic-arc basalts (modified *from* Meschede, 1986).

"ocean-floor basalt" (Pearce and Cann, 1973). Consequently, Meschede (1986) demonstrated that the immobile element Nb can be used to separate ocean-floor basalt, among other basalts, into two types of MORB: 1) N-Type MORB, basalt from a "normal" mid-ocean ridge environment which is depleted in incompatible trace elements, and 2) E-type MORB (also known as P-MORB), ocean-floor basalt from plume-influenced regions which are generally enriched in incompatible trace elements (Rollinson, 1993). On a triangular plot of Zr/4, 2XNb and Y, Meschede (1986) showed that four main basalt field can be identified; within-plate alkali basalts (AI), within-plate alkali basalts and within-plate alkali tholeiites (AII), E-type MORB (B), within-plate tholeiites and volcanic-arc basalts (C) and N-type MORB and volcanic-arc basalts (D) (Figure 3.5). Meschede's (1986) diagram is particularly useful to identify volcanic-arc basalts and it can be applied to intermediate and silicic lavas as well as to basalts (Rollinson, 1993).

Most of the samples from the mafic to intermediate volcanic rocks of the Deloro assemblages are falling in the D-field and four samples (samples 6020, 6026, 6034 and 6052) are included or limit to the C-field (Figure 3.5). This is consistent with the Ayer's tectonic setting interpretation of the Deloro assemblage i.e. within-plate tholeiites, MORB and volcanic-arc basalts.

3.4 LESHER RHYOLITE *ET AL.* CLASSIFICATION SCHEME (1986)

Lesher *et al.* (1986) study of massive sulfide ore-associated and barren felsic metavolcanic rocks allowed them to classify Archean felsic metavolcanic rocks into three majors groups based on the trace-element geochemistry; FI, FII and FIII (FIIIa and FIIIb) (Ropchan, 2000). Most massive base-metal sulfide deposits in the Superior Province are underlain by subvolcanic magma chambers, which have been interpreted to have supplied heat to drive the ore-forming hydrothermal systems (Lesher *et al.*, 1986). FIII and FII felsic metavolcanic rocks are interpreted to have been derived from high-level magma chambers, accounting for their distinctive geochemical signatures and their association with massive base-metal sulfide mineralization (Lesher *et al.*, 1986). In contrast, FI felsic metavolcanic rocks are interpreted to have been derived from a deeper source and are considered to have escaped significant high-level modification, accounting to their distinctive geochemical signatures and the lack of associated base-metal sulfide mineralization (Lesher *et al.*, 1986).

Hart *et al.* (2004) had another category to Lesher's rhyolite classification: FIV also commonly hosting VMS deposits. FIV are high-silica rhyolites and interpreted to have been derived from low-pressure to moderate degree of partial melting of depleted tholeiitic basalt.

In terms of the rhyolite trace element geochemical classification (Lesher *et al.*, 1986) the Red Dome rhyolite and South rhyolite best conform to the type FI group with some FII characteristics (Figures 3.6 and 3.7). In general, the REE spectra are steep, have moderate negative to very slight positive Eu anomalies. Zr/Y ratios are between ≈2 and 22, and have low abundances of HFS elements (e.g. Y ≈5 to 34ppm, Zr ≈73 to 207ppm and Hf ≈3 to 7ppm). The Sr abundances range from ≈15 to 243ppm (Appendix C). In general, none of these rhyolite types host economic base-metal sulfide deposits (Lesher *et al.*, 1986).

3.5 Piché and Jébrak NORMAT calculations (2004)

NORMAT is a method used to quantify the hydrothermal alteration in greenschist facies rocks using normative mineral ratios. This method does not require petrographic observations; it is independent of the rock type and does not need precursor mineral determinations (Piché and Jébrack, 2004). Five indices are used to quantify the global depletion of alkali elements as well as the formation of the following specific alteration minerals: 1) IPARA for paragonite, 2) ISER for sericite, 3) ICHLO for chlorite, 4) IPYRO for pyrophyllite and 5) IFRAIS for no alteration. If IFRAIS=100, the rock is unaltered as well if ICHLO= 100, the rock is totally chloritized. Therefore the sum IPARA+ISER+ICHLO+IPYRO+IFRAIS =100. IPAF is a sub-product of the NORMAT calculations and characterizes the carbonatization of the rocks.

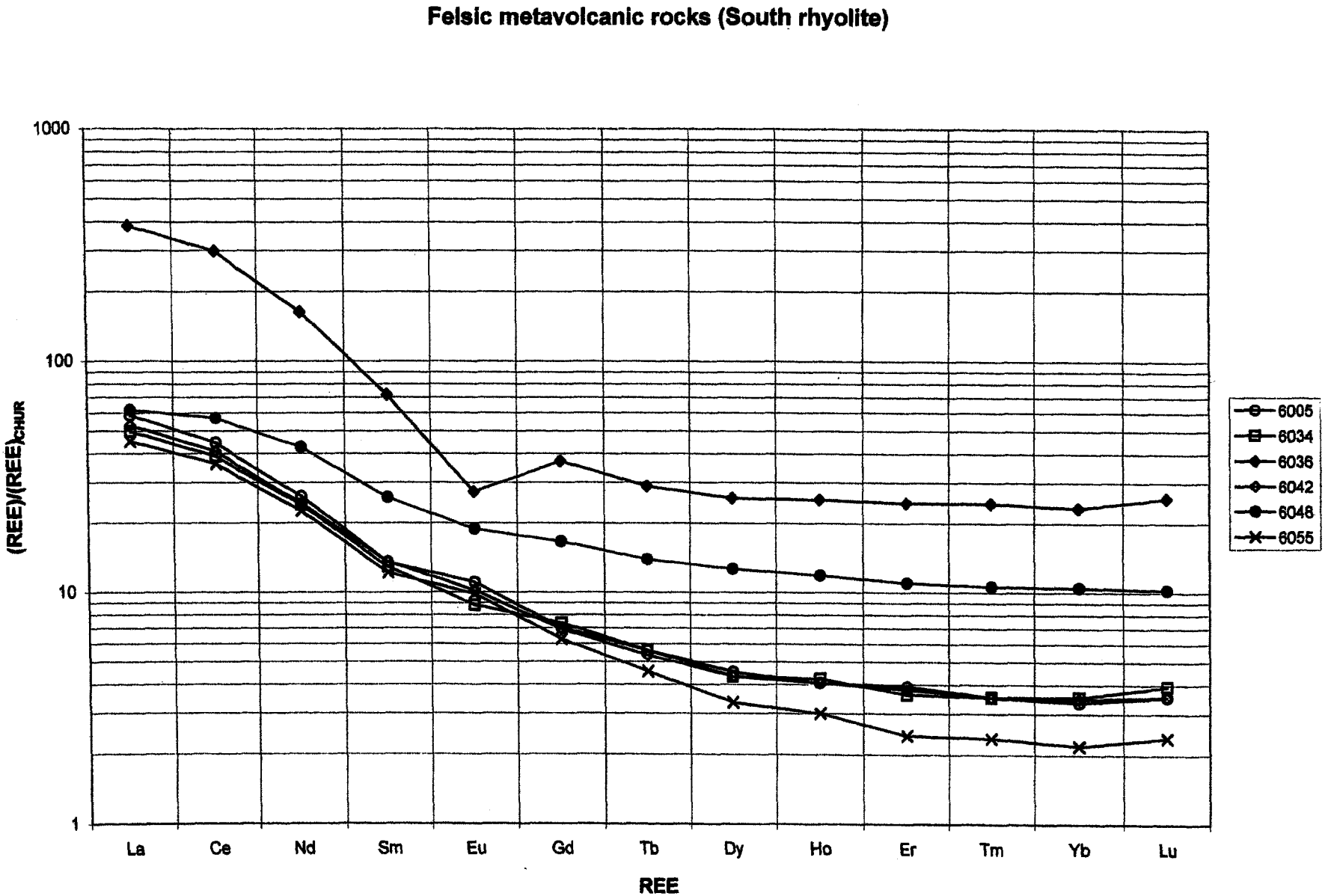

Figure 3.6: Chondrite-normalized REE abundance patterns for South rhyolite (unit 2). Chondrite abundances used for normalization *from* Sun and McDonough (1989).

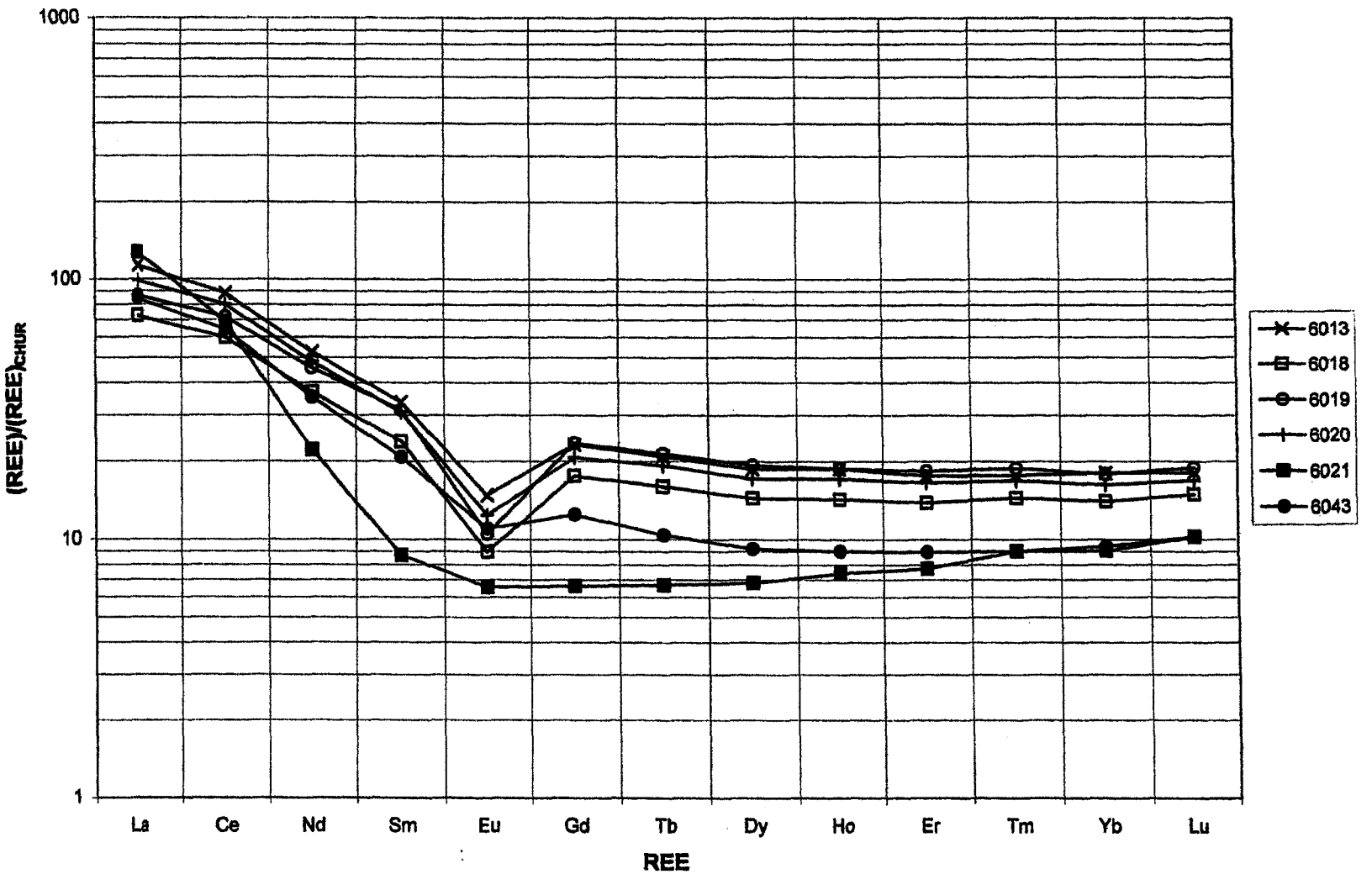

Figure 3.7: Chondrite-normalized REE abundances patterns for Red Dome rhyolite (unit 4). Chondrite abundances used for normalization *from* Sun and McDonough (1989).

IFRAIS= 100 X { (Ab+Or+An+Cpx) /

{ (HChl+HSer+HPar+HPyr) + (Ab+Or+An+Cpx) }}

ICHLO= 100 X {{HChl / { (HChl+HSer+HPar+HPyr) + (Ab+Or+An+Cpx)}}

Ab represents albite; Or represents orthoclase; An represents anorthite; Cpx represents clinopyroxene; HChl represents hydrothermal chlorite; HSer represents hydrothermal sericite; HPar represents hydrothermal paragonite; and HPyr represents hydrothermal pyrophyllite.

Note: The ICHLO formula is the same for each of the alteration minerals indices; only a substitution of the mineral analyzed is needed. The chlorite was used only as an example.

IPAF= 100 X {LOI-LOIMIN) / (LOIMAX-LOIMIN)}

LOI-LOIMIN represents how much of the real LOI value is above LOIMIN.

LOIMAX-LOIMIN represents the range of the sample's normative LOI values between fresh and altered states.

The calculations of NORMAT is based on the following five petrological rules: 1) increasing silica saturation calculations, 2) divergent and reversed Bowen series

calculations, 3) greenschist facies mineral assemblages, 4) calculations for VMS type hydrothermal alterations and 5) virtual CO_2 estimate and normative carbonate minerals (Piché and Jébrak, 2004). NORMAT calculations are based on similar petrological rules used with CIPW norm calculations, except that NORMAT is adapted for hydrous minerals and carbonates.

This method is limited; some rock types can not be used with NORMAT such as pelitic shales and rocks containing spinel, graphite or sulfide minerals.

Because the calculations are relatively complicated and the software is proprietary, a number of 17 samples were analyzed by the company Aur Resources Inc. (Appendix D). The results of samples from the Big Four Lake area, close to the Copper Hill showing and taken by Martin Lapointe of Aur Resources Inc. are presented on figure 3.8. Some samples were rejected: for instance samples R12969, R12975, R12976, B61209 and B61216 contain sulfide minerals and samples B61211 and B61215 are graphitic chemical sediments (chert) also containing sulfide minerals. Four samples (R12970, R12972, R12973 & R12974) were taken from Red Dome rhyolite outcrops. Samples R12970 and R12974 have high "fresh" indices (IFRAIS=93.32 and 94.56) and two others (R12972 & R12973) have a lower, but still significative, IFRAIS (IFRAIS=58.07 and 68.34). Although there are signs of sericitization for those samples (ISER=38.90 and 17.89). The carbonatization of these four Red Dome rhyolite

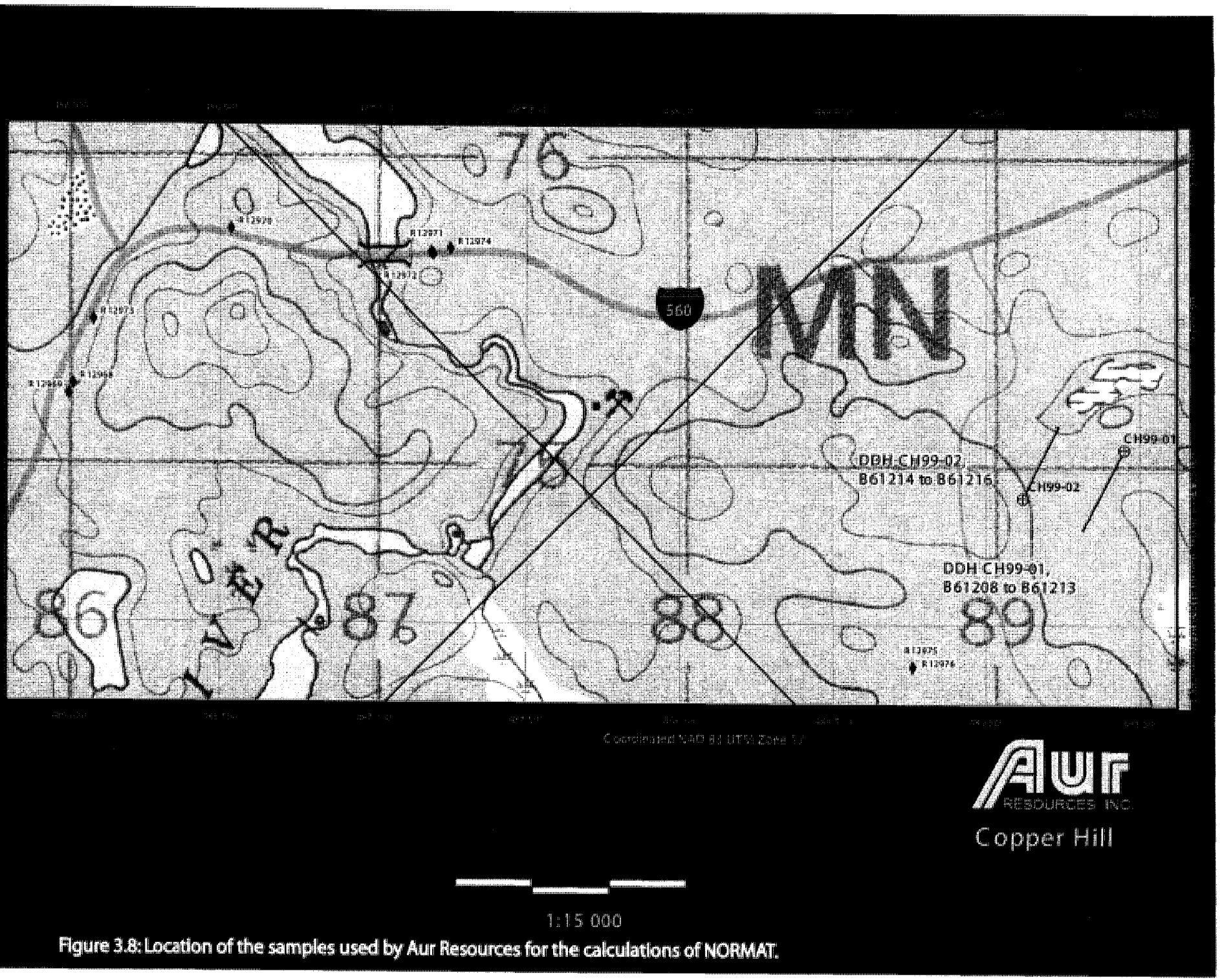

Figure 3.8: Location of the samples used by Aur Resources for the calculations of NORMAT.

samples is also significant (IPAF average 70.38). One core sample (B61214) of South rhyolite was collected and has similar results; IFRAIS=80.97 and IPAF=81.67. Five samples (4 from diamond drill core and 1 from outcrop) from the mafic to intermediate volcanic rocks were collected (R12968, B61208, B61210, B61212 & B61213). All four samples (B61208, B61210, B61212 & B61213) from the drill hole have IFRAIS=100, the carbonatization is pretty low except for sample B61208 which has IPAF=85.13. Outcrop sample (R13968) is relatively fresh with an IFRAIS=95.65 with moderate carbonatization (IPAF=41.16).

Interpretation of the rocks using the NORMAT formulation is difficult because textural and petrologic observations are not included. For instance, in the thesis area the importance of timing is critical; the volcanic rocks were first altered by seawater, then altered due to burial and regional metamorphism and finally variably affected by hydrothermal alteration. "Fresh" rocks do not exist in the area. The samples from Red Dome rhyolite unit appear to be altered hydrothermally and also due to regional metamorphism. The degree of alteration is variable and includes several different types of alteration; hematitization, sericitization, chloritization, carbonatization and also minor silicification. The alteration minerals such as chlorite, minor albite and sericite and sulfide minerals commonly occur as accessory minerals in quartz+carbonates veins and also as veinlets cutting the pervasively hematized and/or sericitized rhyolite. Veinlets of

chlorite or sericite are also quite common in this unit in both pervasive alteration types.

However the results obtained with NORMAT suggest the rock samples from Red Dome rhyolite are relatively fresh with IFRAIS varying from 58.07 to 94.56, ICHLO is nil, ISER varies from 2.6 to 38.90 and IPAF varies from 32.86 to 92.24. Even considering that the NORMAT calculation is designed for greenschist facies rocks the Red Dome rhyolite is not a "fresh" unit because it has late veins cross-cutting it. The NORMAT calculations could be a useful tool in mineral exploration but, as shown here is no substitute for petrographic observations. Presumably it would be useful in the interpretation of a large data base of closely spaced samples over a VMS deposit.

3.6 GRANT ISOCON DIAGRAM (1986)

Grant (1986) developed isocon diagrams to plot appropriately scaled oxide abundances of an unaltered sample against its altered equivalent. Elements considered immobile define a straight line through the origin, called the isocon, with a slope approximately equal to one. Elements having an increase in abundance will plot above the isocon. The elements having a decrease in abundance will plot below.

An attempt was made to evaluate the mobility of elements in the various alteration zones of the Red dome rhyolite unit. Accordingly four samples were taken from two different outcrops representing the hematite, sericite ± epidote alterations and plotted on an isocon diagram (Grant, 1986) and the results are shown in figure 3.9.

For this study, comparison of two samples, with different levels of alteration, taken from the same outcrop were used. Samples 6020 and 6021 from outcrop 00-GL-27 and samples 6018 and 6019 from outcrop 00-GL-38. The samples 6018 and 6021 are hematized (altered samples), sample 6019 is epidotized and sericitized and sample is 6020 is sericitized (unaltered samples).

The immobile elements (e.g. Al, Y, Zr and Ti) do not adequately define a straight line (normally slope = 1 depending on dilution) in these plots, hence the monitoring of mobile elements is not possible. The fact that a straight line was not developed may stem from the fact that the sample localities were widely spaced (max. ~100 meters) or that the rock chemistry of the pre-alteration samples was different.

3.7 MINERAL CHEMISTRY

In order to better characterize the rocks electron microprobe (EMP) analyses were performed on minerals. As shown in chapter 2 the minerals represent an

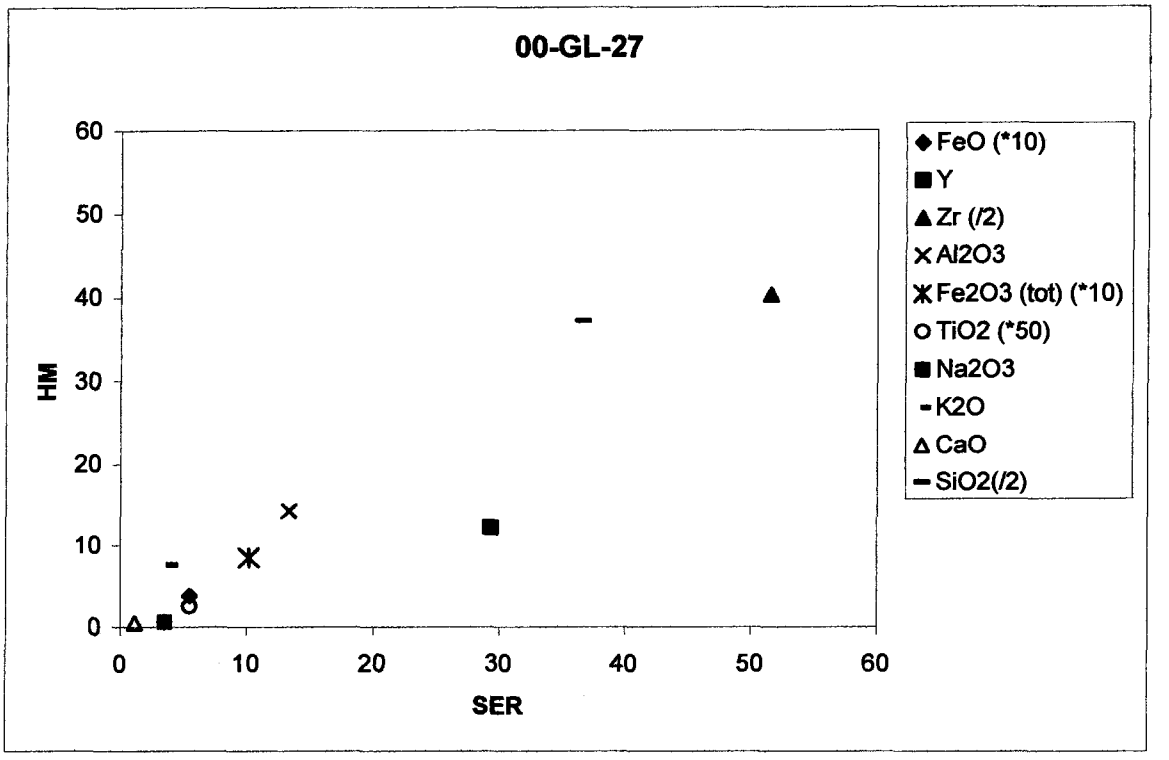

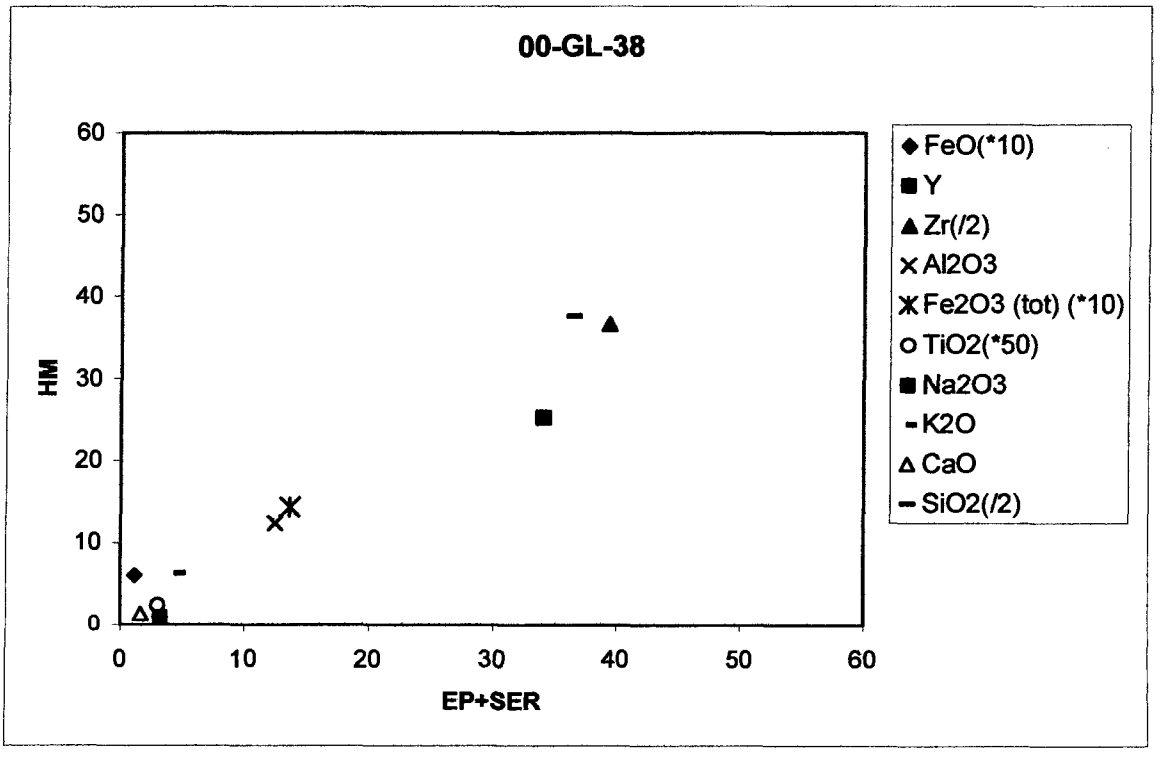

Figure 3.9: Isocon diagrams for outcrops 00-GL-27 and 00-GL-38 both included in Red Dome rhyolite (unit 4). Numbers in parentheses are normalization numbers used to scale the data.

alteration assemblage formed by regional metamorphism and also hydrothermal alteration. Accordingly the mineral chemistry of the chlorite, sericite and carbonate minerals has been compared to that from known VMS hydrothermal deposits such as the Noranda, Cyprus and Mattabi (Franklin, 1996).

3.7.1 FELDSPAR

Appendix E shows the results of 15 analyses of feldspars from the Red Dome & South rhyolites and some mafic volcanic rocks. As expected and in confirmation with the petrography (Chapter 2) the plagioclase are all albite and range in composition from Ab_{95-99} in the South rhyolite and Ab_{96} in the Mafic to intermediate metavolcanic rock units. In the Red Dome rhyolite unit the majority of the analyses are as expected, Or_{96-97} except one that is Ab_{100}. The mineral calculations were performed with the software FORMULA V96.9 developed by T.S. Ercit of the Canadian Museum of Nature, in Ottawa. The names of the minerals are after Deer *et al.* (1992).

3.7.2 CHLORITE

Appendix E shows the results of 33 analyses of chlorite in the Red Dome and South rhyolites, the mafic volcanic rocks, and the Proterozoic intrusions (Matachewan and Nipissing intrusive units). The chlorite occurs as a result of several different metamorphic processes: hydrothermal alteration, seafloor alteration and burial/regional metamorphism. The purpose of the chlorite analyses was to determine the Fe/Fe+Mg ratio of the minerals because Franklin

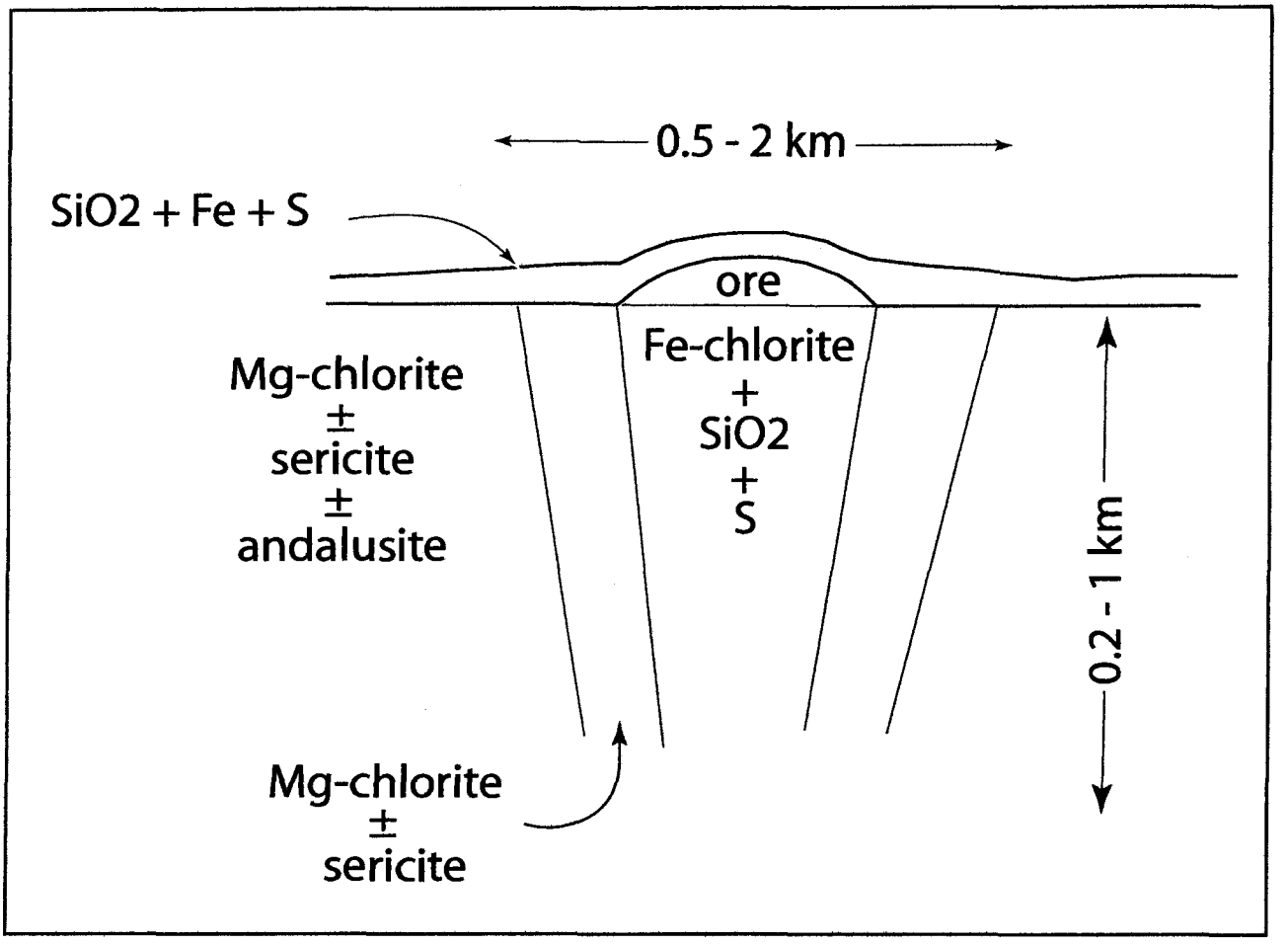

Figure 3.10: Synthesis of alteration zone immediately under Cu-Zn VMS deposits such as at Noranda and Cyprus. This model is applicable to deep water, >500 m depth.
note: Mg-chlorite±sericite zone is grational into both the central Fe-chlorite±SiO2+S and the outer-most andalusite zones (modified *from* Franklin, 1996).

(1996) and Shirozo, 1974) has shown that chlorites proximal to VMS mineralization are enriched in Fe/Fe+Mg relative to those found more proximally (Figure 3.10). Accordingly textural analyses were done to determine the origin of the chlorite and EMP to characterize the Fe/Fe+Mg ratio of hydrothermal chlorite (Table 3.1).

Chlorite analyzed from Red Dome rhyolite is interpreted to be hydrothermal because it is mainly found in veins and veinlets associated with quartz and carbonates. In addition at the Copper Hill showing, the minerals pyrite, chalcopyrite and minor malachite were observed. Although there is no direct evidence showing that these veins cut the metamorphic fabric, they appear to result from late hydrothermal activity. The chlorite analyzed in the South rhyolite occurs as amygdules and as alteration on some albite crystals and not in veins. It is therefore interpreted to be of regional or burial metamorphic origin. In the mafic volcanic rocks, the chlorite is mainly located in veins and veinlets and also found as an alteration of the groundmass implying either hydrothermal veins or a regional/burial metamorphic origin. In the Proterozoic intrusions the chlorite analyzed was found in a relatively fresh groundmass therefore implying a diagenetic or "deuteric" origin.

All the chlorite analyzed is slightly Fe rich (Table 3.1), no matter the geological unit. In the mafic volcanic rocks the chlorite Fe# (Molecular Fe/Fe+Mg) is 0.46 to

South rhyolite

	6048a	6048b	6048c	6048d	6048e	6048f	6048g	6048h	6048i	6048j	6048k	6034a	6034b
FEO	25,55	26,13	25,44	24,97	24,97	25,08	28,17	26,18	25,54	24,16	25,75	27,56	28,22
FeO/71,841	**0,355646**	**0,36372**	**0,354115**	**0,347573**	**0,347573**	**0,349104**	**0,392116**	**0,364416**	**0,355507**	**0,336298**	**0,35843**	**0,383625**	**0,3928**
MGO	14,38	14,16	14,23	14,04	14,16	14,2	13,12	13,97	13,96	13,55	14,15	11,48	11,64
MgO/40,299	**0,356833**	**0,351373**	**0,35311**	**0,348396**	**0,351373**	**0,352366**	**0,325566**	**0,346659**	**0,346411**	**0,336237**	**0,351125**	**0,284871**	**0,2888**
Fe/Fe+Mg	0,50	0,51	0,50	0,50	0,50	0,50	0,55	0,51	0,51	0,50	0,51	0,57	0,58

Red Dome rhyolite

	6018a	32a	32b	32c	32d	32e	32f	27a	27b
FEO	24,01	34,27	38,74	30,47	35,32	31,47	33,17	34,49	33,56
FeO/71,841	**0,33421**	**0,477026**	**0,539246**	**0,424131**	**0,491641**	**0,438051**	**0,461714**	**0,480088**	**0,467143**
MGO	17,07	7,79	6,47	13,03	9,36	11,78	9,17	9,84	10,08
MgO/40,299	**0,423584**	**0,193305**	**0,16055**	**0,323333**	**0,232264**	**0,292315**	**0,227549**	**0,244175**	**0,25013**
Fe/Fe+Mg	0,44	0,71	0,77	0,57	0,68	0,60	0,67	0,66	0,65

Mafic to intermediate metavolcanic rocks

	6056a	6024a	6024b	6024c	6024d	6024e	6046a	6032a	53a
FEO	24,99	26,4	26,9	25,73	28,07	24,67	28,18	27,69	25,99
FeO/71,841	**0,347852**	**0,367478**	**0,374438**	**0,358152**	**0,390724**	**0,343397**	**0,392255**	**0,385435**	**0,361771**
MGO	16,14	15,91	15,4	16,62	13,38	16,19	14,73	14,78	16,71
MgO/40,299	**0,400506**	**0,394799**	**0,382143**	**0,412417**	**0,332018**	**0,401747**	**0,365518**	**0,366758**	**0,41465**
Fe/Fe+Mg	0,46	0,48	0,49	0,46	0,54	0,46	0,52	0,51	0,47

Intrusive rocks (Matachewan)

	6030a	70a	70b
FEO	30,16	28,03	28,28
FeO/71,841	**0,419816**	**0,390167**	**0,393647**
MGO	13,22	14,38	14,38
MgO/40,299	**0,328048**	**0,356833**	**0,356833**
Fe/Fe+Mg	0,56	0,52	0,52

Table 3.1: Chlorite Fe # of Deloro assemblage and Matachewan rocks.

0.54 and 0.52 to 0.56 in the Proterozoic intrusions. In the Red Dome rhyolite the Fe# is 0.44 to 0.77 compared to 0.50 to 0.58 in the South rhyolite. One of the main interests of this study was to evaluate the VMS deposit potential of the Red Dome rhyolite. That being said, the chlorite in the Red Dome rhyolite is interpreted to be hydrothermal in origin and is slightly enriched in Fe. However because all the chlorites analyzed are somewhat Fe-rich and because it is difficult to distinguish between hydrothermal versus metamorphically derived chlorite the Fe# does not appear to be useful as a pathfinder to VMS mineralization.

3.7.3 SERICITE

Eleven EMP analyses of sericite were done to confirm the microscopic observations because the sericite is often observed only as thin wisps in the groundmass of some rocks. The sericite mainly occurs as alteration on plagioclase and as pervasive alteration in the groundmass in the Red Dome and South rhyolites and also in the mafic to intermediate volcanic rocks. The sericite mainly occurs as veins and veinlets in the Red Dome rhyolite and here is coarser grained and easily identified using optical means.

Sericite in both the groundmass and veinlets of the Red Dome rhyolite has anomalously high Fe concentrations ranging from 2.50 to 3.32 wt. % (Appendix E). Because this amount of Fe can not be accommodated in the sericite structure it likely represents Fe (-Ti) oxides minerals (likely hematite) inclusions within the

sericite (André Lalonde, personal communication). The single analysis of sericite from the groundmass of the intermediate to mafic metavolcanic rocks also has anomalously high iron (FeO=3.4 wt. %, Analysis 53a, Appendix E)

South rhyolite sericites occur as fine crystals in the groundmass or as alteration of the albite phenocrysts. The data (Appendix E) are typical of sericites except for a few that they are associated with altered albite that has anomalous FeO.

3.7.4 LARGE *ET AL.* « ALTERATION BOX PLOT » (2001)

Large *et al.* (2001) published a method called the "Alteration Box Plot" based on whole major element chemical data to distinguish VMS deposit hydrothermal alteration from "diagenetic" i.e. burial metamorphism alteration. The technique was employed here to try distinguishing regional metamorphic effect from local hydrothermal effects associated with VMS mineralization. The Alteration Box Plot method employs two well known indices (defined below) to characterize the various alteration trends of rocks associated with volcanic-hosted massive sulfides deposits. The Ishikawa alteration index (AI) and the chlorite-carbonate and pyrite index (CCPI) measure the intensity of sericite, chlorite, carbonate and pyrite replacement of sodic feldpars and glass associated with hydrothermal alteration close to mineralization respectively.

AI, which was designed for the felsic rocks of Kuroko deposits, measures the loss of Na_2O (and CaO) and the gain of K_2O during the alteration of the albite to sericite and quartz. AI can also be used to calculate the loss of K_2O and the gain of FeO and MgO during the alteration of the volcanic glass to chlorite. There are two main limitations on the AI: 1) this index does not take account of the carbonate alteration, hence low values of AI may be attained that are extensively carbonatized, 2) AI does not distinguish between sericitization and chloritization if it is used without petrography.

$$AI= \quad 100 * (K_2O+MgO) / (K_2O+MgO+Na_2O+CaO)$$

CCPI measures the increase of MgO and FeO associated with the development of Mg-Fe chlorite which commonly replaces albite, potassic feldspars or sericite and leads to a loss of Na_2O and K_2O (Large *et al.*, 2001). The main limitation of this index is the strong effect of the magmatic fractionation and the primary composition of the volcanic rock. Therefore if the weight percent of SiO_2 increases because of fractionation, implying a corresponding decrease of MgO and FeO, the CCPI will decrease.

$$CCPI= 100 * \{(MgO+FeO) / (MgO+FeO+Na_2O+K_2O)\}$$

Figures 3.11 and 3.12 resume the different diagenetic and hydrothermal trends AI and CCPI trends. Samples of South and Red Dome rhyolites and mafic to

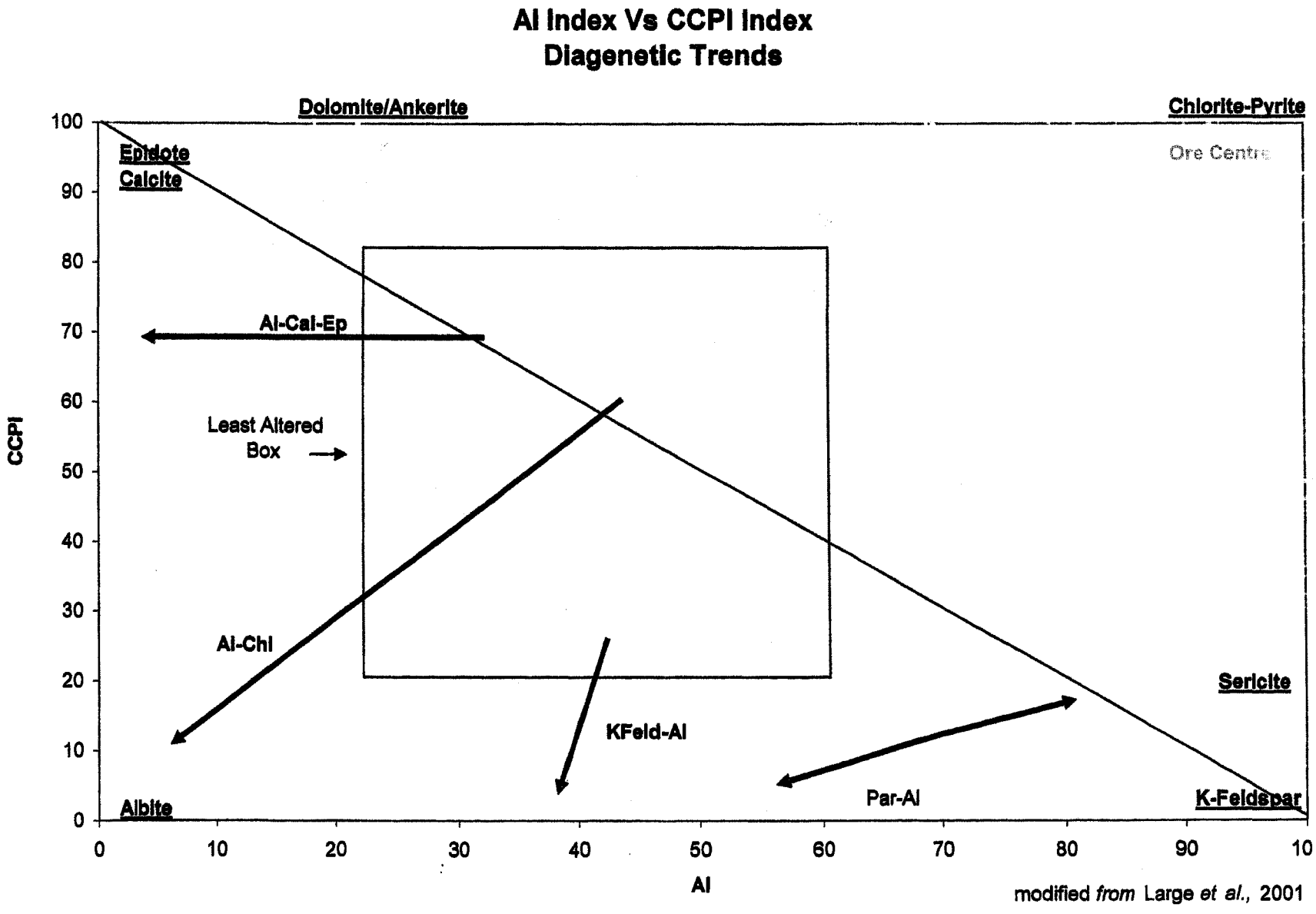

Figure 3.11: Fields for diagenetic alteration (lower left) and the hydrothermal alteration (upper right) in the alteration box plot. The arrows show the common trends for diageneti alteration.

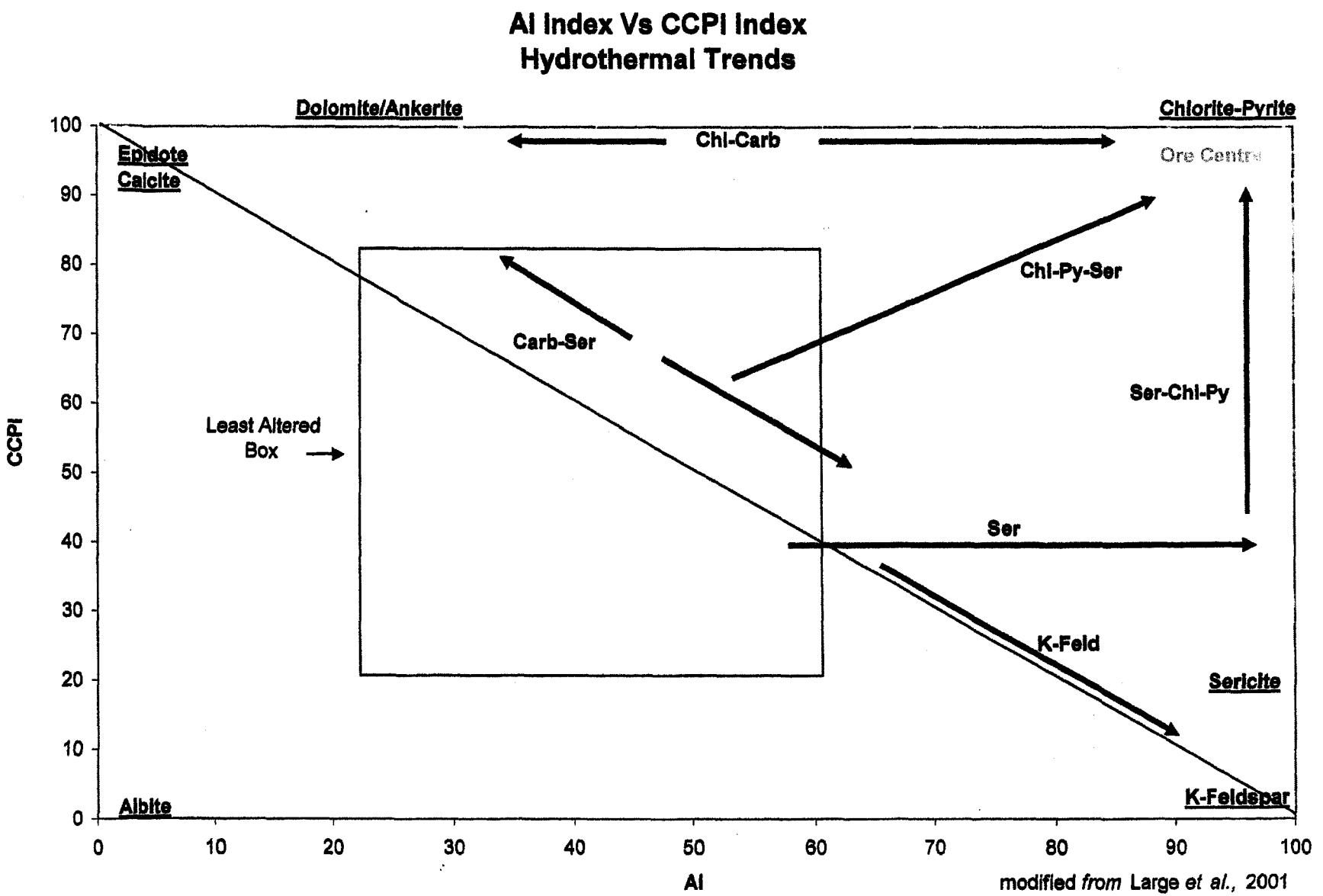

Figure 3.12: Fields for diagenetic alteration (lower left) and the hydrothermal alteration (upper right) in the alteration box plot. The arrows show the common trends for hydrothermal alteration.

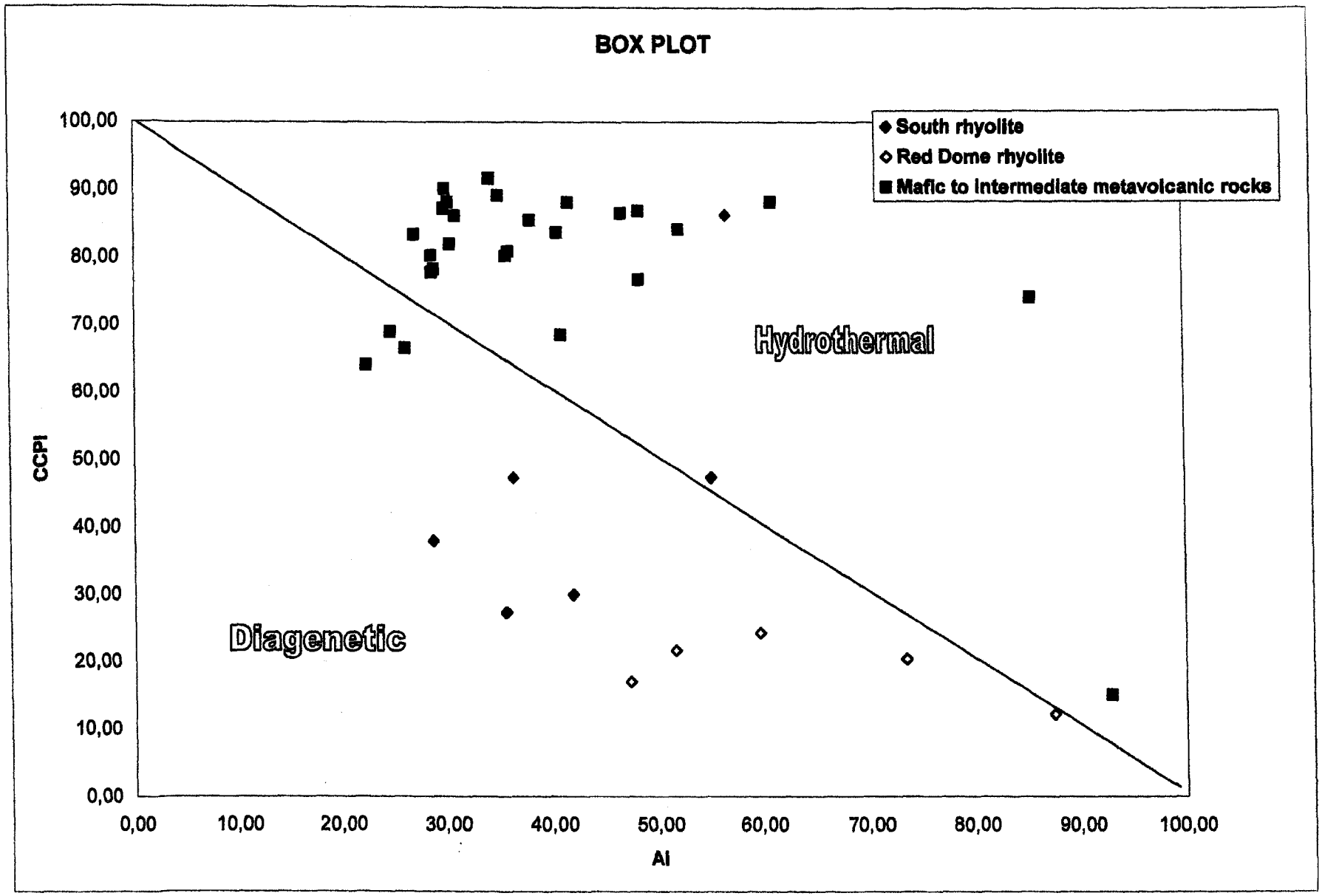

Figure 3.13: Alteration Box plot realized with the samples taken by the author

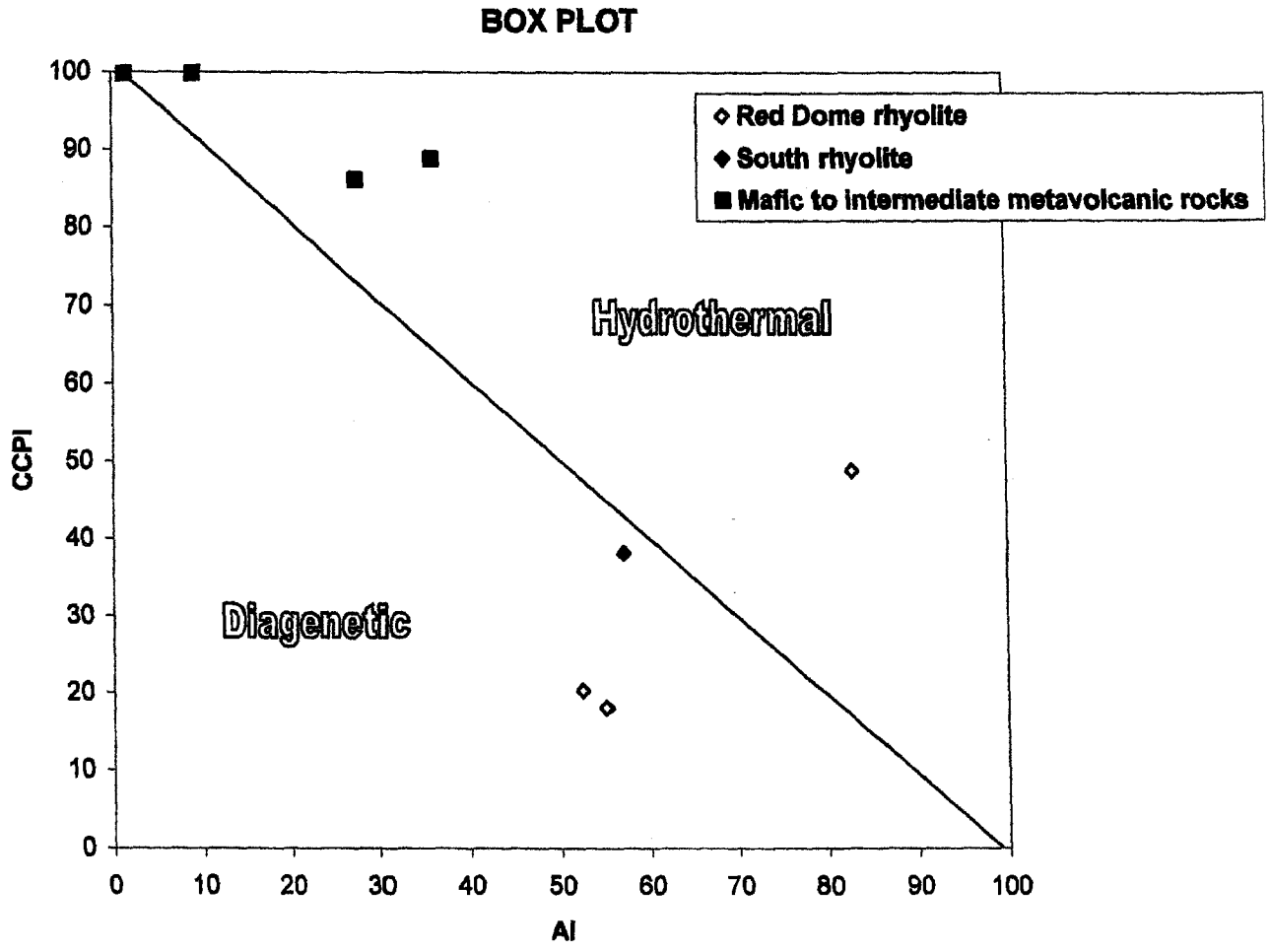

Figure 3.14: Alteration Box plot realized with Aur Resourses Inc. samples

intermediate metavolcanic rocks were plotted on the Alteration Box Plot (Figures 3.13 and 3.14) in order to determine the nature of the alteration i.e. burial metamorphism versus hydrothermal. The results are quite surprising; the majority of the rhyolite samples plot in the "diagenetic" domain, whereas the majority of the mafic to intermediate samples are included in the hydrothermal field. This can probably be explained by the non existence of a massive sulfide ore body.

In the mafic to intermediate volcanic rocks the chlorite and the sericite are pervasive generally not vein hosted and regionally developed, it was likely developed on a regional scale thru seafloor alteration burial and regional metamorphic processes than thru VMS related hydrothermal alteration.

According to the Alteration Box Plot, the alteration in South rhyolite is "diagenetic", this is consistent with field observations as the sericite is defined within a metamorphic fabric within the rock and is rarely in veinlets. However two samples (6036 and 6048) are included in the hydrothermal field.

The alteration of Red Dome rhyolite is also diagenetic according to the Alteration Box Plot method. However this rhyolite unit is cut by veins containing quartz, carbonates, sericite and chlorite that were likely developed late. Precise definition of the timing of these veins with respect of regional metamorphism is not possible because there is no metamorphic mineral fabric developed in these rocks.

3.7.5 Carbonate Minerals

A total of 46 carbonate minerals were analyzed with EMP in other to infer their identity and because they can have Fe enrichment trends in close proximity to VMS mineralization (Figure 3.15). More in particular, petrography demonstrates that there is a Fe-Mg rich carbonates likely formed by hydrothermal processes. The Fe# (Table 3.2) was calculated for carbonates using cation proportions which were computed using the software FORMULA (T.S. Ercit, Canadian Museum of Nature) and the oxide abundance data (Appendix E) determined by EMP.

In the Red Dome rhyolite the Fe# ranges from 0.27 to 0.82. In the South rhyolite it ranges from 0.18 to 0.82. In the Mafic to intermediate metavolcanic rocks the Fe# ranges from 0.55 to 1.00. The only analysis done of the Matachewan rocks give a Fe# of 0.69.

From the FORMULA software calcite was determined to be present in the Mafic to intermediate metavolcanic rocks (unit 1), in both rhyolite units (units 2 and 4) and Matachewan rocks (unit 6). In South rhyolite and Matachewan rocks only calcite was calculated. Fe-Mg carbonates (mostly dolomite) were calculated only in Red Dome rhyolite and unit 1 (Figure 3.16).

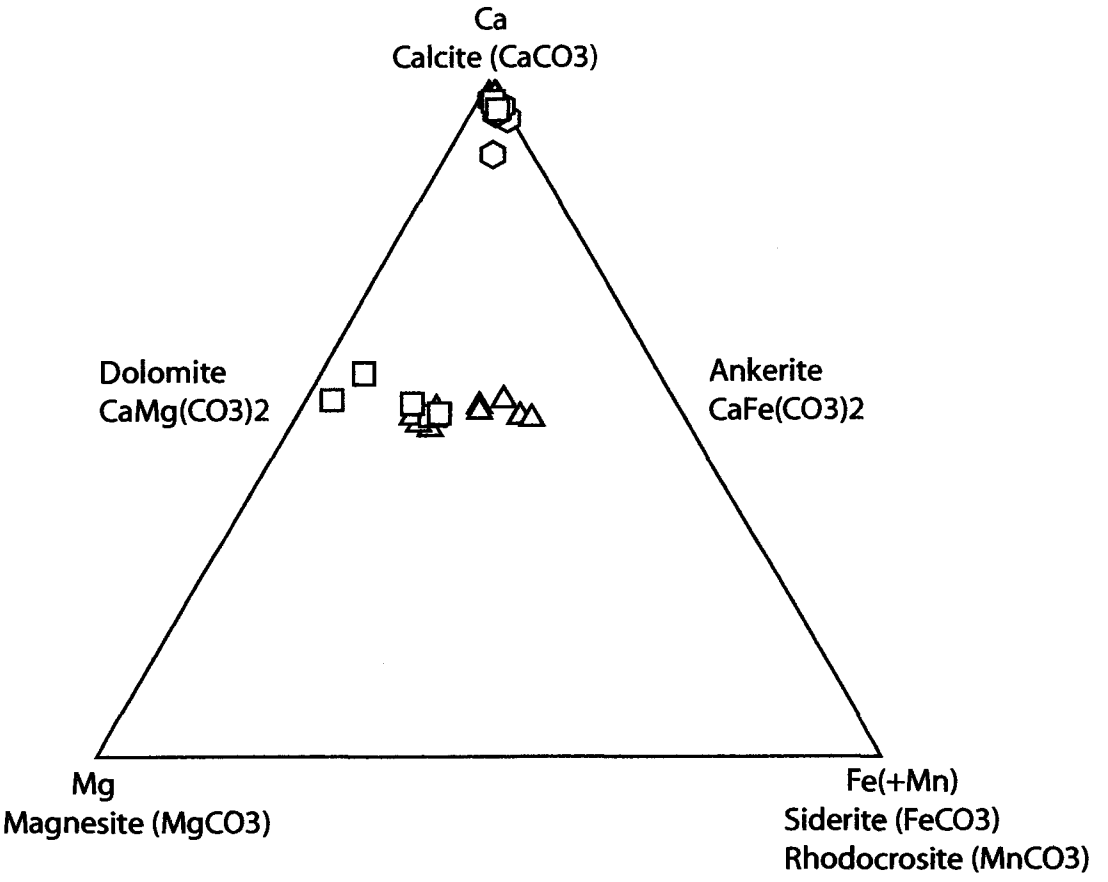

Figure 3.15: Ternary diagram of the carbonates of Deloro assemblage rocks. Squares, mafic to intermediate metavolcanic rocks (unit 1); triangles, Red Dome rhyolite (unit 4); and hexagons, South rhyolite (unit 2)
(modified *from* Klein and Hurlbut, 1985).
N.B. The Matachewan sample is included in the calcite field, and its not visible on this figure.

South rhyolite

	6048a	6048b	6048c	6048d	6048e	6048f	6048g	6048h	6048i	6048j	6048k	6048l	6048m	6034a	6034b	6034c	6034d	6034e	6034f	6034g
FEO	0,093	0,009	0,013	0,014	0,015	0,023	0,036	0,037	0,014	0,048	0,024	0,009	0,044	0,015	0,075	0,043	0,006	0,308	0,300	0,249
MGO	0,097	0,002	0,009	0,012	0,010	0,014	0,012	0,018	0,010	0,016	0,012	0,007	0,017	0,006	0,767	0,877	0,008	0,648	0,626	0,674
Fe/Fe+Mg	0,489	0,818	0,591	0,538	0,600	0,622	0,750	0,673	0,583	0,750	0,667	0,563	0,721	0,714	0,089	0,047	0,500	0,322	0,324	0,270

Red Dome rhyolite

	32a	32b	32c	32d	32e	6019a	6019b	6019c	6019d	6019e	27a	27b	27c	27d	27e	6018a	6018b	6018c	6018d
FEO	0,293	0,285	0,192	0,285	0,173	0,489	0,437	0,556	0,277	0,322	0,016	0,023	0,210	0,021	0,022	0,006	0,029	0,014	0,006
MGO	0,661	0,665	0,800	0,677	0,807	0,436	0,505	0,416	0,685	0,619	0,005	0,005	0,009	0,007	0,007	0,003	0,016	0,011	0,008
Fe/Fe+Mg	0,307	0,300	0,194	0,286	0,177	0,529	0,464	0,572	0,288	0,342	0,762	0,821	0,959	0,750	0,759	0,727	0,817	0,560	0,500

Mafic to intermediate metavolcanic rocks

	6024a	6024b	6056a	6056b	6056c	6056d
FEO	0,001	0,001	0,009	0,000	0,010	0,012
MGO	0,000	0,000	0,000	0,000	0,002	0,010
Fe/Fe+Mg	1,000	1,000	1,000	n/a	0,833	0,545

Intrusive rocks (Matachewan)

	6030a
FEO	0,018
MGO	0,008
Fe/Fe+Mg	0,692

Table 3.2: Carbonate Fe # for Deloro assemblage and Matachewan rocks.

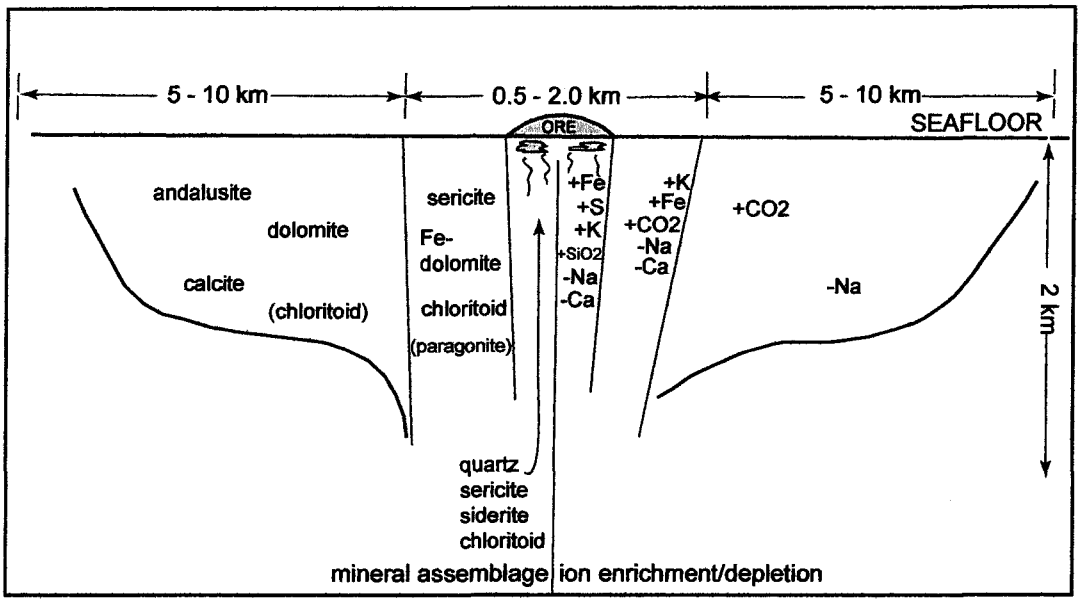

Figure 3.16: Synthesis of alteration zones adjacent to VMS deposits such as the Mattabi deposit. This model is applicable for shallow water, <500 m depth. Minerals in brackets are present in minor amounts
(modified *from* Franklin, 1996).

In the Mafic to intermediate metavolcanic rocks the calcite analyzed occurred in veins and veinlets. In South rhyolite, the calcite analyzed occurred in the groundmass and also in amygdules. In Red Dome rhyolite the analyses were mainly done in veins and also in sericite altered feldspar in the groundmass. In Matachewan rocks, only one analysis was done in the groundmass.

3.7.6 AMPHIBOLES

The amphibole analyses were performed in the mafic to intermediate volcanic rocks as well than on the Proterzoic intrusive rocks. A total of five analyses were done all in the groundmass of the two different units. The results (Appendix E) are consistent with the minerals being amphibole. The results of mineral calculations (based on 23 oxygens and assuming all the iron is Fe2+) show that the amphiboles of the mafic to intermediate volcanic rocks are anthophyllite (samples 6046a and b) and ferro-hornblende (sample 6046c). The amphibole of the Matachewan dike was determine to be ferro-actinolite and ferro-hornblende (respectively samples 6030a and b). These analyses were named according to the IMA nomenclature guidelines of Leake *et al.* (1997).

3.7.7 PYROXENES

A total of seven analyses (Appendix E) were done on the pyroxene within the groundmass of the mafic to intermediate volcanic rocks. Three analyses were performed in the groundmass of the Matachewan dike intrusions. The results were also obtained by FORMULA (Appendix E). All the pyroxene analyzed is

clinopyroxene and this result is concordant with the nature of the rocks. The analyses done on the pyroxene were only performed to verify the mineral composition.

3.7.8 GARNET

Only two analyses (Appendix E) were done on the garnet; one on the groundmass of the mafic to intermediate volcanic rocks and one on the weakly altered groundmass of the Matachewan dikes. Both of the analyses are andradite according to Deer *et al.* (1992).

3.7.9 EPIDOTE

The same samples used for garnet analyses were used for epidote analyses. Three analyses (Appendix E) were done; one on the groundmass of the mafic to intermediate volcanic rocks and two on the Proterozoic intrusive rocks (Matachewan dikes). One analysis was done on the weakly altered groundmass and the other in a vein. The results were obtained only to verify the composition of the minerals.

3.7.10 Fe-Ti OXIDE MINERALS

The Fe-Ti oxide minerals were done mainly on the mafic to volcanic rocks and on the Matachewan dikes. A total of eight analyses on the volcanic rocks had been done and only two on the intrusive rocks (Appendix E).

In the mafic to intermediate volcanic rocks, a variety of Fe-Ti oxides minerals were analyzed. In sample 6046, titanite was analyzed in the relatively fresh groundmass. In sample 00-GL-53, ilmenite crystals were also analyzed in the relatively fresh groundmass. In sample 6046, the groundmass is altered and it is hard to tell which Fe-Ti oxides were analyzed, it could be magnetite or hematite but, no specific name can be given. Finally in sample 6024, ilmenite was analyzed in a vein. One analysis was rejected because of the results not concordant with any Fe-Ti oxides.

In the Matachewan samples, titanite is found in a vein of 00-GL-70 and ilmenite was analyzed in the groundmass of sample 6030 (André Lalonde, personal communication).

CHAPTER FOUR: SUMMARY AND CONCLUSIONS

Figure 4.1 depicts a conjectural model of the geological evolution of the Big Four Lake area. Figure 4.1a shows the formation of the Deloro assemblage at the regional scale in a volcanic arc environment based upon the interpretation of the geochemical data. Figure 4.1b shows the formation of the mafic volcanic rocks of tholeiitic affinity MORB type basalts (unit 1), possibly due to back-arc spreading. It also contains chemical metasedimentary horizons (unit 1a) likely deposited from hot springs during periods of volcanic quiescence. Unit 2 (Figure 4.1c) depicts the calc-alkalic South rhyolite intruding into the Mafic volcanic rocks as a dome edifice. The unit 2a volcaniclastic rock is shown as a breccia formed by autoclastic processes. The unit 3 volcaniclastic rock is interpreted (Figure 4.1d) to have formed as an epiclastic deposit of volcanic-rock-derived sandstone and conglomerate proximal to the South rhyolite dome. Figure 4.1e pictures the calc-alkalic Red Dome rhyolite (unit 4) intruding the mafic volcanic rocks (units 1 and 1a) east of South rhyolite (unit 2). A regional chemical sedimentary horizon (unit 5) seals regionally the Deloro assemblage, suggesting a break in the volcanism. This could be the time when the sparse mineralization of the Brunet occurence was emplaced. Figure 4.1f represents folding and subsequent faulting of Deloro assemblage and finally, the introduction of the rocks by the Proterozoic intrusions.

Figure 4.1: Schematic diagram of the formation of Big Four Lake area on a roughly east-west section.

ARCHEAN

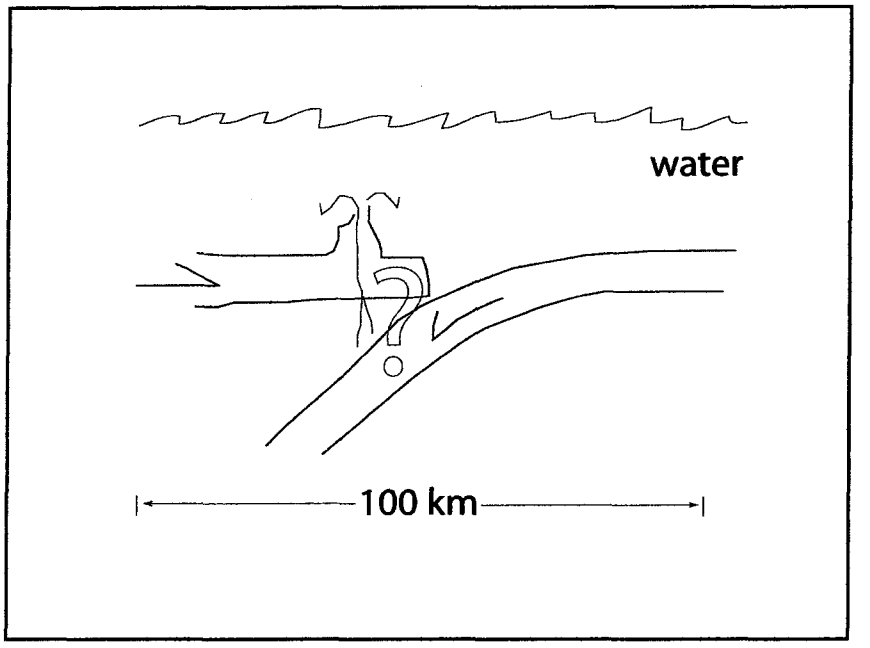

a) Formation of Deloro assemblage regionnaly in a compressive system, i.e. volcanic-arc or mid-oceanic ridge environment.
N.B. The interpretation is only based on geochemical data.

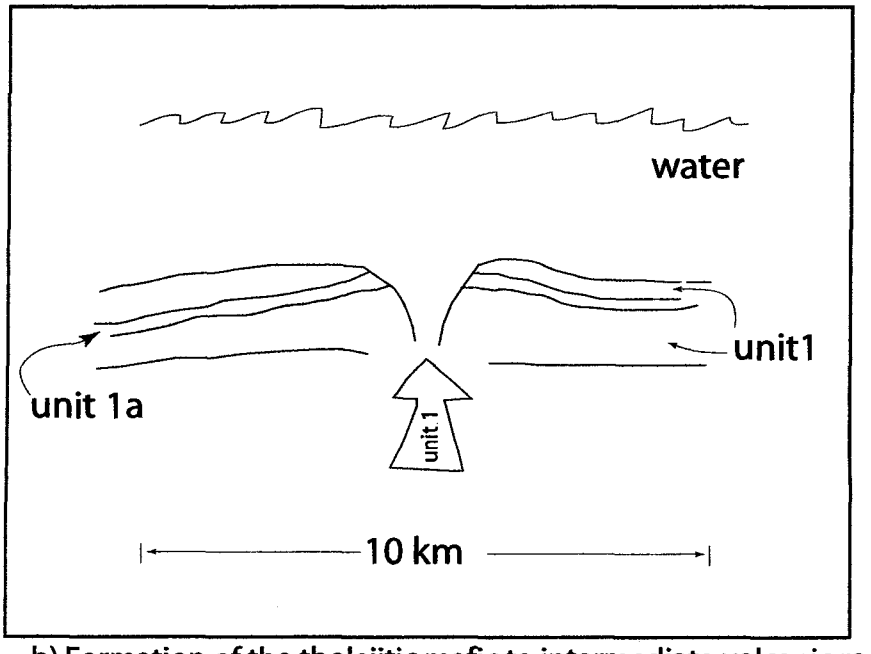

b) Formation of the tholeiitic mafic to intermediate volcanic rocks (unit 1) in back-arc, and the chemical sedimentary horizons (unit 1a during a break in volcanism) in Big Four Lake area.
Unit 1 is interpreted to be N-MORB type and volcanic-arc basalts from Meschede (1986) basalt classification (see Chapter 3).

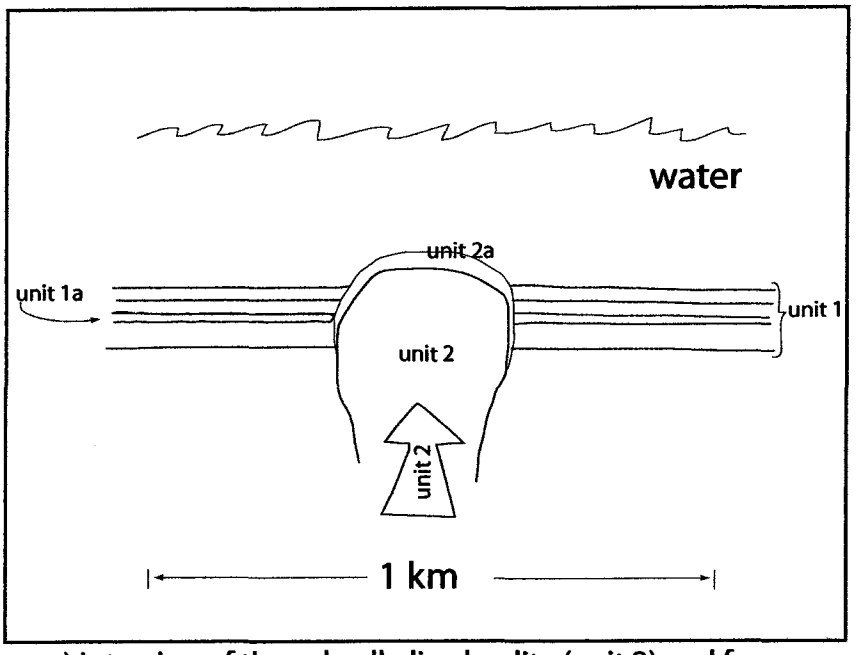

c) Intrusion of the calc-alkalic rhyolite (unit 2) and formation of minor brecciated rocks (unit 2a) during the intrusive event.

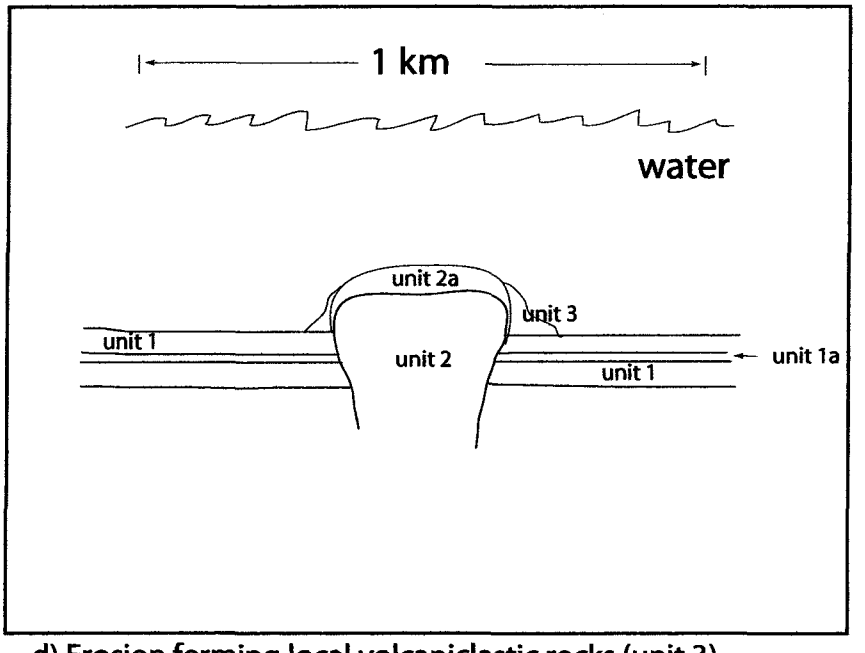

d) Erosion forming local volcaniclastic rocks (unit 3)

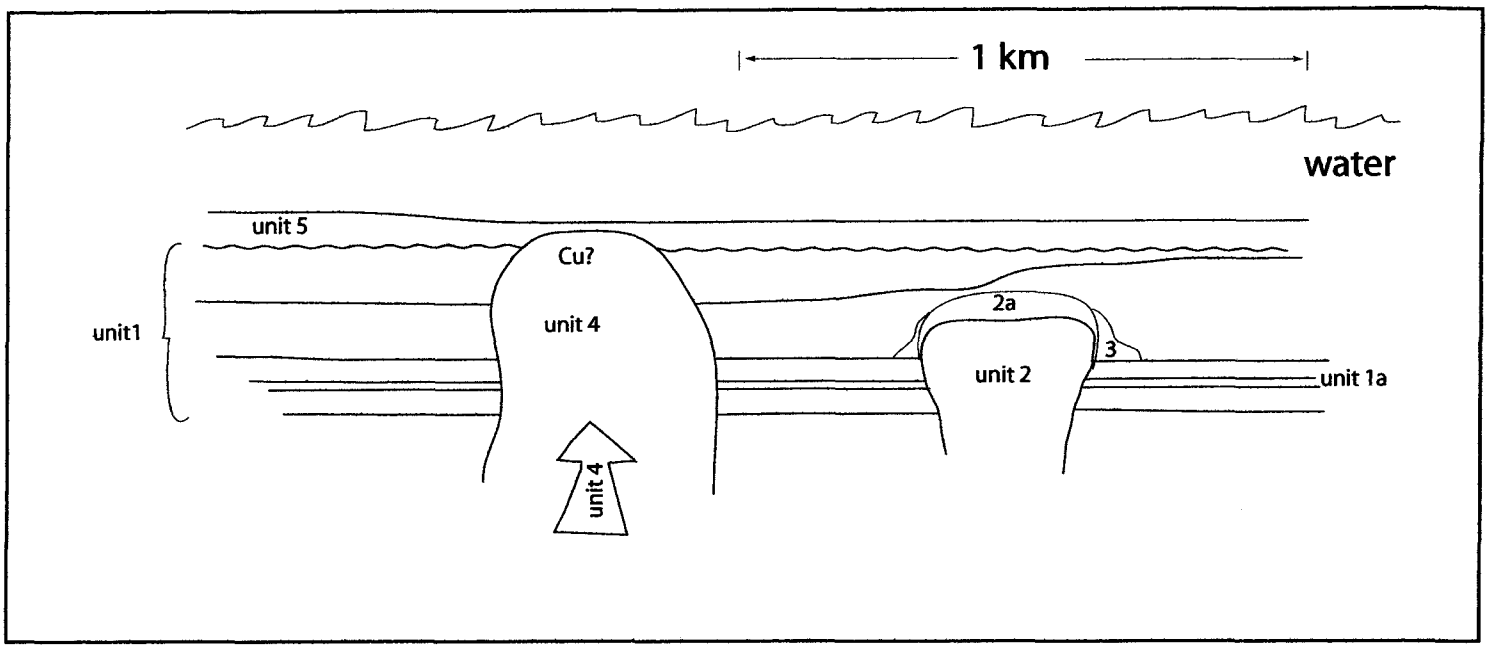

e) Intrusion of the calc-alkalic rhyolite (unit 4) of Red Dome rhyolite. Followed by the formation of a regional chemical sedimentary (unit 5) horizon overlying an unconformity. Possible formation (if VMS) of the hydrothermal system and copper mineralization.

PROTEROZOIC

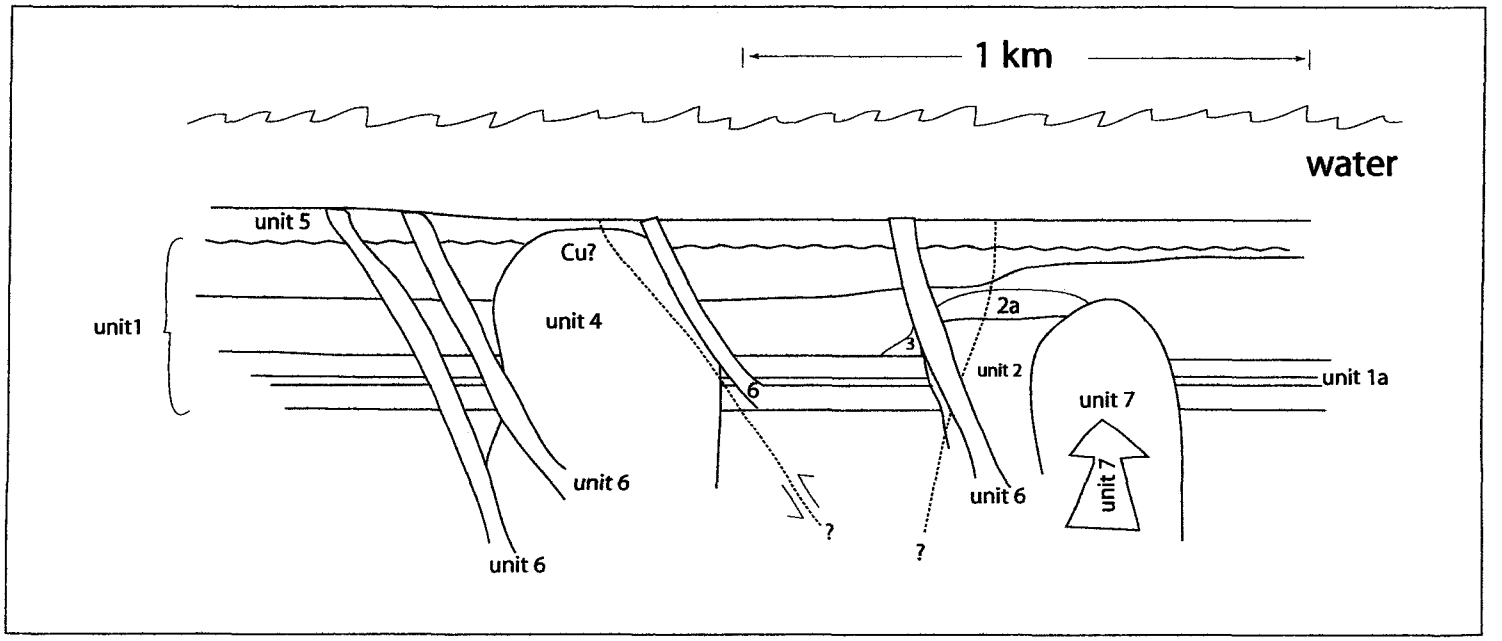

f) After some Archean regional folding and faulting , the area was intruded by the Proterozoic rocks. The first intrusion is the Matachewan dike swarm closely followed by the Nipissing gabbros. These intrusions are also found at a regional scale and may be in part related to Cu mineralization in the area (Chapter 3 for discussion).

CONTRIBUTIONS TO KNOWLEDGE

The following are items in point form and represent new knowledge discovered by the author during the course of this work.

- Production of 1: 10,000 map of the Big Four Lake Area showing the distribution of Deloro and other rocks.

- Determination of the rock types in Big Four Lake area ⇒ Deloro assemblage and Proterozoic intrusions

- Distribution of facies, textures and the setting of the volcanic rocks ⇒ timing between each unit of Big Four Lake area

- Complete geochemical characterization of the rocks including major and trace elements, REE ... The data were interpreted using the following means to demonstrate the presumed tectonic affiliations and the nature of the mineralization. In addition EMP was used to better define the minerals, the results were used to calculate mineral compositions and compare with VMS mineralization & alteration elsewhere.

- There is no evidence the rocks of the Big Four Lake area belong to the Pacaud or Kidd Munro assemblages (as initially thought) ⇒ no major geochemical differences, unconformities, faults or breaks in the mafic rocks south and north of the rhyolites.

- Red Dome rhyolite (unit 4) is a dome facies ⇒ autoclastic brecciated and massive facies and columnar jointing observed. New SHRIMP results imply that the Red Dome rhyolite is younger than initially thought. Therefore it is possibly a sub-volcanic intrusion intruding the Deloro assemblage. It is also geochemically dfferent from the South rhyolite (unit

2) as it is richer it potassium and has distinctive REE patterns. It is also different in that it contains microcline phenocrysts and shows intensive pervasive hematite alteration. This unit seems to have similarities to the intrusions hosting the Tyranite gold deposit located ~50 km east of Brunet Cu occurence and to the gold deposits in the Matachewan area. Given the interpretation for relatively late timing of alteration and mineralization of the Red Dome rhyolite and the new data indicating a possible intrusive origin, perhaps the emphasis of exploration should be changed to also consider the possibility of porphyry style Cu ± Au mineralization rather than VMS.

- South rhyolite (unit 2) is massive with associated volcaniclastic rocks (unit 2a). The rhyolite is a dome and associated with epiclastic rocks (unit 3). There is no evidence of explosive and hot emplacement of the fragmental rocks therefore this unit is not pyroclastic and most likely a dome.

- Origin of the Copper Hill mineralization
  - Presence of the typical hydrothermal alteration minerals of VMS deposits but regionally distributed not locally zoned in the rocks.
  - The metallic mineral assemblage of Brunet copper occurrence conforms to VMS model.
  - Stratigraphy of units conforms to VMS model; Red Dome rhyolite is more altered and show more evidence of hydrothermalism than South rhyolite, the presence of chemical sediments capping the system is also supporting the VMS model, and the mafic volcanic rocks are older and more abundant than Red Dome rhyolite.
  - The volcanic assemblage does not seem to be bimodal because of the presence of intermediate rocks.
  - All EMP analysis do not conform to the zoning pattern expected to be formed as a result of VMS alteration. The chlorite and carbonate do not show an enrichment of Fe.

- As an alternative is it possible that the mineralization is related to Matachewan or Nippising intrusions because of the veinlets aligned with S_0 and emanating from Matachewan dikes and also Brunet Cu occurence vein similar orientation to Matachewan swarm. The Cu mineralization (Brunet Cu occurrence), is interpreted to have a hydrothermal origin. However, the mineralization system does not have a VMS signature even though it was initially thought too. The hydrothermal activity could possibly be explained by the heat generated from intrusions remobilizing chemical elements. The source of the heat could be either from the intrusions of the felsic rocks in the area or from the Proterozoic intrusions of Nippissing and Matachewan. However the mineralization appears to cut regional deformation and it is therefore interpreted to have occurred in the Archean prior to the Proterozoic intrusions.
- Missing the ore body.
- Concludes: no VMS or VMS not found or very small hydrothermal system not entirely developed.

REFERENCES

Ayer, J.A., Trowell, N.F., Amelin, Y., Corfu, F., 1998. Geological Compilation of the Abitibi Greenstone Belt in Ontario: Towards a Revised Stratigraphy Based on Compilation and New Geochronology results. *In*: Summary of Field Work and Other activities 1999, Ontario Geological Survey, Miscellaneous Paper 169, pp. 14-24.

Ayer, J.A., Ketchum, J.W.F., Trowell, N.F., 2002a. New Geochronological and Neodymium Isotopic Results from the Abitibi Greenstone Belt, with Emphasis on the Timing and the Tectonic Implications of Neoarchean Sedimentation and Volcanism. *In*: Summary and Field Work and Other Activities 2002, Ontario Geological Survey, Open File Report 6100, pp. 5-1 to 5-16.

Ayer, J.A., Amelin, Y., Corfu, F., Kamo, S., Ketchum, J., Kwok, K., Trowell, N., 2002. Evolution of the Southern Abitibi Greenstone Belt Based on U-Pb Geochronology: Autochthonous Volcanic Construction Followed by Plutonism, Regional Deformation and Sedimentation. Precambrian Research **115**, 63-95.

Ayer. J.A., Thurston, P.C., Bateman, R., Dubé, B., Gibson, H.L., Hamilton, M.A., Hathway, B., Hocker, S.M., Houlé, M.G., Hudack, G., Ispolatov, V.O., Lafrance, B., Lesher, C.M., MacDonald, P.J., Péloquin, A.S., Piercey, S.J., Reed, L.E, Thompson, P.H., 2005. Overview of Results from the Greenstone Architecture Project: Discover Abitibi Initiative. Ontario Geological Survey, Open File Report 6154, 1-107pp.

Born, P., 1995. A Sedimentary Basin Analysis of the Abitibi Greenstone Belt in the Timmins Area, Northern Ontario, Canada; Unpublished Ph.D. thesis, Carleton University, Ottawa, 489 pp.

Burnwash, E.M., 1897. Geology of the Nipissing-Algoma Line. Ontario Bureau of Mines, Vol. 6, Sec. 5, pp. 167-183.

Card, K.D., 1990. A Review of the Superior Province of the Canadian Shield, a Product of Archean Accretion. Precambrian Research **48**, 99-156.

Card, K.D., and Poulsen, K.H., 1998. Geology and Mineral Deposits of the Superior Province of the Canadian Shield. *In*: Geology of the Precambrian Superior and Grenville Provinces and Precambrian Fossils in North America, Geological Survey of Canada, Geology of North America, Vol. C-1, Geology of Canada No. 7, pp. 13-204.

Caldbick, P., 2004. Summary Report on the Golden Sylvia Iron Formation, 2004 Drill Program and Shining Tree Area Properties *prepared for* International KRL Resources Corp., 130 pp.

Carter, M.W., 1977. Geology of Macmurchy and Tyrrell Townships, Districts of Sudbury and Timiskaming. Ontario Division Mines, Report 152, 69 pp.

Carter, M.W., 1987. Geology of the Shining Tree Area, Districts of Sudbury and Timiskaming. Ontario Geological Survey, Report 240, 48 pp.

Chown, E.H., Daignault, R., Mueller, W., 1992. Tectonic evolution of the northern Volcanic Zone, Abitibi Belt, Quebec. Canadian Journal of Earth Sciences **29**, 2211-2225.

Coleman, A.P., 1901. Iron Ranges of the Lower Huronian. Ontario Bureau of Mines, Vol. 10, pp. 181-212.

Collins, W.H., 1911. Geology of Onaping Sheet, Ontario. Portion of Map-area between West Shining Tree and Onaping Lakes. pp. 244-252 *In:* Geological Survey of Canada Summary Report for 1911, 356 pp., (published 1912).

Collins, W.H., 1912. Geology of Onaping Sheet, Ontario. pp. 301-314 *In:* Geological Survey of Canada, Summary Report for 1912, 396 pp., (published 1914).

Collins, W.H., 1917. Onaping Map-Area. Geological Survey of Canada, Mem. No. 95, 157 pp. Accompanied by Maps 153A, 179A.

Corfu, F., 1993. The Evolution of the Southern Abitibi Greenstone Belt in Light of Precise U-Pb Geochronology. Economic Geology **88**, 1323-1340.

Corfu, F., and Andrews, A.J., 1986. A U-Pb Age for Mineralized Nipissing Diabase, Gowganda, Ontario. Canadian Journal of Earth Sciences **23**, 107-109.

Davis, W.J., Lacroix, S., Gariepy, C., Machado, N., 2000. Geochronology and Radiogenic Isotope Geochemistry of Plutonic Rocks from the Central Abitibi Sub-province: Significance to the Internal Subdivision and Plutono-Tectonic Evolution of the Abitibi Belt. Canadian Journal of Earth Sciences **37**, 117-133.

Deer, W.A., Howie, R.A., Zussman, J., 1992. An Introduction to the Rock-Forming Minerals. 2nd Edition, Pearson Prenctice Hall, 696 pp.

Dimroth, E., Imreh, L., Goulet, N., Rocheleau, M., 1983a. Evolution of the South Central Segment of the Archean Abitbi Belt, Quebec, Part II. Plutonic and Metamorphic Evolution and Geotectonic Model. Canadian Journal of Earth Sciences **20**, 1355-1373.

Dimroth, E., Imreh, L., Goulet, N., Rocheleau, M., 1983b. Evolution of the South Central Segment of the Archean Abitbi Belt, Quebec, Part III. Plutonic and Metamorphic Evolution and Geotectonic Model. Canadian Journal of Earth Sciences **20**, 1374-1388.

Finley, F.L., 1926. Wasapika Section, West Shiningtree Gold Area, District of Sudbury. Ontario Department of Mines, Vol. 35, pt. 6, pp. 83-96.

Fowler, A.D., and Jensen, L.S., 1989. Quantitive Trace-Element Modeling of the Crystallization History of the Kinojevis and Blake River Groups, Abitibi Greenstone Belt, Ontario. Canadian Journal of Earth Sciences **26**, 1356-1367.

Franklin, J.M., 1996. Gîtes de sulfures massifs à métaux communs associés à des roches volcaniques. *In* Géologie des gîtes minéraux du Canada, *Revised by* O.R. Eckstrand, W.D. Sinclair and R.I. Thorpe, Commission Géologique du Canada, No. 8, (*Also in* The Geology of North America, Vol. P-1, Geological Society of America, pp. 174-199.

Gledhill, T.L., 1926. Note on the South Part of Grassy River Area. Ontario Department of Mines, Vol. 35, pt. 6, pp. 77-82. Accompanied by Map 35J, scale 1 inch to ½ mile.

Goodwin, A.M., 1977. Archean Basin-Craton Complexes and the Growth of Precambrian Shields. Canadian Journal of Earth Sciences **14**, 2737-2759.

Goodwin, L.H., 1919. West Shining Tree Gold District, Ontario. Engineering and Mining Journal Press **108**, No. 7, 261-264.

Graham, A.R., 1932. Tyrrell-Knight Gold Area. Ontario Department of Mines, Vol. 41, pt. 2, pp. 25-61. Accompanied by Map 41b, scale ¾ inch to 1 mile.

Grant, J.A., 1986. The Isocon Diagram – A Simple Solution to Gresens' Equation for Metasomatic Alteration. Economic Geology **81**, 1976-1982.

Grunsky, E.C., Easton, R.M., Thurston, P.C., and Jeansen, L.S., 1992. Characterization ans statistcal classification of Archean volcanic rocks of the Superior Province using major element geochemistry. *In*: Geology of Ontario; OGS Special Volume 4, Part 2. *Edited by* P.C. thurston, H.R. Williams, R.H. Sutcliffe, and G.M. Stott, Ontario Geological Survey, Ontario, pp. 1397-1438.

Hart, T.R, Gibson, H.L., Lesher, C.M., 2004. Trace Element Geochemistry and Petrogenesis of Felsic Volcanic Rocks Associated with Volcanogenic Massive Cu-Zn-Pb Sulphide Deposits. Economic Geology **99**, 1003-1013.

Heaman, L.M., 1988. A Precise U-Pb Zircon Age for Hearst Dikes. *In*: Program with Abstracts, Annual Meeting Geological Association of Canada-Mineralogical Association of Canada **13**, A53.

Heather, K.B., 1998. New Insights on the Stratigraphy and Structural Geology of the Southwestern Abitibi Greenstone belt: Implications for the Tectonic Evolution and Setting of Mineral Deposits in the Superior Province. *In*: The first Age of Giant Ore Formation: Stratigraphy, Tectonics and Mineralization in the Late Archean and Early Proterozoic, Prospector Development Association Canadian Anniversery Convention, Toronto, pp. 63-101.

Hodge, W.R., 1912. West Shining Tree Gold District. The Engineering and Mining Journal **94**, No. 8, pp. 343-345.

Hopkins, P.E., 1920a. West Shiningtree Gold Area. Ontario Department of Mines, Vol. 29, pt. 3, pp. 28-52. Accompanied by Map 29a, scale 1 inch to ½ mile.

Hopkins, P.E., 1920b. West Shiningtree Gold Area. Ontario Department of Mines, Bulletin No. 39, 26 pp. Accompanied by Map 29a, scale 1 inch to ½ mile.

Hopkins, P.E., 1922. Ontario Gold Deposits: Their Character, Distribution and Productiveness. Ontario Department of Mines, Vol. 30, pt. 2, 73 pp.

Hore, R.E., 1918. Gold Deposits in Macmurchy and Churchill Townships. Canadian Mining Journal **39**, No. 16, pp. 276-281.

Hore, R.E., 1919a. The Wasapika Gold Area. Canadian Mining Journal **40**, 490-500.

Hore, R.E., 1919b. Recent Developments in Wasapika Gold Area. Canadian Mining Journal **40**, 677-678.

Hore, R.E., 1919c. Some Notes on Ores and Rocks of Wasapika Gold Area. Canadian Mining Journal **40**, 749-751.

Hore, R.E., 1919d. A New Goldfield in Ontario. Mining and Scientific Press **119**, 595-596.

Hunter, D.A., 1998. The Copper Hill Property, Technical report and Recommendations, Macmurchy and Churchill Townships, Larder Lake Mining Division, Northeastern Ontario, NTS: 41P/11 *prepared for* International KRL Resources Corp., 16 pp.

Irvine, T.N., and Baragar, W.R.A., 1971. A Guide to the Classification of the Common Volcanic Rocks. Canadian Journal of Earth Sciences **8**, 523-548.

Jackson, S.L., Fyon, A.J., Corfu, F., 1994. Review of Archean Supracrustal Assemblages of the Southern Abitibi Greenstone Belt in Ontario, Canada: Products of Microplate Interaction within Large-Scale Plate-Tectonic Setting. Precambrian Research **65**, 183-205.

Jackson, S.L., and Fyon, A.J., 1991. The Western Abitibi Subprovince in Ontario. *In*: Geology of Ontario, Ontario Geological Survey, Special Volume 4/1, pp. 405-482.

Jensen, L.S., and Langford, F.F., 1985. Geology and Petrogenesis of the Archean Abitibi Belt in Kirkland Lake Area, Ontario. Ontario Geological Survey, Miscellaneous Paper 123, 130 pp.

Jensen, L.S., 1976. A New Cation Plot for Classifying Subalkalic Volcanic Rocks. Ontario Division of Mines, Miscellaneous Paper 66, 45 pp.

Jolly, W.T., 1980. Development and Degradation of Archean Lavas, Abitibi Area, Canada. Journal of Petrology **21**, 323-363.

Johns, G.W., 1996. Reappraisal of the Geology of the Shining Tree Area, Districts of Sudbury and Timiskaming. *In*: Summary of Field Work and Other activities 1996, Ontario Geological Survey, Miscellaneous Paper 166, pp. 13-15.

Johns, G.W., 1999. Reappraisal of the Geology of the Shining Tree Area (Tyrrell Township), Districts of Sudbury and Timiskaming. *In*: Summary of Field Work and Other activities 1999, Ontario Geological Survey, Miscellaneous Paper 168, pp. 26-29.

Johns, G.W., 1999a. Shining Tree Area (East Half), Precambrian Geology, Map P. 3389, Ontario Geological Survey, scale 1: 30,000.

Johns, G.W., and Amelin, Y., 1999. Reappraisal of the Geology of the Shining Tree Area (East Part), Districts of Sudbury and Timiskaming. *In*: Summary of Field Work and Other Activities 1999, Ontario Geological Survey, Miscellaneous Paper 169, pp. 43-49.

Johns, G.W., 2000. Shining Tree Area (West Half), Precambrian Geology, Map P. 3420, Ontario Geological Survey, scale 1: 30,000.

Johns, G.W., 2003. Shining Tree Area, Precambrian Geology, Map P. 3521, Ontario Geological Survey, scale 1: 50,000.

Klein, C., and Hurlbut Jr, C.S., 1985. Manual of Mineralogy. 21st Edition, John Wiley and Sons, Inc., 681 pp.

Laird, H.C., 1935. Recent Development in Swayze and West Shiningtree Area. Ontario Department of Mines, Vol. 44, pt. 7, pp. 38-47.

Lajoie, J., and Stix, J., 1992. Volcaniclastic Rocks. *In*: Facies Models response to sea level change, Geological Association of Canada, pp. 101-118.

Langford, G. B., 1927. Wasapika Section, West Shiningtree Gold Area, District of Sudbury. Ontario Department of Mines, Vol. 36, pt. 2, pp. 100-104. Map insert to face p.100, scale 1 inch to ¼ mile.

Large, R.R., Gemmel, J.B., Paulik, H., Huston, D.L., 2001. The Alteration Box Plot: A Simple Approach to Understanding the Relationship between Alteration Mineralogy and Lithogeochemistry Associated with Volcanic-Hosted Massive Sulfide Deposits. Economic Geology **96**, 957-971.

Leake, B.E, Woolley, A.R., Arps, C.E.S., Birch, W.D., Gilbert, M.C., Grice, J.D., Hawthorne, F.C., Kato, A., Kish, H.J., Krivivichev, V.G., Linthout, K., laird, J., Mandarino, J.A., Maresh, W.V., Nickel, E.H., Rock, N.M.S., Schumacher, J.C., Smith, D.C., Stephenson, N.C.N., Ungaretti, L., Whittaker, E.J.W., Youzhi, G., 1997. Nomenclature of Amphiboles: Report on the Subcommittee on Amphiboles of the International Mineralogical Association, Commission on New Minerals and Minerals Names. The Canadian Geologist **35**, 219-246.

Lebel, J.L., 2000. Report on the Copper Hill Property, Larder Lake Mining Division, Ontario, NTS 41P/11 *prepared for* International KRL Resources Corp., 12 pp.

Lesher, C.M., Goodwin, A.M., Campbell, I.H., Gorton, M.P., 1986. Trace-Element Geochemistry of Ore-Associated and Barren, Felsic Metavolcanic Rocks in the Superior Province, Canada. Canadian Journal of Earth Sciences **23**, 222-237.

Ludden, J., Hubert, C., Gariepy, C., 1986. The Tectonic Evolution of the Abitibi Greenstone Belt of Canada. Geology Magazine **123**, 153-166.

Meschede, M., 1986. A Method of Discriminating Between Bifferent Types of Mid-Ocean Ridge Basalts and Continental Tholeiites with the Nb-Zr-Y Diagram. Chemical Geology 56, pp. 207-218.

Michard, A., 1989. Rare Earth Element Systematics in Hydrothermal Fluids. Geochimica et Cosmochimica Acta **53**, 745-750.

Mortensen, J.K., 1993a. U-Pb Geochronology of the Eastern Abitibi Subprovince. Part 1: Chibougamau-Matagami-Joutel Region. Canadian Journal of Earth Sciences **30**, 11-28.

Mortensen, J.K., 1993b. U-Pb Geochronology of the Eastern Abitibi Subprovince. Part 2: Noranda-Kirkland Lake Area. Canadian Journal of Earth Sciences **30**, 29-41.

Oliver, H.S., Hughes, R.P., Hall, R.P., Johns, G.W., 1999. Lithogeochemistry of the Shining Tree Area. *In*: Summary of Field Work and Other activities 1999, Ontario Geological Survey, Open File Report 6032, pp. 6-1 to 6-14.

Oliver, H.S., Hughes, R.P., Hall, R.P., Johns, G.W., 1999a. Preliminary Geochemistry of Metavolcanic rocks of the Shining Tree Area; Abitibi Subprovince, Ontario. *In*: Summary of Field Work and Other activities 1999, Ontario Geological Survey, Miscellaneous Paper 169, pp. 51-58.

Oliver, H.S., Hughes, R.P., Hall, R.P., Johns, G.W., 1999b. The Mafic and Ultramafic rocks of the Shining Tree Greenstone Belt, Northeastern Ontario, Canada. *In*: Summary of Field Work and Other activities 1999, Ontario Geological Survey, Open File Report 6000, pp. 11-1 to 11-12.

Pearce, J.A., and Cann, J.R., 1973. Tectonic Setting of Basic Volcanic Rocks Determined Using Trace Element Analysis. Earth Planet Science Letters **19**, 290-300.

Percival, J.A., and Card, K.D., 1983. Archean Crust as Revealed in the Kapuskasing Uplift, Superior Province, Canada. Geology **11**, 323-326.

Piché, M., and Jébrak, M., 2004. Normative Minerals and Alteration Indices Developed for Mineral Exploration. Journal of Geochemical Exploration **82**, 59-77.

Powell, W.G., Carmichael, D.M., Hodgson C.J., 1995. Conditions and Timing of Metamorphism in the Southern Abitibi Greenstone Belt, Quebec. Canadian Journal of Earth Sciences **32**, 787-805.

Rollinson, H.R., 1993. Using Geochemical Data: Evaluation, Presentation, interpretation, Longman, Syngapore, 352 pp.

Ropchan, J.C., 2000. Petrographic and Geochemical Studies of the Alteration Zones Associated with Gold Mineralization at the Holloway Mine, Southwestern Abitibi Greenstone Belt, Canada. Master Thesis, Ottawa University, 133 pp.

Saumur, B.-M., 2005. The Contorted Lobe and Breccia Facies of the V10B Flow Unit (Vipond Formation, Abitibi Greenstone Belt): a Detailed Study at the Firetower Outcrop, Schumacher, Ontario. Undergrad Thesis, Ottawa University, 69 pp.

Stewart, R.B., 1912. West Shining Tree Gold District. Ontario Department of Mines, Bulletin No. 134, 29 pp.

Stewart, R.B., 1913. The West Shining Tree Gold Area. Ontario Department of Mines, Vol. 22, pt. 1, pp. 233-237.

Sun, S.S., and McDonough, W.F., 1989. Chemical and Isotopic Systematics of Oceanic Basalts: Implications for Mantle Composition and Processes. *In:* Magmatism in the Ocean Basins, Edited by A.D. Saunders, and M.J. Norry, Geological Society Special Publication No. 42, pp. 313-345.

Sutcliffe, R.H., Barrie, C.T., Burrows, D.R., Beakhouse, G.P., 1993. Plutonism in the Southern Abitibi Subprovince: a Tectonic and Petrogenic Framework. Economic Geology **88**, 1359-1375.

Watkins, J.J., 2000. Progress Report on the Copper Hill Property, Shining Tree Area, Larder Lake Mining Division, Ontario, Canada, NTS: 41P/11 *prepared for* International KRL Resources Corp., 18 pp.

Weed, W.H., 1923. West Shining Tree Gold Prospects. Engineering and Mining Journal Press **116**, No. 2, 68-69.

Wilson, A.D., 1960. The Micro-Determination of Ferrous Iron in Minerals by a Volumetric and Colorimetric Method. Analyst **85**, 823-827.

APPENDIX A: GEOCHEMISTRY DATA

Appendix A: Major elements

Sample No.	Al2O3	CaO	Fe2O3	K2O	LOI	MgO	MnO	Na2O	P2O5	SiO2	TiO2	TOTAL
6005	15.44	2.05	2.39	1.42	3.99	1.24	0.07	4.53	0.08	68.22	0.35	99.77
6006	14.32	4.80	13.02	0.35	10.48	6.59	0.25	2.60	0.06	47.47	0.80	100.74
6042	15.64	3.27	3.16	2.18	5.85	1.28	0.07	2.79	0.07	64.76	0.36	99.44
6032	15.65	9.40	12.94	0.06	3.31	7.84	0.21	3.45	0.05	46.94	0.80	100.64
6034	19.29	1.80	1.98	3.13	3.73	1.08	0.03	4.03	0.07	64.10	0.29	99.52
6008	16.46	2.62	5.43	2.83	5.97	1.64	0.11	1.35	0.11	62.08	0.69	99.29
6014	16.63	3.93	7.38	0.63	7.86	2.25	0.12	4.23	0.15	56.93	0.80	100.92
6016	13.96	6.42	7.78	0.96	7.55	2.40	0.10	1.95	0.14	57.90	0.77	99.93
6012	14.08	2.99	12.31	0.13	5.15	6.95	0.20	3.49	0.10	53.98	1.37	100.76
6013	13.89	1.10	1.51	4.31	2.63	0.57	0.03	2.18	0.02	73.46	0.09	99.80
6020	13.31	1.15	1.02	3.74	2.18	0.47	0.03	3.53	0.02	73.27	0.11	98.82
6021	14.18	0.49	0.85	7.60	1.80	0.29	N.D.	0.64	0.01	74.36	0.05	100.28
6036	12.66	2.15	2.25	2.69	4.88	0.70	0.05	0.60	0.02	74.18	0.14	100.32
6039	14.90	6.46	6.29	1.12	7.25	1.71	0.11	3.38	0.20	57.90	0.99	100.31
6017	15.12	7.66	12.24	0.21	7.55	5.79	0.18	2.38	0.06	48.78	0.80	100.78
6019	12.46	1.66	1.36	4.45	3.19	0.75	0.04	3.20	0.02	72.98	0.06	100.18
6018	12.34	1.42	1.43	6.36	2.19	0.46	0.03	1.03	0.01	75.26	0.05	100.57
6023	11.70	5.86	16.33	0.67	9.02	2.69	0.30	1.87	0.26	50.34	1.57	100.60
6024	13.68	7.15	14.05	0.03	9.97	7.08	0.19	2.81	0.07	45.06	1.01	101.11
6026	12.96	6.79	16.19	0.64	11.79	3.18	0.26	2.18	0.16	44.91	1.58	100.65
6029	13.74	5.96	17.34	0.47	11.44	3.88	0.24	2.10	0.10	44.15	1.35	100.76
6030	14.86	6.29	15.81	0.21	3.68	5.05	0.19	3.95	0.11	49.56	1.42	101.12
6043	13.40	0.04	1.18	8.25	1.16	0.39	N.D.	0.61	0.01	75.39	0.06	100.50
6044	12.79	2.85	17.05	0.16	3.72	4.55	0.18	4.05	0.24	53.46	1.80	100.86
6045	12.90	5.18	15.50	0.06	4.49	3.91	0.20	4.72	0.24	51.63	1.78	100.61
6046	13.92	3.67	16.65	0.10	1.94	3.65	0.20	5.56	0.23	52.90	1.77	100.59
6047	13.65	5.07	16.34	0.05	7.11	3.64	0.23	3.14	0.25	49.54	1.87	100.90
6048	16.79	3.56	13.10	0.93	7.44	6.63	0.13	2.19	0.22	48.77	1.18	100.95
6049	15.13	4.69	15.81	0.44	6.41	6.27	0.19	2.97	0.10	47.65	1.26	100.90
6050	16.09	2.81	11.89	1.35	7.44	4.35	0.14	0.81	0.07	54.16	0.81	99.92
6051	14.80	7.22	8.78	0.81	12.97	4.58	0.22	2.36	0.05	47.57	0.74	100.09
6052	14.53	4.72	15.77	0.09	6.43	3.00	0.18	3.64	0.30	48.62	2.57	99.84
6053	18.99	4.33	9.41	2.58	8.91	2.42	0.17	1.01	0.08	50.80	0.92	99.62
6054	14.70	9.34	8.59	1.05	15.82	3.78	0.28	1.67	0.06	44.09	0.71	100.08
6055	15.86	2.50	1.74	2.76	4.24	0.70	0.04	3.74	0.06	67.88	0.30	99.83
6056	15.14	6.65	10.83	0.05	4.55	5.94	0.25	4.09	0.06	52.34	0.83	100.72
6057	17.64	3.58	6.62	1.93	7.36	1.94	0.20	2.01	0.05	57.13	0.85	99.32
6058	18.03	5.08	8.78	0.59	5.90	2.56	0.16	4.54	0.06	53.70	0.84	100.25
6059	13.73	5.68	21.76	0.62	15.52	3.20	0.82	1.65	0.05	37.03	0.74	100.82
6060	13.75	9.50	12.40	0.41	11.06	4.26	0.28	1.41	0.08	46.39	0.95	100.50

*major oxides abundances are express in wt%

Appendix A: FeO by titration

Sample No.	FeO (wt%)
6005	1.69
6006	14.48
6042	7.59
6032	12.81
6034	1.36
6008	3.97
6014	5.22
6016	6.18
6012	8.37
6013	0.75
6020	0.55
6021	0.38
6036	1.69
6039	4.85
6017	9.06
6019	1.18
6018	0.61
6023	12.91
6024	10.61
6026	13.15
6029	14.19
6030	9.31
6043	0.76
6044	10.45
6045	9.52
6046	8.80
6047	12.63
6048	10.20
6049	11.00
6050	9.59
6051	7.28
6052	12.27
6053	7.88
6054	7.26
6055	1.19
6056	8.35
6057	4.97
6058	6.77
6059	18.23
6060	10.23

Appendix A: REE elements

Sample No.	Ce	Cs	Dy	Er	Eu	Gd	Hf	Ho	La	Lu	Nb	Nd	Pr
6005	27.26	0.63	1.15	0.65	0.64	1.44	2.99	0.23	13.89	0.09	2.64	12.17	3.29
6006	6.72	0.71	3.27	2.24	0.68	2.62	1.39	0.79	2.36	0.36	1.68	6.14	1.14
6042	25.05	1.17	1.10	0.63	0.59	1.42	3.34	0.23	12.55	0.09	2.66	11.31	3.00
6032	6.34	0.56	2.93	1.98	0.67	2.40	1.31	0.66	2.36	0.31	1.55	5.50	1.04
6034	23.84	0.83	1.10	0.60	0.51	1.51	3.49	0.24	11.82	0.10	2.70	11.19	2.95
6008	46.76	1.09	4.10	2.48	1.12	4.49	5.86	0.92	20.84	0.40	10.35	24.94	6.18
6014	23.11	0.52	2.51	1.48	0.90	2.87	3.17	0.56	9.82	0.22	6.21	13.87	3.18
6016	26.45	0.70	2.87	1.73	0.93	3.20	3.21	0.64	12.08	0.26	6.02	14.58	3.50
6012	11.92	0.84	4.77	3.35	1.20	4.34	2.40	1.14	4.60	0.49	3.27	10.05	1.96
6013	54.10	1.21	4.74	2.91	0.86	4.75	3.98	1.06	26.78	0.46	11.39	24.52	6.54
6020	49.01	1.30	4.35	2.74	0.72	4.25	3.92	0.97	23.44	0.43	11.34	22.56	6.04
6021	42.11	1.16	1.73	1.28	0.38	1.36	3.55	0.42	30.22	0.26	9.34	10.31	3.74
6036	182.73	1.20	6.50	4.04	1.58	7.63	6.63	1.43	91.14	0.65	13.55	76.19	22.03
6039	38.83	0.70	3.26	1.90	1.24	3.74	3.49	0.73	16.52	0.30	6.79	22.48	5.37
6017	8.13	0.65	2.86	1.94	0.69	2.40	1.39	0.67	3.28	0.32	1.96	6.25	1.26
6019	43.96	0.96	4.90	3.04	0.61	4.81	3.32	1.06	20.54	0.48	11.40	21.30	5.54
6018	36.62	1.35	3.67	2.30	0.52	3.61	3.04	0.81	17.21	0.38	8.39	17.16	4.56
6023	20.16	0.31	7.82	5.07	1.78	6.81	3.54	1.82	7.62	0.81	4.94	16.91	3.30
6024	4.56	0.20	3.08	2.13	0.52	2.18	1.80	0.72	1.72	0.35	2.27	3.78	0.72
6026	15.59	0.28	6.10	4.04	1.41	5.25	3.07	1.38	6.06	0.64	4.17	13.46	2.50
6029	9.54	0.38	4.31	2.92	0.90	3.47	2.06	1.00	3.80	0.47	2.94	7.35	1.51
6030	12.10	0.85	4.66	3.06	1.05	3.82	2.34	1.05	4.52	0.49	3.21	9.97	1.97
6043	39.33	1.29	2.34	1.48	0.64	2.57	3.53	0.51	20.03	0.26	11.65	16.42	4.52
6044	20.07	0.83	8.10	5.38	1.76	7.12	4.11	1.88	7.55	0.84	5.55	17.21	3.27
6045	23.41	0.77	8.44	5.75	1.94	7.33	4.04	1.99	9.16	0.88	5.50	19.05	3.75
6046	20.35	0.38	8.20	5.25	1.75	7.04	4.09	1.89	7.62	0.83	5.54	16.89	3.30
6047	23.21	0.49	8.73	5.51	2.14	7.72	4.20	1.98	9.12	0.84	5.73	19.08	3.74
6048	34.78	0.78	3.21	1.82	1.09	3.41	4.07	0.67	14.65	0.26	7.62	19.91	4.72
6049	13.23	1.52	4.63	3.06	1.04	4.00	2.40	1.04	5.24	0.48	3.42	10.44	2.05
6050	10.98	1.96	2.72	1.82	0.76	2.46	1.56	0.65	3.68	0.27	1.56	9.17	1.82
6051	6.78	2.32	2.81	1.88	0.61	2.25	1.46	0.65	2.74	0.32	1.52	5.46	1.08
6052	21.66	0.60	5.20	3.96	1.42	4.78	5.03	1.26	7.20	0.76	11.52	18.68	3.62
6053	8.98	2.11	3.81	2.84	0.60	2.80	1.89	0.95	4.26	0.44	1.86	6.02	1.31
6054	6.40	1.74	2.84	1.89	0.58	2.10	1.48	0.65	2.50	0.32	1.49	4.99	0.97
6055	22.15	2.02	0.85	0.40	0.57	1.29	2.91	0.17	10.72	0.06	2.11	10.51	2.73
6056	8.69	0.97	3.09	2.05	0.76	2.53	1.48	0.71	3.51	0.33	1.99	6.60	1.35
6057	7.28	2.80	2.50	1.70	0.48	1.78	1.67	0.57	2.80	0.27	1.66	4.70	1.06
6058	4.25	0.97	2.03	1.41	0.32	1.65	1.64	0.48	1.59	0.21	1.65	3.62	0.66
6059	5.08	0.90	2.32	1.59	0.62	1.99	1.26	0.55	1.83	0.26	1.55	4.88	0.90
6060	9.63	0.40	3.91	2.63	0.73	3.18	1.87	0.88	3.85	0.42	2.10	7.56	1.52

* REE abundances are express in ppm

Trace

Appendix A: ~~REE~~ elements

Sample No.	Rb	Sm	Sr	Ta	Tb	Th	Tm	U	Y	Yb	Zr
6005	42.41	2.07	181.64	N.D.	0.21	1.44	0.09	0.38	6.59	0.57	107.92
6006	12.86	2.09	38.30	N.D.	0.48	0.21	0.33	0.06	21.38	2.19	46.77
6042	50.31	2.08	123.31	N.D.	0.20	1.54	0.09	0.28	6.37	0.59	110.05
6032	1.21	1.81	181.50	N.D.	0.43	0.19	0.30	0.05	18.51	1.95	44.12
6034	58.34	1.97	195.04	N.D.	0.21	1.39	0.09	0.45	6.45	0.60	119.39
6008	53.79	4.96	140.95	0.82	0.68	3.72	0.37	1.12	24.72	2.41	199.89
6014	20.42	3.12	124.10	0.47	0.42	1.29	0.23	0.38	15.40	1.47	120.26
6016	31.95	3.36	183.17	0.47	0.49	1.55	0.25	0.40	17.24	1.59	123.53
6012	2.52	3.23	71.65	N.D.	0.74	0.45	0.48	0.13	31.34	2.98	81.17
6013	100.87	5.14	16.38	1.51	0.78	8.03	0.45	2.42	31.59	3.07	105.87
6020	94.51	4.71	47.45	1.38	0.72	7.51	0.43	2.37	29.34	2.77	103.21
6021	126.84	1.33	15.34	1.45	0.25	8.21	0.23	2.06	12.23	1.54	80.67
6036	55.08	10.98	72.28	0.98	1.08	7.77	0.62	0.61	37.08	3.94	207.08
6039	45.30	4.36	181.50	0.50	0.56	1.57	0.28	0.36	19.08	1.80	133.08
6017	5.66	1.90	102.72	N.D.	0.43	0.28	0.30	0.08	18.13	1.83	45.98
6019	83.65	4.81	53.80	1.53	0.80	6.75	0.48	1.92	34.06	3.04	78.75
6018	114.91	3.64	18.16	1.24	0.60	7.04	0.37	2.01	25.26	2.39	73.39
6023	19.01	5.40	58.90	0.36	1.19	0.62	0.76	0.16	48.42	4.98	120.21
6024	0.91	1.28	62.02	N.D.	0.43	0.28	0.32	0.08	19.72	2.14	57.96
6026	20.84	4.02	73.10	0.32	0.89	0.53	0.63	0.13	37.35	3.90	99.51
6029	15.80	2.45	59.89	N.D.	0.65	0.36	0.42	0.10	26.79	2.88	68.05
6030	4.62	3.13	173.25	0.32	0.69	0.40	0.46	0.11	27.63	3.07	76.73
6043	134.23	3.17	17.69	1.46	0.39	7.58	0.23	1.54	14.45	1.60	86.38
6044	3.50	5.52	71.46	0.46	1.25	0.70	0.81	0.19	50.05	5.13	133.05
6045	1.71	5.80	71.62	0.46	1.30	0.71	0.86	0.18	52.30	5.52	135.95
6046	2.13	5.49	79.80	0.46	1.22	0.70	0.80	0.18	49.76	5.20	134.19
6047	1.38	5.88	52.82	0.47	1.34	0.69	0.83	0.18	53.22	5.22	138.19
6048	31.04	3.94	105.06	0.59	0.52	1.70	0.27	0.43	18.12	1.78	151.57
6049	12.28	3.18	71.04	0.34	0.68	0.48	0.46	0.13	28.19	2.92	78.30
6050	49.28	2.45	45.79	N.D.	0.41	0.15	0.27	0.13	17.46	1.68	50.28
6051	32.92	1.75	95.55	N.D.	0.42	0.29	0.30	0.08	17.48	1.92	48.92
6052	2.12	4.97	23.76	0.81	0.80	2.26	0.64	0.54	33.22	4.53	183.88
6053	45.18	1.76	53.31	N.D.	0.55	0.30	0.42	0.09	26.19	2.72	63.84
6054	33.42	1.51	97.78	N.D.	0.40	0.28	0.30	0.08	17.56	2.00	49.33
6055	87.26	1.86	243.35	N.D.	0.17	1.06	0.06	0.30	4.58	0.37	100.52
6056	1.05	2.04	124.70	N.D.	0.48	0.29	0.34	0.08	18.91	2.04	51.60
6057	39.32	1.45	90.81	N.D.	0.36	0.25	0.26	0.09	14.46	1.66	54.44
6058	21.45	1.12	88.11	N.D.	0.31	0.28	0.22	0.08	13.08	1.37	55.75
6059	21.26	1.59	70.39	N.D.	0.35	0.18	0.24	0.07	15.75	1.67	41.97
6060	17.04	2.35	55.22	N.D.	0.56	0.37	0.41	0.10	24.80	2.76	64.70

* REE abundances are express in ppm

REE

Appendix A: ~~Trace~~ elements

Sample No.	Ce	Cs	Dy	Er	Eu	Gd	Hf	Ho	La	Lu	Nb	Nd	Pr	Rb	Sm
6005	27.26	0.63	1.15	0.65	0.64	1.44	2.99	0.23	13.89	0.09	2.64	12.17	3.29	42.41	2.07
6006	6.72	0.71	3.27	2.24	0.68	2.62	1.39	0.79	2.36	0.36	1.68	6.14	1.14	12.86	2.09
6042	25.05	1.17	1.10	0.63	0.59	1.42	3.34	0.23	12.55	0.09	2.66	11.31	3.00	50.31	2.08
6032	6.34	0.56	2.93	1.98	0.67	2.40	1.31	0.66	2.36	0.31	1.55	5.50	1.04	1.21	1.81
6034	23.84	0.83	1.10	0.60	0.51	1.51	3.49	0.24	11.82	0.10	2.70	11.19	2.95	58.34	1.97
6008	46.76	1.09	4.10	2.48	1.12	4.49	5.86	0.92	20.84	0.40	10.35	24.94	6.18	53.79	4.96
6014	23.11	0.52	2.51	1.48	0.90	2.87	3.17	0.56	9.82	0.22	6.21	13.87	3.18	20.42	3.12
6016	26.45	0.70	2.87	1.73	0.93	3.20	3.21	0.64	12.08	0.26	6.02	14.58	3.50	31.95	3.36
6012	11.92	0.84	4.77	3.35	1.20	4.34	2.40	1.14	4.60	0.49	3.27	10.05	1.96	2.52	3.23
6013	54.10	1.21	4.74	2.91	0.86	4.75	3.98	1.06	26.78	0.46	11.39	24.52	6.54	100.87	5.14
6020	49.01	1.30	4.35	2.74	0.72	4.25	3.92	0.97	23.44	0.43	11.34	22.56	6.04	94.51	4.71
6021	42.11	1.16	1.73	1.28	0.38	1.36	3.55	0.42	30.22	0.26	9.34	10.31	3.74	126.84	1.33
6036	182.73	1.20	6.50	4.04	1.58	7.63	6.63	1.43	91.14	0.65	13.55	76.19	22.03	55.08	10.98
6039	38.83	0.70	3.26	1.90	1.24	3.74	3.49	0.73	16.52	0.30	6.79	22.48	5.37	45.30	4.36
6017	8.13	0.65	2.86	1.94	0.69	2.40	1.39	0.67	3.28	0.32	1.96	6.25	1.26	5.66	1.90
6019	43.96	0.96	4.90	3.04	0.61	4.81	3.32	1.06	20.54	0.48	11.40	21.30	5.54	83.65	4.81
6018	36.62	1.35	3.67	2.30	0.52	3.61	3.04	0.81	17.21	0.38	8.39	17.16	4.56	114.91	3.64
6023	20.16	0.31	7.82	5.07	1.78	6.81	3.54	1.82	7.62	0.81	4.94	16.91	3.30	19.01	5.40
6024	4.56	0.20	3.08	2.13	0.52	2.18	1.80	0.72	1.72	0.35	2.27	3.78	0.72	0.91	1.28
6026	15.59	0.28	6.10	4.04	1.41	5.25	3.07	1.38	6.06	0.64	4.17	13.46	2.50	20.84	4.02
6029	9.54	0.38	4.31	2.92	0.90	3.47	2.06	1.00	3.80	0.47	2.94	7.35	1.51	15.80	2.45
6030	12.10	0.85	4.66	3.06	1.05	3.82	2.34	1.05	4.52	0.49	3.21	9.97	1.97	4.62	3.13
6043	39.33	1.29	2.34	1.48	0.64	2.57	3.53	0.51	20.03	0.26	11.65	16.42	4.52	134.23	3.17
6044	20.07	0.83	8.10	5.38	1.76	7.12	4.11	1.88	7.55	0.84	5.55	17.21	3.27	3.50	5.52
6045	23.41	0.77	8.44	5.75	1.94	7.33	4.04	1.99	9.16	0.88	5.50	19.05	3.75	1.71	5.80
6046	20.35	0.38	8.20	5.25	1.75	7.04	4.09	1.89	7.62	0.83	5.54	16.89	3.30	2.13	5.49
6047	23.21	0.49	8.73	5.51	2.14	7.72	4.20	1.98	9.12	0.84	5.73	19.08	3.74	1.38	5.88
6048	34.78	0.78	3.21	1.82	1.09	3.41	4.07	0.67	14.65	0.26	7.62	19.91	4.72	31.04	3.94
6049	13.23	1.52	4.63	3.06	1.04	4.00	2.40	1.04	5.24	0.48	3.42	10.44	2.05	12.28	3.18
6050	10.98	1.96	2.72	1.82	0.76	2.46	1.56	0.65	3.68	0.27	1.56	9.17	1.82	49.28	2.45
6051	6.78	2.32	2.81	1.88	0.61	2.25	1.46	0.65	2.74	0.32	1.52	5.46	1.08	32.92	1.75
6052	21.66	0.60	5.20	3.96	1.42	4.78	5.03	1.26	7.20	0.76	11.52	18.68	3.62	2.12	4.97
6053	8.98	2.11	3.81	2.84	0.60	2.80	1.89	0.95	4.26	0.44	1.86	6.02	1.31	45.18	1.76
6054	6.40	1.74	2.84	1.89	0.58	2.10	1.48	0.65	2.50	0.32	1.49	4.99	0.97	33.42	1.51
6055	22.15	2.02	0.85	0.40	0.57	1.29	2.91	0.17	10.72	0.06	2.11	10.51	2.73	87.26	1.86
6056	8.69	0.97	3.09	2.05	0.76	2.53	1.48	0.71	3.51	0.33	1.99	6.60	1.35	1.05	2.04
6057	7.28	2.80	2.50	1.70	0.48	1.78	1.67	0.57	2.80	0.27	1.66	4.70	1.06	39.32	1.45
6058	4.25	0.97	2.03	1.41	0.32	1.65	1.64	0.48	1.59	0.21	1.65	3.62	0.66	21.45	1.12
6059	5.08	0.90	2.32	1.59	0.62	1.99	1.26	0.55	1.83	0.26	1.55	4.88	0.90	21.26	1.59
6060	9.63	0.40	3.91	2.63	0.73	3.18	1.87	0.88	3.85	0.42	2.10	7.56	1.52	17.04	2.35

* trace element abundances express in ppm

Appendix A: Trace elements

Sample No.	Sr	Ta	Tb	Th	Tm	U	Y	Yb	Zr
6005	181.64	N.D.	0.21	1.44	0.09	0.38	6.59	0.57	107.92
6006	38.30	N.D.	0.48	0.21	0.33	0.06	21.38	2.19	46.77
6042	123.31	N.D.	0.20	1.54	0.09	0.28	6.37	0.59	110.05
6032	181.50	N.D.	0.43	0.19	0.30	0.05	18.51	1.95	44.12
6034	195.04	N.D.	0.21	1.39	0.09	0.45	6.45	0.60	119.39
6008	140.95	0.82	0.68	3.72	0.37	1.12	24.72	2.41	199.89
6014	124.10	0.47	0.42	1.29	0.23	0.38	15.40	1.47	120.26
6016	183.17	0.47	0.49	1.55	0.25	0.40	17.24	1.59	123.53
6012	71.65	N.D.	0.74	0.45	0.48	0.13	31.34	2.98	81.17
6013	16.38	1.51	0.78	8.03	0.45	2.42	31.59	3.07	105.87
6020	47.45	1.38	0.72	7.51	0.43	2.37	29.34	2.77	103.21
6021	15.34	1.45	0.25	8.21	0.23	2.06	12.23	1.54	80.67
6036	72.28	0.98	1.08	7.77	0.62	0.61	37.08	3.94	207.08
6039	181.50	0.50	0.56	1.57	0.28	0.36	19.08	1.80	133.08
6017	102.72	N.D.	0.43	0.28	0.30	0.08	18.13	1.83	45.98
6019	53.80	1.53	0.80	6.75	0.48	1.92	34.06	3.04	78.75
6018	18.16	1.24	0.60	7.04	0.37	2.01	25.26	2.39	73.39
6023	58.90	0.36	1.19	0.62	0.76	0.16	48.42	4.98	120.21
6024	62.02	N.D.	0.43	0.28	0.32	0.08	19.72	2.14	57.96
6026	73.10	0.32	0.89	0.53	0.63	0.13	37.35	3.90	99.51
6029	59.89	N.D.	0.65	0.36	0.42	0.10	26.79	2.88	68.05
6030	173.25	0.32	0.69	0.40	0.46	0.11	27.63	3.07	76.73
6043	17.69	1.46	0.39	7.58	0.23	1.54	14.45	1.60	86.38
6044	71.46	0.46	1.25	0.70	0.81	0.19	50.05	5.13	133.05
6045	71.62	0.46	1.30	0.71	0.86	0.18	52.30	5.52	135.95
6046	79.80	0.46	1.22	0.70	0.80	0.18	49.76	5.20	134.19
6047	52.82	0.47	1.34	0.69	0.83	0.18	53.22	5.22	138.19
6048	105.06	0.59	0.52	1.70	0.27	0.43	18.12	1.78	151.57
6049	71.04	0.34	0.68	0.48	0.46	0.13	28.19	2.92	78.30
6050	45.79	N.D.	0.41	0.15	0.27	0.13	17.46	1.68	50.28
6051	95.55	N.D.	0.42	0.29	0.30	0.08	17.48	1.92	48.92
6052	23.76	0.81	0.80	2.26	0.64	0.54	33.22	4.53	183.88
6053	53.31	N.D.	0.55	0.30	0.42	0.09	26.19	2.72	63.84
6054	97.78	N.D.	0.40	0.28	0.30	0.08	17.56	2.00	49.33
6055	243.35	N.D.	0.17	1.06	0.06	0.30	4.58	0.37	100.52
6056	124.70	N.D.	0.48	0.29	0.34	0.08	18.91	2.04	51.60
6057	90.81	N.D.	0.36	0.25	0.26	0.09	14.46	1.66	54.44
6058	88.11	N.D.	0.31	0.28	0.22	0.08	13.08	1.37	55.75
6059	70.39	N.D.	0.35	0.18	0.24	0.07	15.75	1.67	41.97
6060	55.22	N.D.	0.56	0.37	0.41	0.10	24.80	2.76	64.70

* trace element abundances express in ppm

APPENDIX B: LOCATION OF THE OUTCROPS AND THE GEOCHEMISTRY SAMPLES IN BIG FOUR LAKE AREA

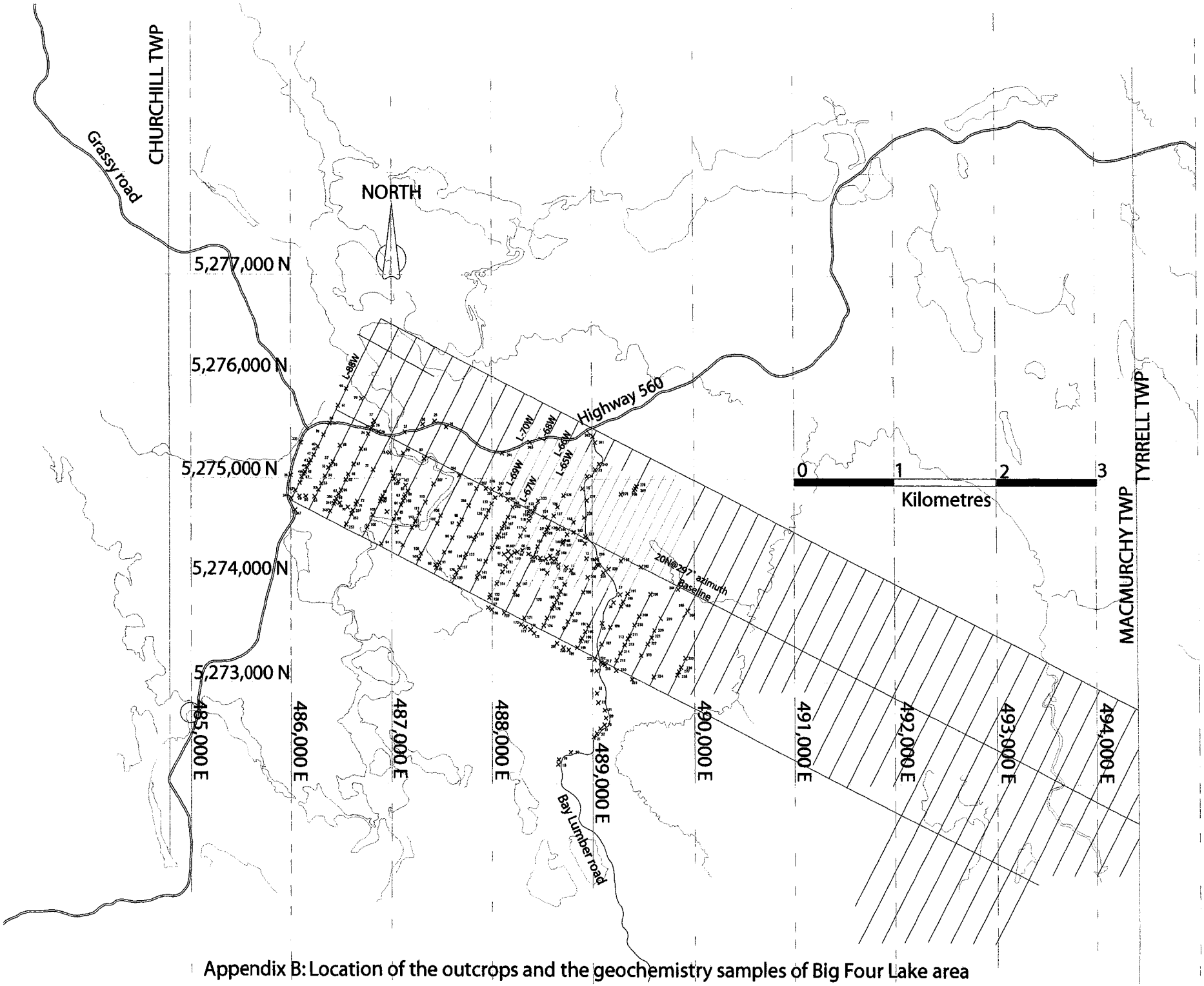

Appendix B: Location of the outcrops and the geochemistry samples of Big Four Lake area

Appendix B: Geochemistry sample with their associated location and unit

Geochemistry No.	GPS Coord.		Line	Station	Station No.	Unit
	17T	UTM				
6005	0488251 E	5274291 N			00-GL-04	2
6006	0488587 E	5274295 N			00-GL-09	1
6012	0487543 E	5275459 N			00-GL-24	3
6013	0487217 E	5275498 N			00-GL-27	4
6014	0489025 E	5272481 N			00-GL-21	1
6016	0489112 E	5272543 N			00-GL-23	1
6017	0489180 E	5273816 N			00-GL-36	7
6018	0486470 E	5275568 N			00-GL-38A	4
6019	0486470 E	5275568 N			00-GL-38B	4
6020	0487217 E	5275498 N			00-GL-27A	4
6021	0487217 E	5275498 N			00-GL-27B	4
6023	0486080 E	5274850 N	87+45 W	11+00 N	00-GL-49	1
6024	0486140 E	5274830 N	86+89 W	11+00 N	00-GL-50	1
6026	0486335 E	5275010 N	86+00 W	13+50 N	00-GL-54	1
6029	0487480 E	5274170 N	72+00 W	11+25 N	00-GL-91	1
6030	0486885 E	5274530 N	80+00 W	14+05 N	00-GL-99	6
6032	0486946 E	5274667 N			00-GL-101	1
6034	0487745 E	5274225 N	70+00 W	13+10 N	00-GL-135	2
6036	0489141E	5272662 N			00-GL-29	2
6039	0489062 E	5272812 N			00-GL-32	1
6042	0488587 E	5274295 N			00-GL-09	2
6043	0486391 E	5275583 N			00-GL-38B	1
6044	0486010 E	5275030 N			00-GL-28A	1
6045	0486010 E	5275030 N			00-GL-28B	1
6046	0486010 E	5275030 N			00-GL-28C	2
6047	0486010 E	5275030 N			00-GL-28C1	1
6048	0489109 E	5273591 N			00-GL-35	4
6049	0488449 E	5275417 N			00-GL-243	1

Geochemistry No.	Depth		Drill Hole No.	Unit
	from (m)	to (m)		
6050	245.20	245.50	CH99-01	1
6051	076.60	076.98	CH99-01	1
6052	361.60	361.83	CH99-01	1
6053	342,35	342.85	CH99-01	1
6054	129,8	130.25	CH00-08	1
6055	237,13	237.41	CH00-08	2
6056	011.00	011.35	CH00-08	1
6057	153,05	153.38	CH00-08	1
6058	144,76	145.06	CH00-07	1
6059	404,74	404.92	CH00-07	1
6060	010.63	010.83	CH00-11	1

Appendix B: Station location with their associated GPS and grid coordinates and units.

Station No.	GPS Coord. (17T)		Line	Station	Unit(s)
	UTM (E)	UTM (N)			
00-GL-01	488121	5274259			1
00-GL-01A	488159	5274289			1
00-GL-02	488160	5274218			1
00-GL-03	488223	5274279			1
00-GL-04	488252	5274285			1
00-GL-05	488301	5274303			1
	few m east of -05				1
00-GL-06	488369	5274266			1
00-GL-07	488436	5274239			1
00-GL-07A	488483	5274227			1
00-GL-08	488539	5274221			1
00-GL-09	488578	5274251			1
00-GL-09A	488591	5274228			2 and 6
00-GL-10	488638	5274219			2 and 6
	between -11 and -17				3
00-GL-11	488782	5274142			3
	few m west of -11				6
00-GL-12	488941	5274231			6 and 2?
00-GL-13	489026	5275108			1
00-GL-14	488954	5275034			5
00-GL-15	488900	5274912			5
00-GL-16	488661	5274168			3
00-GL-17	488737	5274137			3
00-GL-18	488651	5272193			1 and 3
00-GL-19	488653	5272228			3
	100 m N of -18				3
00-GL-20	488778	5272312			1
00-GL-21	489020	5272473			1
00-GL-22	489052	5272511			1
00-GL-23	489083	5272552			1
00-GL-24	487543	5275516			1
00-GL-25	487433	5275571			1
00-GL-26	487315	5275541			4
00-GL-27	487141	5275464			4 and 6
00-GL-28	486010	5275030			1
00-GL-29	489141	5272662			4 and 1?
00-GL-30	489124	5272594			1
	few m N of -30				1
00-GL-31	489130	5272737			1
	S of -31				1
00-GL-32	489065	5272812			1
00-GL-33	489051	5272904			2
00-GL-34	489047	5273131			2 or 4?
00-GL-35	489109	5273591			2a
00-GL-36	489209	5273797			7
00-GL-37	489274	5273869			7
00-GL-38	486391	5275583			4 and 6
00-GL-39	486326	5275433	88+00 W	15+30 N	4
00-GL-40	486269	5275321	88+00 W	15+94 N	4
00-GL-41	486231	5275242	88+00 W	15+00 N	4

Appendix B: Station location with their associated GPS and grid coordinates and units.

Station No.	GPS Coord. (17T)		Line	Station	Unit(s)
	UTM (E)	UTM (N)			
00-GL-42	486198	5275185	88+00 W	14+25 N	4
00-GL-43	486183	5275152	88+00 W	14+05 N	4
			88+00 W	13+75 N	1
00-GL-44	486161	5275112	88+05 W	13+55 N	1 and 4
00-GL-45	486143	5275073	87+75 W	13+50 N	1
			88+00 W	13+50 N	1
00-GL-46	486132	5275050	88+00 W	12+85 N	4
00-GL-47	486112	5275016	88+00 W	12+75 N	1
			88+00 W	12+50 N	1
00-GL-48	486090	5274960	88+00 W	12+00 N	1
00-GL-49	486100	5274860	87+45 W	11+00 N	1
00-GL-50	486150	5274827	86+89 W	11+00 N	1
00-GL-51	486241	5274822	86+00 W	11+40 N	1
00-GL-52	486277	5274897	86+00 W	12+15 N	1
00-GL-53	486306	5274954	86+00 W	12+80 N	1
	few m N				1
00-GL-54	486341	5275026	86+00 W	13+50 N	1 or 6?
			86+00 W	14+00 N	6
00-GL-55	486377	5275107	86+00 W	14+50 N	1
00-GL-56	486397	5275133	86+00 W	14+75 N	6
00-GL-57	486417	5275173	86+00 W	15+25 N	6
00-GL-58	486493	5275328	86+00 W	17+00 N	4
00-GL-59	486702	5275788			4
	486685	5275845			4
	close to the river				1
00-GL-60	486556	5275890	88+00 W	20+25 N	4
00-GL-61	486471	5275724	88+00 W	18+40 N	4
00-GL-62	486699	5275296	84+00 W	17+70 N	4
	under the bridge				4
	between L82W and L84W				4
00-GL-63	486633	5275156	84+00 W	16+07 N	1 or 6?
			84+00 W	15+80 N	4
00-GL-64	486574	5275044	84+00 W	15+00 N	6
00-GL-65	486551	5274993	84+00 W	14+50 N	6
			84+00W	14+07 N	6
			84+00 W	13+75 N	6
00-GL-66	486496	5274888	84+00 W	13+25 N	1 or 6?
			84+00 W	13+08 N	1 or 6?
00-GL-67	486478	5274848	84+00 W	12+87 N	1 or 6?
00-GL-68	486452	5274804	84+00 W	12+50 N	6
00-GL-69	486489	5274765	83+60 W	12+00 N	6
				12+00 N	6
00-GL-70	486573	5274725	82+30 W	12+00 N	6
00-GL-71	486653	5274753	82+00 W	12+75 N	6
00-GL-72	486664	5274778	82+00 W	13+00 N	6
00-GL-73	486822	5275086	82+00 W	16+50 N	4
				16+75N	4
			82+00 W	18+00 N	4 and 6
00-GL-74	486771	5275439	84+00 W	18+30 N	4
00-GL-75	486804	5275501	84+00 W	19+05 N (B.L.?)	4

Appendix B: Station location with their associated GPS and grid coordinates and units.

Station No.	GPS Coord. (17T)		Line	Station	Unit(s)
	UTM (E)	UTM (N)			
00-GL-76	486822	5275534	84+00 W	19+38 N	4
00-GL-77	486833	5275563	84+00 W	19+75 N	4
00-GL-78	486878	5275461	83+25 W	19+00 N	4
	under the bridge				4
	S side, on top of -27				4
00-GL-79	487123	5275247	80+00 W	19+25 N	4
00-GL-80	487327	5275202	78+00 W	19+75 N	4
00-GL-81	487167	5274882	78+00 W	16+20 N	1
00-GL-82	487143	5274841	78+00 W	15+68 N	1
00-GL-83	487133	5274821	78+00 W	15+63 N	1
00-GL-84	487099	5274750	78+00 W	14+75 N	1
00-GL-85	487053	5274662	78+00 W	13+65 N	1
00-GL-86	487022	5274602	78+00 W	13+00 N	6
00-GL-87	487679	5274556	72+00 W	15+65 N	1
00-GL-88	487698	5274605	72+00 W	16+20 N	6
00-GL-89	487606	5274420	72+00 W	14+00 N	2?
00-GL-90	487533	5274280	72+00 W	12+50 N	1
			72+00 W	12+35 N	1
00-GL-91	487482	5274175	72+00 W	11+25 N	1
00-GL-92	487456	5274124	72+00 W	10+75 N	1 or 7?
00-GL-93	487438	5274156	72+52 W	10+00 N	2
00-GL-94	486902	5274356	78+00 W	9+70 N	1
00-GL-95	486962	5274476	78+00 W	10+30 N	1
			76+00 W	12+25N	1
00-GL-96	487028	5274998	78+95 W	16+50 N	1
			79+40 W	16+50 N	1
00-GL-97	486917	5274833	80+00 W	14+50 N	1
00-GL-98	486899	5274801	80+00 W	14+30 N	1
00-GL-99	486892	5274778	80+00 W	14+05 N	6
			80+00 W	12+03 N	6
00-GL-100	486763	5274530	80+00 W	11+25 N	6
00-GL-101	486956	5274670			1
00-GL-102	487120	5274790	78+00 W	15+25 N	6
00-GL-103	487146	5274934	78+50 W	river	1
00-GL-104	487073	5274977	79+50 W	river	1
00-GL-105	486823	5274644	80+00 W	12+03 N	1
00-GL-106	487492	5274641	74+00 W	15+50 N	1
00-GL-107	487458	5274568	74+00 W	14+70 N	1
00-GL-108	487300	5274262	74+00 W	11+25 N	6
00-GL-109	487277	5274214	74+00 W	10+90 N	1
00-GL-110	487337	5274776	76+00 W	16+00 N	1
00-GL-111	487280	5274662	76+00 W	14+75 N	1
00-GL-112	487241	5274585	76+00 W	14+00 N	1
00-GL-113	487207	5274526	76+00 W	13+25 N	1
00-GL-114	487120	5274349	76+00 W	10+25 N	1
00-GL-115	488194	5274257	66+00 W	15+25 N	2
00-GL-116	488288	5274445	66+00 W	17+25 N	1
			66+00 W	17+43 N	6
00-GL-117	488322	5274511	66+00 W	18+00 N	1
00-GL-118	488366	5274596	66+00 W	19+00 N	1

Appendix B: Station location with their associated GPS and grid coordinates and units.

Station No.	GPS Coord. (17T)		Line	Station	Unit(s)
	UTM (E)	UTM (N)			
	from S19+30 N to S19+50 N				6
00-GL-119	488389	5274645	66+00 W	19+05 N	1
00-GL-120	488406	5274682	66+00 W	19+95 N	1
00-GL-121	488428	5274718	66+00 W	20+32 N	1
00-GL-122	488446	5274756	66+00 W	20+75 N	6
00-GL-123	488465	5274791	66+00 W	21+10 N	6
00-GL-124	488526	5274630	64+90 W	20+00 N	1
			64+25 W	20+00 N	6
00-GL-125	488714	5274844	64+00 W	22+75 N	6
00-GL-126	488658	5274733	64+00 W	21+50 N	1
			64+00 W	21+00 N	1
00-GL-127	488615	5274641	64+00 W	20+50 N	6
00-GL-128	488558	5274531	64+00 W	19+30 N	1
00-GL-129	488546	5274508	64+00 W	19+10 N	1
00-GL-130	487935	5274636	70+00 W	17+35 N	1
00-GL-131	487965	5274695	70+00 W	18+05 N	1
	few m N of -131				1
00-GL-132	488003	5274759	70+00 W	18+75 N	1 or 6?
00-GL-133	487839	5274448	70+00 W	15+20 N	1
00-GL-134	487823	5274410	70+00 W	14+80 N	1
00-GL-135	487744	5274258	70+00 W	13+10 N	2?
00-GL-136	487728	5274224	70+00 W	12+75 N	2
00-GL-137	487677	5274129	70+00 W	11+65 N	2a
00-GL-138	487651	5274079	70+00 W	11+10 N	6
00-GL-139	487625	5274017	68+00 W	10+75 N	1
			68+00 W	10+45 N	1
			68+00 W	10+75 N	1
			68+00 W	11+00 N	1
00-GL-140	487854	5274033	68+00 W	11+75 N	2
00-GL-141	487871	5274073	68+00 W	12+00 N	2
00-GL-142	487934	5274191	68+00 W	13+40 N	2
00-GL-143	488003	5274327	68+00 W	14+95 N	2
			68+00 W	15+25 N	2a
00-GL-144	488056	5274433	68+00 W	16+00 N	6
00-GL-145	488069	5274455	68+00 W	16+25 N	1
			68+00 W	16+50 N	1
00-GL-146	488098	5274514	68+00 W	17+00 N	1
00-GL-147	488122	5274563	68+00 W	17+50 N	1
00-GL-148	488161	5274633	68+00 W	18+30 N	1
00-GL-149	488524	5274462	64+00 W	18+50 N	1
			64+00 W	18+25 N	1
00-GL-150	488461	5274341	64+00 W	17+10 N	6
00-GL-151	488406	5274241	64+00 W	16+00 N	2
			64+00 W	15+50 N	2
00-GL-152	488134	5274140	66+00 W	13+90 N	2
00-GL-153	488105	5274088	66+00 W	13+25 N	2
00-GL-154	488048	5273973	66+00 W	12+00 N	2
			66+00 W	11+72 N	2
00-GL-155	487988	5273864	66+00 W	10+75 N	1
	few m S of -155				1

Appendix B: Station location with their associated GPS and grid coordinates and units.

Station No.	GPS Coord. (17T)		Line	Station	Unit(s)
	UTM (E)	UTM (N)			
00-GL-156	487976	5273834	66+00 W	10+50 N	1
00-GL-157	487965	5273737	65+65 W	9+50N	1
00-GL-158	488006	5273714	65+20 W	9+50 N	1
			65+40 W	9+50 N	1
00-GL-159	488126	5273682	64+00 W	10+85 N	2
00-GL-160	488228	5273891	64+00 W	12+10 N	2
00-GL-161	488266	5273963	64+00 W	12+87 N	2
00-GL-162	488810	5274585	62+00 W	20+95 N	1
00-GL-163	488812	5274484	62+00 W	20+00 N	1
00-GL-164	488748	5274461	62+00 W	19+50 N	1
00-GL-165	488713	5274396	62+00 W	18+80 N	1
00-GL-166	488707	5274383	62+00 W	18+70 N	1
00-GL-167	488702	5274373	62+00 W	18+50 N	1
00-GL-168	488659	5274294	62+00 W	17+65 N	1
00-GL-169	488548	5274081	62+00 W	15+25 N	2
00-GL-170	488417	5273818	62+00 W	12+25 N	1
00-GL-171	488324	5273639	62+00 W	10+25 N	1
			62+00 W	10+00 N	1
00-GL-172	488294	5273571	62+00 W	09+60 N	1
00-GL-173	488341	5273548	61+50 W	09+50 N	1
00-GL-174	488389	5273523	61+00 W	09+50 N	1 or 2?
00-GL-175	488423	5273489	60+53 W	10+00 N	1 or 2?
00-GL-176	488510	5273567	60+00 W	10+25 N	1
	from S10+25 N	to S10+75 N			1
00-GL-177	488550	5273641	60+00 W	11+25 N	1
00-GL-178	488601	5273733	60+00 W	12+40 N	2?
			60+00 W	12+50N	1
00-GL-179	488620	5273775	60+00 W	12+75 N	1
00-GL-180	488641	5273817	60+00 W	13+15 N	1
			60+00 W	13+30 N	1
00-GL-181	488668	5273872	60+00 W	13+90 N	2
00-GL-182	488687	5273907	60+00 W	14+25 N	2
			60+00 W	14+35 N	2
			60+00 W	14+75 N	2
00-GL-183	488721	5273971	60+00 W	15+00 N	2
			60+00 W	15+75 N	2
00-GL-184	488788	5274105	60+00 W	16+75 N	2
00-GL-185	488926	5274371	60+00 W	19+50 N	6
00-GL-186	489045	5274169	58+00 W	18+25 N	1?
00-GL-187	489098	5273387	54+00 W	11+50 N	2
00-GL-188	489181	5273555	54+00 W	13+40 N	2
00-GL-189	489288	5273765	54+00 W	15+75 N	6
00-GL-190	489312	5273808	54+00 W	16+25 N	7?
00-GL-191	489348	5273880	54+00 W	17+00 N	7?
00-GL-192	489483	5274143	54+00 W	19+90 N	1
00-GL-193	489287	5274200	56+00 W	19+60 N	1
00-GL-194	488964	5273569	56+00 W	12+50 N	2?
00-GL-195	488932	5273505	56+00 W	11+80 N	1?
00-GL-196	488902	5273446	56+00 W	11+05 N	1
00-GL-197	488888	5273415	56+00 W	10+90 N	1

Appendix B: Station location with their associated GPS and grid coordinates and units.

Station No.	GPS Coord. (17T)		Line	Station	Unit(s)
	UTM (E)	UTM (N)			
00-GL-198	488854	5273355	56+00 W	10+07 N	2
00-GL-199	488764	5273328	56+75 W	B.L.	1
00-GL-200	488712	5273353	57+25 W	B.L.	1
			57+68 W	B.L. (9+75 N)	2
00-GL-201	488648	5273390	58+00 W	9+80 N	2
00-GL-202	488727	5273546	58+00 W	11+20 N	1
00-GL-203	488757	5273603	58+00 W	11+90 N	1
00-GL-204	488798	5273682	58+00 W	10+80 N	1
00-GL-205	488904	5273890	57+95 W	15+15 N	2
00-GL-206	488950	5274039	58+05 W	16+75 N	1
00-GL-207	489062	5274160	57+95 W	18+30 N	6
00-GL-208	489573	5273876	52+00 W	18+00 N	2
00-GL-209	489464	5273661	52+00 W	15+70 N	7?
			52+00 W	15+15 N	7?
00-GL-210	489419	5273576	52+00 W	14+60 N	7?
00-GL-211	489368	5273473	52+00 W	13+45 N	2
00-GL-212	489353	5273443	52+00 W	13+10 N	2
00-GL-213	489323	5273382	52+00 W	12+48 N	2
00-GL-214	489281	5273302	52+00 W	11+50 N	1
00-GL-215	489246	5273227	52+75 W	10+75 N	1
00-GL-216	489128	5273184	52+75 W	10+00 N	1
00-GL-217	489110	5273197	52+85 W	10+00 N	1
00-GL-218	489086	5271321			1
	489554	5273918	drill road		2
00-GL-219	489678	5273645	50+00 W	16+58 N	2
00-GL-220			50+00 W	15+25 N	2
00-GL-221	489583	5273453	50+00 W	14+50 N	7
00-GL-222	489549	5273392	50+00 W	13+80 N	7?
00-GL-223	489490	5273279	50+00 W	12+48 N	2
00-GL-224	489609	5273074	48+00 W	11+25 N	2
00-GL-225	489925	5273252	46+00 W	14+08 N	2a
00-GL-226	489881	5273166	46+00 W	13+32 N	2a
			46+00 W	13+22 N	2a
00-GL-227	489858	5273123	46+00 W	12+75 N	1
			46+00 W	12+42 N	1
			46+ 00 W	11+75 N	1
00-GL-228	489847	5273093	46+00 W	11+70 N	1
			46+00 W	11+02 N	6
00-GL-229	489398	5273045	49+35 W	10+00 N	2?
			49+85 W	10+00 N	2?
			50+50 W	10+00 N	2
00-GL-230	489239	5273129	51+50 W	10+00 N	1?
00-GL-231	486095	5275325			2
	same location, more W				6
00-GL-232	489090	5273207	53+50 W	10+00 N	1 or 2?
00-GL-233	489033	5273237	53+55 W	10+00 N	1
00-GL-234	489112	5274090			7
00-GL-235	489093	5274153			6 and 7
00-GL-236	489048	5274219			1
00-GL-237	488929	5274437			1

Appendix B: Station location with their associated GPS and grid coordinates and units.

Station No.	GPS Coord. (17T)		Line	Station	Unit(s)
	UTM (E)	UTM (N)			
00-GL-238	488914	5274631			1
			62+00 W	20+80 N	1 and 5?
	10-12 m N of -238				5?
00-GL-239	488940	5274801			5
	50m S of -239				5
00-GL-240	489068	5275166			1
	15 B186m S of -241				1
00-GL 241	489024	5275378			1
00-GL-242	489002	5275435			6
00-GL-243	488449	5275417			1 and 6
00-GL-244	488146	5275309			1 and 6
00-GL-245	486047	5274886	87+99 W	10+77 N	1
00-GL-246	486010	5274806	87+98 W	10+26 N	1
00-GL-247	486045	5274693	87+07 W	09+50 N	1
00-GL-248	486396	5274686	84+00 W	11+00 N	6
			84+00 W	11+32 N	6
00-GL-249	486430	5274755	84+00 W	11+75 N	6
			84+00 W	11+80 N	6
00-GL-250	486441	5274778	84+00 W	12+10 N	6
			84+00 W	12+00 N	6
			84+00 W	12+00 N	6
00-GL-251	486622	5274691	82+10 W	12+00 N	6
00-GL-252	486605	5274657	82+00 W	11+60 N	1
00-GL-253	486554	5274555	82+00 W	10+50 N	2
			82+00 W	10+25 N	2
				09+80 N	2
00-GL-254	487675	5275042	73+90 W	20+00 N	4
00-GL-255	487852	5274906	72+00 W	19+50 N	4
			72+00 W	19+00 N	4
			72+00 W	18+40 N	4
00-GL-256	487771	5274745	72+00 W	17+75 N	6
00-GL-257	487945	5274912	71+10 W	20+00 N	4
00-GL-258	488001	5274884	70+50 W	20+00 N	4
00-GL-259	488035	5274822	70+00 W	19+55 N	6
			70+00 W	19+25 N	6
00-GL-260	488093	5274850	69+60 W	20+00 N	4
00-GL-261	488160	5274800	68+75 W	20+00 N	4
			68+25 W	20+00 N	4
00-GL-262	488208	5274726	68+00 W	19+50 N	1
			68+00 W	19+25 N	1
00-GL-263	488080	5274913	70+00 W	20+45 N	5
00-GL-264	489852	5273931	49+75 W	19+97 N	7
00-GL-265	489942	5273723	48+00 W	18+50 N	2
00-GL-266	489915	5273673	48+00 W	18+07 N	1
00-GL-267	487423	5274952	76+00 W	18+00 N	4
			76+00 W	18+25 N	4
			76+00 W	18+55 N	4
			76+00 W	19+15 N	4
00-GL-268	489418	5274904	57+00 W	26+50 N	1
00-GL-269	489430	5274918	57+00 W	26+70 N	1

Appendix B: Station location with their associated GPS and grid coordinates and units.

Station No.	GPS Coord. (17T)		Line	Station	Unit(s)
	UTM (E)	UTM (N)			
00-GL-270	489439	5274936	57+00 W	26+87 N	1
00-GL-271	489286	5274861	59+00 W	25+50N	1

APPENDIX C: TABLE OF RHYOLITES (UNITS 4 AND 6) GEOCHEMICAL DATA FOR LESHER'S RHYOLITE CLASSIFICATION

Appendix C: Geochemistry data for Lesher's classification

	South rhyolite						Red Dome rhyolite					
	(6005)	(6034)	(6036)	(6042)	(6048)	(6055)	(6018)	(6013)	(6019)	(6020)	(6021)	(6043)
SiO_2 (%)	71,22	66,91	77,72	69,20	52,16	71,02	76,49	75,61	75,25	75,81	75,52	75,90
TiO_2	0,37	0,30	0,15	0,38	1,26	0,31	0,05	0,09	0,06	0,11	0,05	0,06
Al_2O_3	16,12	20,14	13,26	16,71	17,96	16,59	12,54	14,30	12,85	13,77	14,40	13,49
Fe_2O_3	2,50	2,07	2,36	3,38	14,01	1,82	1,45	1,55	1,40	1,06	0,86	1,19
MnO	0,07	0,03	0,05	0,07	0,14	0,04	0,03	0,03	0,04	0,03	0,00	0,00
MgO	1,29	1,13	0,73	1,37	7,09	0,73	0,47	0,59	0,77	0,49	0,29	0,39
CaO	2,14	1,88	2,25	3,49	3,81	2,62	1,44	1,13	1,71	1,19	0,50	0,04
Na_2O	4,73	4,21	0,63	2,98	2,34	3,91	1,05	2,24	3,30	3,65	0,65	0,61
K_2O	1,48	3,27	2,82	2,33	0,99	2,89	6,46	4,44	4,59	3,87	7,72	8,31
P_2O_5	0,08	0,07	0,02	0,07	0,24	0,06	0,01	0,02	0,02	0,02	0,01	0,01
Rb (ppm)	42,41	58,34	55,08	50,31	31,04	87,26	114,91	100,87	83,65	94,51	126,84	134,23
Ba	253,27	484,57	395,33	359,43	165,03	486,11	664,93	376,66	654,23	503,26	466,80	754,88
Sr	181,64	195,04	72,28	123,31	105,06	243,35	18,16	16,38	53,80	47,45	15,34	17,69
Sc	5,00	4,00	6,00	5,00	18,00	4,00	1,00	2,00	2,00	3,00	1,00	1,00
Cr	56,24	58,50	53,20	55,26	76,18	22,67	53,83	50,43	56,12	51,66	50,94	63,88
La	13,89	11,82	91,14	12,55	14,65	10,72	17,21	26,78	20,54	23,44	30,22	20,03
Ce	27,26	23,84	182,73	25,05	34,78	22,15	36,62	54,10	43,96	49,01	42,11	39,33
Nd	12,17	11,19	76,19	11,31	19,91	10,51	17,16	24,52	21,30	22,56	10,31	16,42
Sm	2,07	1,97	10,98	2,08	3,94	1,86	3,64	5,14	4,81	4,71	1,33	3,17
Eu	0,64	0,51	1,58	0,59	1,09	0,57	0,52	0,86	0,61	0,72	0,38	0,64
Tb	0,21	0,21	1,08	0,20	0,52	0,17	0,60	0,78	0,80	0,72	0,25	0,39
Yb	0,57	0,60	3,94	0,59	1,78	0,37	2,39	3,07	3,04	2,77	1,54	1,60
Lu	0,09	0,10	0,65	0,09	0,26	0,06	0,38	0,46	0,48	0,43	0,26	0,26
Y	6,59	6,45	37,08	6,37	18,12	4,58	25,26	31,59	34,06	29,34	12,23	14,45
Zr	107,92	119,39	207,08	110,05	151,57	100,52	73,39	105,87	78,75	103,21	80,67	86,38
Th	1,44	1,39	7,77	1,54	1,70	1,06	7,04	8,03	6,75	7,51	8,21	7,58
U	0,38	0,45	0,61	0,28	0,43	0,30	2,01	2,42	1,92	2,37	2,06	1,54
Hf	2,99	3,49	6,63	3,34	4,07	2,91	3,04	3,98	3,32	3,92	3,55	3,53
Ta			0,98		0,59		1,24	1,51	1,53	1,38	1,45	1,46
La/La_{CHUR}	36,75	31,27	241,11	33,20	38,76	28,36	45,53	70,85	54,34	62,01	79,95	52,99
Yb/Yb_{CHUR}	2,29	2,41	15,82	2,37	7,15	1,49	9,60	12,33	12,21	11,12	6,18	6,43
(La/Yb)n	13,38	10,81	12,70	11,68	4,52	15,90	3,95	4,79	3,71	4,65	10,77	6,87
Eu*	10,00	9,50	52,50	9,75	20,71	8,75	21,43	28,57	28,57	27,14	8,00	17,08
Eu/Eu*	0,0640	0,0537	0,0301	0,0605	0,0526	0,0651	0,0243	0,0301	0,0214	0,0265	0,0475	0,0375
Zr/Y	16,38	18,51	5,58	17,28	8,36	21,95	2,91	3,35	2,31	3,52	6,60	5,98

note:
Eu* was calculated by linear interpolation between chondrite-normalized Sm and Tb.
n represents chondrite normalized values from Sum and McDonough, 1989.
Chondrite abundances used from Sun and McDonought, 1989.

APPENDIX D: NORMAT RESULTS AND GEOCHEMICAL DATA FROM AUR RESOURCES INC.

Appendix D: NORMAT results from Aur Resources Inc.

SAMPLE ID	LOCATION X	LOCATION Y	LOCATION Z		IFRAIS	ICHLO	IPARA	IPYRO	ISER		IPAF
R12968	485995,65	5275048,82	3367,511		95,6449966	0	4,26800013	0	0,087		41,1559982
R12969	485983,093	5275015,89	3363,728		16,2719994	0	65,0630035	0	18,6660004		12,8360004
R12970	486519,698	5275551,3	3375,38		93,3160019	0	2,57800007	0	4,10599995		83,4240036
R12972	487181,799	5275473,19	3352,213		58,0690002	0	3,03200007	0	38,8989983		32,8590012
R12973	486063,311	5275255,21	3351,286		68,3389969	0	13,7700005	0	17,8910008		92,2360001
R12974	487238,162	5275491,01	3352,788		94,5630035	0	2,83500004	0	2,602		72,9830017
R12975	488751,982	5274139,9	3387,239		62,5960007	0	24,7159996	0	12,6879997		46,6609993
R12976	488751	5274139	3387,239		37,7109985	0	29,8260002	0	32,4630013		64,7060013

SAMPLE ID	HOLE ID	FROM (m)			IFRAIS	ICHLO	IPARA	IPYRO	ISER		IPAF
B61208	CH99-01	142,5			100	0	0	0	0		85,1289978
B61209	CH99-01	278,1			100	0	0	0	0		5,44199991
B61210	CH99-01	290,2			100	0	0	0	0		0,72799999
B61211	CH99-01	294,3			0	98,3199997	0,74500001	0,60900003	0,32699999		3,37599993
B61212	CH99-01	298,1			100	0	0	0	0		-10,694109
B61213	CH99-01	304,4			100	0	0	0	0		-8,1529913
B61214	CH99-02	11			80,9700012	0	13,3190002	0	5,71099997		81,6669998
B61215	CH99-02	89			0	76,3990021	3,56900001	0,52499998	19,507		2,171
B61216	CH99-02	98			100	0	0	0	0		105,133003

Appendix D: Aur Resources Inc. geochemical data

SAMPLE_ID	UNIT	SIO2	TIO2	AL2O3	FE2O3	MGO	MNO
R12968	1	49,36	1,8	12,39	15,2	3,52	0,22
R12969	n/a	67,75	0,45	11,49	11,46	2,19	0,07
R12970	4	73,33	0,13	12,8	1,07	0,41	0,02
R12972	4	73,68	0,09	11,8	4,01	1,06	0,02
R12973	4	73,17	0,06	12,3	1,47	1,42	0,04
R12974	4	75,8	0,08	11,8	1,24	0,54	0,03
R12975	n/a	65,08	0,62	14,17	7,31	1,12	0,11
R12976	n/a	57,12	0,42	12,34	14,52	1,98	0,38

SAMPLE_ID	UNIT	CAO	NA2O	K2O	LOI	TOTAL	ZR
R12968	1	6,52	2,92	0,09	7,5	99,77	136
R12969	n/a	0,14	2,11	0,92	3,16	99,84	155
R12970	4	2,26	1,97	4,77	2,95	99,77	125
R12972	4	1,01	0,26	5,07	2,46	99,54	103
R12973	4	1,83	1,58	3,12	4,5	99,53	88
R12974	4	1,26	2,94	4,1	1,96	99,82	95
R12975	n/a	2,24	2,73	2,13	4,19	99,84	184
R12976	n/a	2,3	1,07	1,77	7,97	99,94	158

SAMPLE_ID	UNIT	Y	ZR_Y	AL2O3_TIO2	TIO2_ZR	RB	SR
R12968	1	35	3,9	7	132	13	125
R12969	n/a	21	7,4	26	29	37	27
R12970	4	30	4,2	98	10	110	63
R12972	4	36	2,9	131	9	116	29
R12973	4	34	2,6	205	7	90	25
R12974	4	32	3	148	8	90	25
R12975	n/a	25	7,4	23	34	69	108
R12976	n/a	20	7,9	29	27	63	66

SAMPLE_ID	UNIT	AU30	AG	CU	ZN
R12968	1	3	0,1	50	106
R12969	n/a	3	0,1	85	84
R12970	4	3	0,2	3	4
R12972	4	3	0,1	99	19
R12973	4	3	0,1	3	8
R12974	4	3	0,1	9	6
R12975	n/a	3	0,5	17	44
R12976	n/a	3	0,1	47	90

Appendix D: Aur Resources Inc. geochemical data

SAMPLE_ID	UNIT	SIO2	TIO2	AL2O3	FE2O3	MGO	MNO
B61208	1	41,17	0,68	13,08	12,11	4,41	0,54
B61209	n/a	71,9	0,04	0,36	9,25	0,64	0,26
B61210	1	36,26	0,04	0,38	18,64	1,9	0,65
B61211	n/a	39,15	2,74	13,12	33,57	3,64	0,09
B61212	1	26,41	0,03	0,52	14,82	0,23	0,38
B61213	1	26,94	0,05	0,61	11,63	0,46	0,45
B61214	2	74,73	0,09	10,67	3,81	0,47	0,14
B61215	n/a	57,06	1,09	13,13	18,34	4,5	0,06
B61216	n/a	74,84	0,02	0,23	14,67	0,9	0,93

SAMPLE_ID	UNIT	CAO	NA2O	K2O	LOI	TOTAL	ZR
B61208	1	9,58	0,7	1,39	15,9	99,69	50
B61209	n/a	9,67	0,04	0,02	6,27	98,46	14
B61210	1	19,17	0,01	0,02	11,7	88,78	15
B61211	n/a	1,52	0,03	0,02	5,59	99,79	167
B61212	1	30,47	0,01	0,01	19,6	92,5	15
B61213	1	30,83	0,02	0,01	20,2	91,22	19
B61214	2	1,2	2,9	1,89	3,19	99,14	88
B61215	n/a	0,16	0,13	1,08	4,25	99,91	73
B61216	n/a	0,32	0,05	0,02	7,81	99,8	14

SAMPLE_ID	UNIT	Y	ZR_Y	AL2O3_TIO2	TIO2_ZR	RB	SR
B61208	1	16	3,1	0	136	51	67
B61209	n/a	14	1	0	29	12	77
B61210	1	14	1,1	0	27	16	55
B61211	n/a	17	9,8	0	164	21	29
B61212	1	17	0,9	0	20	15	49
B61213	1	15	1,3	0	26	13	62
B61214	2	25	3,5	0	10	66	110
B61215	n/a	17	4,3	0	149	46	101
B61216	n/a	10	1,4	0	14	15	19

SAMPLE_ID	UNIT	AU30	AG	CU	ZN
B61208	1	3	0,1	7	46
B61209	n/a	3	0,3	14	8
B61210	1	3	1,2	59	19
B61211	n/a	3	0,1	9	83
B61212	1	3	0,8	40	15
B61213	1	3	0,3	36	16
B61214	2	3	0,1	4	11
B61215	n/a	3	0,1	7	82
B61216	n/a	3	0,2	7	22

APPENDIX E: EMP AND FORMULA RESULTS

FELDSPAR Mafic to Intermediate metavolcanic rocks

GROUNDMASS

	6046a	53a
SIO2	70.25	69.57
AL2O3	20.00	20.34
TIO2	.00	.00
CR2O3	.00	.00
FEO	.34	.38
MNO	.00	.00
MGO	.00	.00
K2O	.07	.07
CAO	.15	.56
NA2O	11.56	11.63
BAO	.00	.06
CL	.00	.00
F	.00	.00
TOTAL	102.37	102.61
TOT-O	102.37	102.61
Or	0.004	0.008
An	0.007	0.013
Alb	0.956	0.956

ASSOCIATED WITH FELDSPAR

	6046b
SIO2	68.26
AL2O3	19.98
TIO2	.00
CR2O3	.00
FEO	.19
MNO	.00
MGO	.00
K2O	.15
CAO	.28
NA2O	11.34
BAO	.00
CL	.00
F	.00
TOTAL	100.20
TOT-O	100.20
Or (%)	0.4
An (%)	2.6
Alb (%)	96.3

FELDSPAR South Rhyolite

GROUNDMASS

	6034a	6034b	6034c	6048a	6048b
SIO2	70.07	70.55	69.62	68.97	67.56
AL2O3	19.99	19.75	19.89	19.55	20.71
TIO2	.00	.00	.00	.00	.00
CR2O3	.00	.00	.00	.00	.00
FEO	.00	.03	.03	.09	.23
MNO	.00	.00	.00	.00	.00
MGO	.00	.00	.00	.00	.00
K2O	.01	.06	.12	.05	.88
CAO	.02	.05	.03	.13	.37
NA2O	11.65	11.42	11.79	11.77	11.25
BAO	.00	.00	.00	.01	.04
CL	.00	.00	.00	.00	.00
F	.00	.00	.00	.00	.00
TOTAL	101.74	101.86	101.48	100.57	101.04
TOT-O	101.74	101.86	101.48	100.57	101.04
Or (%)	0.1	0.3	0.7	0.3	4.9
An (%)	0.1	0.2	0.1	0.6	1.7
Alb (%)	96.7	94.6	98.3	99.1	94.9

FELDSPAR Red Dome rhyolite

VEINS

	6018a	27a
SIO2	65.49	64.65
AL2O3	18.94	19.13
TIO2	.00	.00
CR2O3	.00	.00
FEO	.07	.28
MNO	.00	.00
MGO	.00	.00
K2O	16.59	16.57
CAO	.01	.02
NA2O	.35	.27
BAO	.14	.35
CL	.00	.00
F	.00	.00
---	---	---
TOTAL	101.59	101.27
---	---	---
TOT-O	101.59	101.27
Or (%)	96.5	97.0
An (%)	0.0	0.1
Alb (%)	3.1	2.4

GROUNDMASS

	6018b	6018c	6019a	6019b	27b
SIO2	65.80	65.35	64.74	65.39	70.70
AL2O3	18.92	18.90	19.31	19.15	20.24
TIO2	.00	.00	.00	.00	.00
CR2O3	.00	.00	.00	.00	.00
FEO	.25	.15	.08	.00	.16
MNO	.00	.00	.00	.00	.00
MGO	.00	.00	.00	.00	.00
K2O	16.58	16.64	16.40	16.66	.05
CAO	.02	.00	.00	.00	.03
NA2O	.19	.18	.32	.33	12.39
BAO	.31	.20	.47	.50	.00
CL	.00	.00	.00	.00	.00
F	.00	.00	.00	.00	.00
---	---	---	---	---	---
TOTAL	102.07	101.42	101.32	102.03	103.57
---	---	---	---	---	---
TOT-O	102.07	101.42	101.32	102.03	103.57
Or (%)	96.1	97.0	95.8	96.7	0.3
An (%)	0.1	1.0	0.0	0.0	0.1
Alb (%)	1.7	1.6	2.8	2.9	101.5

FELDSPAR

	6034a	6034b	6034c	6048a	6048b	6046a	6046b	GL53a	6018a	GL27a
SIO2	70.07	70.55	69.62	68.97	67.56	70.25	68.26	69.57	65.49	64.65
AL2O3	19.99	19.75	19.89	19.55	20.71	20.00	19.98	20.34	18.94	19.13
TIO2	0.00	0.00	0.00	0.00	0.00	0.00	0.00	0.00	0.00	0.00
CR2O3	0.00	0.00	0.00	0.00	0.00	0.00	0.00	0.00	0.00	0.00
FEO	0.00	0.03	0.03	0.09	0.23	0.34	0.19	0.38	0.07	0.28
MNO	0.00	0.00	0.00	0.00	0.00	0.00	0.00	0.00	0.00	0.00
MGO	0.00	0.00	0.00	0.00	0.00	0.00	0.00	0.00	0.00	0.00
K2O	0.01	0.06	0.12	0.05	0.88	0.07	0.15	0.07	16.59	16.57
CAO	0.02	0.05	0.03	0.13	0.37	0.15	0.28	0.56	0.01	0.02
NA2O	11.65	11.42	11.79	11.77	11.25	11.56	11.34	11.63	0.35	0.27
BAO	0.00	0.00	0.00	0.01	0.04	0.00	0.00	0.06	0.14	0.35
CL	0.00	0.00	0.00	0.00	0.00	0.00	0.00	0.00	0.00	0.00
F	0.00	0.00	0.00	0.00	0.00	0.00	0.00	0.00	0.00	0.00
O=CL	0.00	0.00	0.00	0.00	0.00	0.00	0.00	0.00	0.00	0.00
O=F	0.00	0.00	0.00	0.00	0.00	0.00	0.00	0.00	0.00	0.00
TOTAL	101.74	101.86	101.48	100.57	101.04	102.37	100.20	102.61	101.59	101.27
SI4+	3.001	3.015	2.995	2.996	2.941	2.996	2.978	2.971	2.985	2.967
AL3+	1.009	0.995	1.008	1.001	1.062	1.005	1.027	1.024	1.017	1.035
TI4+	0.000	0.000	0.000	0.000	0.000	0.000	0.000	0.000	0.000	0.000
CR3+	0.000	0.000	0.000	0.000	0.000	0.000	0.000	0.000	0.000	0.000
FE2+	0.000	0.001	0.001	0.003	0.008	0.012	0.007	0.014	0.003	0.011
MN2+	0.000	0.000	0.000	0.000	0.000	0.000	0.000	0.000	0.000	0.000
MG2+	0.000	0.000	0.000	0.000	0.000	0.000	0.000	0.000	0.000	0.000
K+	0.001	0.003	0.007	0.003	0.049	0.004	0.008	0.004	0.965	0.970
CA2+	0.001	0.002	0.001	0.006	0.017	0.007	0.013	0.026	0.000	0.001
NA+	0.967	0.946	0.983	0.991	0.949	0.956	0.959	0.963	0.031	0.024
BA2+	0.000	0.000	0.000	0.000	0.001	0.000	0.000	0.001	0.003	0.006
CL-	0.000	0.000	0.000	0.000	0.000	0.000	0.000	0.000	0.000	0.000
F-	0.000	0.000	0.000	0.000	0.000	0.000	0.000	0.000	0.000	0.000
O2-	8.000	8.000	8.000	8.000	8.000	8.000	8.000	8.000	8.000	8.000
CATSUM	4.979	4.962	4.996	5.001	5.027	4.981	4.992	5.001	5.004	5.013
AN SUM	8	8	8	8	8	8	8	8	8	8

-Formula contents on a basis of 8 anions

FELDSPAR

	6018b	6018c	6019a	6019b	GL27b
SIO2	65.80	65.35	64.74	65.39	70.70
AL2O3	18.92	18.90	19.31	19.15	20.24
TIO2	0.00	0.00	0.00	0.00	0.00
CR2O3	0.00	0.00	0.00	0.00	0.00
FEO	0.25	0.15	0.08	0.00	0.16
MNO	0.00	0.00	0.00	0.00	0.00
MGO	0.00	0.00	0.00	0.00	0.00
K2O	16.58	16.64	16.40	16.66	0.05
CAO	0.02	0.00	0.00	0.00	0.03
NA2O	0.19	0.18	0.32	0.33	12.39
BAO	0.31	0.20	0.47	0.50	0.00
CL	0.00	0.00	0.00	0.00	0.00
F	0.00	0.00	0.00	0.00	0.00
O=CL	0.00	0.00	0.00	0.00	0.00
O=F	0.00	0.00	0.00	0.00	0.00

TOTAL	102.07	101.42	101.32	102.03	103.57
SI4+	2.988	2.986	2.966	2.976	2.986
AL3+	1.013	1.018	1.043	1.027	1.008
TI4+	0.000	0.000	0.000	0.000	0.000
CR3+	0.000	0.000	0.000	0.000	0.000
FE2+	0.009	0.006	0.003	0.000	0.006
MN2+	0.000	0.000	0.000	0.000	0.000
MG2+	0.000	0.000	0.000	0.000	0.000
K+	0.961	0.970	0.958	0.967	0.003
CA2+	0.001	0.000	0.000	0.000	0.001
NA+	0.017	0.016	0.028	0.029	1.015
BA2+	0.006	0.004	0.008	0.009	0.000
CL-	0.000	0.000	0.000	0.000	0.000
F-	0.000	0.000	0.000	0.000	0.000
O2-	8.000	8.000	8.000	8.000	8.000
CATSUM	4.994	4.998	5.007	5.009	5.018
AN SUM	8	8	8	8	8

-Formula contents on a basis of 8 anions

CHLORITE Mafic to Intermediate metavolcanic rocks

VEINS

	6024a	6024b	6024c	6024d	6024e	6056a
SIO2	27.15	26.95	27.71	24.93	26.16	27.71
AL2O3	17.78	18.43	17.64	20.37	20.17	18.33
TIO2	.00	.04	.01	.00	.04	.00
CR2O3	.05	.01	.00	.00	.00	.00
FEO	26.40	26.90	25.73	28.07	24.67	24.99
MNO	.25	.26	.13	.14	.33	.55
MGO	15.91	15.40	16.62	13.38	16.19	16.14
K2O	.02	.00	.00	.00	.00	.00
CAO	.02	.03	.04	.20	.05	.05
NA2O	.07	.02	.01	.03	.01	.00
BAO	.00	.00	.00	.00	.00	.00
CL	.02	.00	.02	.00	.01	.02
F	.01	.01	.04	.01	.03	.00
TOTAL	87.68	88.05	87.95	87.13	87.66	87.79
TOT-O	87.67	88.05	87.93	87.13	87.65	87.79

ALTERED GROUNDMASS

	6046a	53a
SIO2	28.01	30.57
AL2O3	15.43	14.15
TIO2	.07	.00
CR2O3	.00	.03
FEO	28.18	25.99
MNO	.57	.50
MGO	14.73	16.71
K2O	.01	.01
CAO	.19	.21
NA2O	.06	.04
BAO	.00	.00
CL	.10	.01
F	.00	.00
TOTAL	87.35	88.22
TOT-O	87.33	88.22

GROUNDMASS

	6032a
SIO2	27.33
AL2O3	18.56
TIO2	.00
CR2O3	.00
FEO	27.69
MNO	.43
MGO	14.78
K2O	.00
CAO	.09
NA2O	.00
BAO	.00
CL	.01
F	.04
TOTAL	88.93
TOT-O	88.91

CHLORITE South rhyolite

AMYGDULES

	6048a	6048b	6048c	6048d	6048e	6048f	6048g	6048h	6048i
SIO2	24.99	24.81	25.08	25.25	25.47	25.82	25.34	25.17	25.39
AL2O3	22.19	22.36	22.13	22.83	22.48	22.16	20.99	22.39	22.71
TIO2	.02	.05	.00	.01	.03	.05	.03	.03	.01
CR2O3	.01	.01	.00	.21	.00	.01	.03	.00	.05
FEO	25.55	26.13	25.44	24.97	24.97	25.08	28.17	26.18	25.54
MNO	.25	.20	.25	.15	.19	.12	.28	.26	.21
MGO	14.38	14.16	14.23	14.04	14.16	14.20	13.12	13.97	13.96
K2O	.02	.00	.03	.00	.05	.02	.01	.01	.01
CAO	.03	.10	.51	.04	.02	.03	.17	.20	.26
NA2O	.03	.00	.06	.00	.00	.00	.03	.02	.06
BAO	.00	.00	.00	.00	.00	.03	.00	.00	.00
CL	.02	.01	.02	.00	.01	.01	.01	.03	.01
F	.05	.01	.03	.03	.01	.04	.05	.00	.06
TOTAL	87.54	87.84	87.78	87.53	87.39	87.57	88.23	88.26	88.27
TOT-O	87.51	87.83	87.76	87.52	87.38	87.55	88.21	88.25	88.24

ASSOCIATED WITH FELDSPAR

	6048j	6048k	6034a
SIO2	26.06	25.88	25.34
AL2O3	22.54	21.36	22.93
TIO2	.77	.04	.03
CR2O3	.27	.00	.01
FEO	24.16	25.75	27.56
MNO	.11	.15	.16
MGO	13.55	14.15	11.48
K2O	.36	.04	.06
CAO	.08	.02	.01
NA2O	.02	.20	.13
BAO	.00	.10	.00
CL	.02	.00	.00
F	.09	.04	.01
TOTAL	88.03	87.73	87.72
TOT-O	87.99	87.71	87.72

GROUNDMASS

	6034b
SIO2	24.88
AL2O3	22.28
TIO2	.03
CR2O3	.02
FEO	28.22
MNO	.04
MGO	11.64
K2O	.09
CAO	.01
NA2O	.18
BAO	.00
CL	.00
F	.00
TOTAL	87.39
TOT-O	87.39

CHLORITE Red Dome rhyolite

VEINS

	32a	32b	32c	32d	32e	32f
SIO2	24.25	23.80	26.05	24.54	25.15	25.13
AL2O3	23.02	20.74	19.53	20.77	19.99	21.80
TIO2	.01	.01	.00	.00	.00	.00
CR2O3	.03	.00	.00	.03	.00	.01
FEO	34.27	38.74	30.47	35.32	31.47	33.17
MNO	.05	.05	.05	.10	.08	.09
MGO	7.79	6.47	13.03	9.36	11.78	9.17
K2O	.06	.02	.00	.00	.01	.02
CAO	.03	.01	.00	.04	.04	.06
NA2O	.04	.03	.01	.01	.02	.02
BAO	.10	.01	.00	.00	.00	.06
CL	.00	.02	.01	.01	.01	.02
F	.00	.04	.06	.01	.00	.00
TOTAL	89.65	89.94	89.21	90.19	88.55	89.55
TOT-O	89.65	89.92	89.18	90.18	88.55	89.55

	6018a
SIO2	26.70
AL2O3	21.05
TIO2	.00
CR2O3	.00
FEO	24.01
MNO	.13
MGO	17.07
K2O	.00
CAO	.04
NA2O	.01
BAO	.00
CL	.00
F	.07
TOTAL	89.08
TOT-O	89.05

	27a	27b
SIO2	24.28	24.38
AL2O3	20.86	20.78
TIO2	.03	.05
CR2O3	.00	.01
FEO	34.49	33.56
MNO	.10	.15
MGO	9.84	10.08
K2O	.01	.04
CAO	.08	.02
NA2O	.01	.01
BAO	.05	.01
CL	.00	.02
F	.00	.00
TOTAL	89.75	89.11
TOT-O	89.75	89.11

CHLORITE Intrusive rocks (Matachewan)

GROUNDMASS

	6030a
SIO2	26.98
AL2O3	16.86
TIO2	.00
CR2O3	.03
FEO	30.16
MNO	.43
MGO	13.22
K2O	.03
CAO	.12
NA2O	.02
BAO	.00
CL	.02
F	.02
TOTAL	87.89
TOT-O	87.88

ALTERED GROUNDMASS

	70a	70b
SIO2	26.66	26.41
AL2O3	19.11	19.12
TIO2	.02	.00
CR2O3	.02	.01
FEO	28.03	28.28
MNO	.41	.44
MGO	14.38	14.38
K2O	.02	.00
CAO	.04	.04
NA2O	.00	.00
BAO	.00	.00
CL	.01	.00
F	.00	.00
TOTAL	88.70	88.68
TOT-O	88.70	88.68

SERICITE Mafic to intermediate metavolcanic rocks

GROUNDMASS

	53a
SIO2	51.28
AL2O3	30.03
TIO2	.08
CR2O3	.00
FEO	3.37
MNO	.04
MGO	.86
K2O	9.48
CAO	.32
NA2O	1.88
BAO	.16
CL	.00
F	.00
-------	-------
TOTAL	97.50
-------	-------
TOT-O	97.50

SERICITE South Rhyolite

ASSOCIATED WITH FELDSPAR

	6034a	6034b	6034c	6048a	6048b
SIO2	48.13	47.94	48.23	47.55	49.79
AL2O3	34.51	34.94	34.08	32.47	31.55
TIO2	.08	.11	.09	.09	.05
CR2O3	.00	.00	.00	.00	.00
FEO	.99	1.15	1.33	2.88	2.59
MNO	.00	.00	.06	.00	.00
MGO	.88	.81	.94	1.02	1.12
K2O	9.78	9.54	9.78	10.35	9.69
CAO	.01	.06	.03	.02	.02
NA2O	.42	.53	.49	.35	.91
BAO	.00	.07	.10	.05	.15
CL	.00	.02	.00	.01	.00
F	.10	.15	.11	.10	.07
TOTAL	94.90	95.32	95.24	94.89	95.94
TOT-O	94.86	95.25	95.19	94.85	95.91

GROUNDMASS

	6034d
SIO2	47.24
AL2O3	34.98
TIO2	.11
CR2O3	.03
FEO	.94
MNO	.00
MGO	.53
K2O	9.04
CAO	.04
NA2O	1.32
BAO	.13
CL	.00
F	.11
TOTAL	94.47
TOT-O	94.42

SERICITE Red Dome rhyolite

GROUNDMASS

	32a	27a	6019a
SIO2	48.71	47.06	50.87
AL2O3	33.16	33.02	29.38
TIO2	.09	.25	.17
CR2O3	.00	.00	.02
FEO	2.50	2.80	3.82
MNO	.02	.00	.00
MGO	1.17	1.21	1.54
K2O	11.08	10.67	10.70
CAO	.01	.00	.04
NA2O	.13	.08	.09
BAO	.02	.00	.10
CL	.02	.01	.01
F	.16	.09	.21
TOTAL	97.07	95.19	96.95
TOT-O	97.00	95.15	96.86

VEIN

	27b
SIO2	48.60
AL2O3	32.43
TIO2	.17
CR2O3	.01
FEO	3.32
MNO	.00
MGO	1.52
K2O	10.86
CAO	.00
NA2O	.05
BAO	.00
CL	.01
F	.14
TOTAL	97.11
TOT-O	97.05

CARBONATES Mafic to intermediate metavolcanic rocks

VEINS

	6024a	6024b	6056a	6056b	6056c	6056d
CAO	58.35	58.81	58.37	56.44	55.25	56.80
FEO	.05	.05	.32	.00	.37	.45
MNO	.15	.05	.13	.06	.28	.55
MGO	.00	.00	.00	.01	.04	.20
SRO	.00	.01	.00	.01	.00	.00
BAO	.04	.04	.02	.00	.01	.03
NA2O	.01	.02	.01	.00	.03	.03
SIO2	.01	.00	.07	.04	.21	2.12
TOTAL	58.61	58.98	58.92	56.56	56.19	60.18

CARBONATES South rhyolite

AMYGDULES

	6048a	6048b	6048c	6048d	6048e	6048f	6048g	6048h	6048i	6048j	6048k	6048l	6048m
CAO	49.17	55.66	57.11	54.71	55.07	54.58	55.87	55.13	56.84	55.49	57.98	57.52	58.12
FEO	3.26	.31	.49	.51	.52	.84	1.33	1.40	.52	1.80	.92	.34	1.72
MNO	.79	.18	.98	.21	.16	2.36	.98	1.96	.96	.98	1.04	1.00	.86
MGO	1.91	.04	.18	.24	.21	.28	.24	.38	.20	.33	.26	.14	.30
SRO	.00	.00	.04	.00	.00	.00	.00	.00	.00	.00	.02	.03	.00
BAO	.00	.00	.00	.01	.00	.02	.00	.00	.00	.02	.00	.00	.00
NA2O	.01	.01	.00	.02	.04	.04	.01	.00	.00	.01	.00	.00	.00
SIO2	3.35	.79	.21	2.70	2.62	1.84	.00	.01	.03	.00	.13	.03	.00
TOTAL	58.49	56.99	59.01	58.40	58.62	59.96	58.43	58.88	58.55	58.63	60.35	59.06	61.00

GROUNDMASS

	6034a	6034b	6034c	6034d	6034e	6034f	6034g
CAO	56.81	34.01	31.92	58.06	29.55	28.16	29.17
FEO	.54	2.88	1.68	.21	11.33	10.48	8.91
MNO	.52	.67	.79	.25	.51	1.35	1.16
MGO	.13	16.43	19.00	.12	13.37	12.26	13.52
SRO	.00	.00	.00	.00	.03	.00	.00
BAO	.00	.00	.04	.06	.01	.00	.00
NA2O	.00	.02	.03	.00	.04	.05	.05
SIO2	.12	.67	.04	.04	.22	3.88	1.37
TOTAL	58.12	54.68	53.50	58.74	55.06	56.18	54.18

CARBONATES Red Dome rhyolite

GROUNDMASS

	32a	32b	32c
CAO	28.54	28.80	28.26
FEO	10.65	10.40	7.10
MNO	1.52	1.35	1.15
MGO	13.49	13.60	16.64
SRO	.00	.01	.00
BAO	.01	.00	.00
NA2O	.00	.00	.04
SIO2	.00	.01	.36
TOTAL	54.21	54.17	53.55

VEINS

	32d	32e
CAO	28.64	28.74
FEO	10.42	6.47
MNO	1.31	1.19
MGO	13.90	16.90
SRO	.00	.01
BAO	.00	.06
NA2O	.02	.01
SIO2	.03	.00
TOTAL	54.32	53.38

	6019a	6019b	6019c	6019d	6019e
CAO	29.55	29.53	28.52	29.51	29.94
FEO	17.46	15.75	19.95	10.27	11.87
MNO	.46	.09	.36	.54	.47
MGO	8.73	10.21	8.37	14.25	12.79
SRO	.04	.19	.03	.18	.20
BAO	.00	.01	.03	.01	.03
NA2O	.03	.06	.00	.00	.00
SIO2	.00	.04	.00	.00	.04
TOTAL	56.27	55.88	57.26	54.76	55.34

	27a	27b	27c	27d	27e
CAO	55.82	54.06	53.21	56.85	59.03
FEO	.58	.82	.75	.80	.87
MNO	1.04	1.11	1.17	1.13	1.23
MGO	.11	.10	.18	.14	.16
SRO	.00	.04	.05	.03	.03
BAO	.02	.00	.00	.01	.05
NA2O	.01	.06	.00	.00	.01
SIO2	.00	.04	.01	.03	.00
TOTAL	57.58	56.23	55.37	58.99	61.38

	6018a	6018b	6018c	6018d
CAO	54.77	54.48	55.98	55.82
FEO	.27	1.06	.51	.22
MNO	.77	1.39	.65	.40
MGO	.07	.36	.23	.13
SRO	.00	.00	.01	.00
BAO	.03	.00	.00	.03
NA2O	.00	.01	.02	.00
SIO2	.09	.20	.02	.05
TOTAL	56.00	57.50	57.42	56.65

CARBONATES Intrusive rocks (Matachewan)

GROUNDMASS

	6030a
CAO	55.04
FEO	.65
MNO	.25
MGO	.16
SRO	.01
BAO	.01
NA2O	.00
SIO2	.58
TOTAL	56.70

CARBONATES

	6024a	6024b	6056a	6056b	6056c	6056d	6030a	GL32a	GL32b	GL32c
CAO	58.35	58.81	58.37	56.44	55.25	56.80	55.04	28.54	28.80	28.26
FEO	0.05	0.05	0.32	0.00	0.37	0.45	0.65	10.65	10.40	7.10
MNO	0.15	0.05	0.13	0.06	0.28	0.55	0.25	1.52	1.35	1.15
MGO	0.00	0.00	0.00	0.01	0.04	0.20	0.16	13.49	13.60	16.64
SRO	0.00	0.01	0.00	0.01	0.00	0.00	0.01	0.00	0.01	0.00
BAO	0.04	0.04	0.02	0.00	0.01	0.03	0.01	0.01	0.00	0.00
CO2 *	45.93	46.23	46.09	44.35	43.81	45.42	43.93	44.60	44.66	45.41
TOTAL	104.52	105.19	104.93	100.87	99.76	103.45	100.05	98.81	98.82	98.56
CA2+	1.994	1.997	1.988	1.998	1.980	1.963	1.967	1.004	1.012	0.977
FE2+	0.001	0.001	0.009	0.000	0.010	0.012	0.018	0.293	0.285	0.192
MN2+	0.004	0.001	0.003	0.002	0.008	0.015	0.007	0.042	0.038	0.031
MG2+	0.000	0.000	0.000	0.000	0.002	0.010	0.008	0.661	0.665	0.800
SR2+	0.000	0.000	0.000	0.000	0.000	0.000	0.000	0.000	0.000	0.000
BA2+	0.000	0.000	0.000	0.000	0.000	0.000	0.000	0.000	0.000	0.000
C4+	2.000	2.000	2.000	2.000	2.000	2.000	2.000	2.000	2.000	2.000
CATSUM	4.000	4.000	4.000	4.000	4.000	4.000	4.000	4.000	4.000	4.000
O	6	6	6	6	6	6	6	6	6	6

* Determined by stoichiometry

-Formula contents on a basis of 6 anions

CARBONATES

	GL32d	GL32e	6019a	6019b	6019c	6019d	6019e	GL27a	GL27b	GL27c
CAO	28.64	28.74	29.55	29.53	28.52	29.51	29.94	55.82	54.06	53.21
FEO	10.42	6.47	17.46	15.75	19.95	10.27	11.87	0.58	0.82	0.75
MNO	1.31	1.19	0.46	0.09	0.36	0.54	0.47	1.04	1.11	1.17
MGO	13.90	16.90	8.73	10.21	8.37	14.25	12.79	0.11	0.10	0.18
SRO	0.00	0.01	0.04	0.19	0.03	0.18	0.20	0.00	0.04	0.05
BAO	0.00	0.06	0.00	0.01	0.03	0.01	0.03	0.02	0.00	0.00
CO2 *	44.85	45.73	43.72	44.11	43.99	45.42	45.12	44.93	43.74	43.16
TOTAL	99.12	99.10	99.96	99.89	101.25	100.18	100.42	102.50	99.87	98.52
CA2+	1.002	0.986	1.061	1.051	1.018	1.020	1.042	1.950	1.940	1.935
FE2+	0.285	0.173	0.489	0.437	0.556	0.277	0.322	0.016	0.023	0.021
MN2+	0.036	0.032	0.013	0.003	0.010	0.015	0.013	0.029	0.031	0.034
MG2+	0.677	0.807	0.436	0.505	0.416	0.685	0.619	0.005	0.005	0.009
SR2+	0.000	0.000	0.001	0.004	0.001	0.003	0.004	0.000	0.001	0.001
BA2+	0.000	0.001	0.000	0.000	0.000	0.000	0.000	0.000	0.000	0.000
C4+	2.000	2.000	2.000	2.000	2.000	2.000	2.000	2.000	2.000	2.000
CATSUM	4.000	4.000	4.000	4.000	4.000	4.000	4.000	4.000	4.000	4.000
O	6	6	6	6	6	6	6	6	6	6

* Determined by stoichiometry

-Formula contents on a basis of 6 anions

CARBONATES

	GL27d	GL27e	6018a	6018b	6018c	6018d	6048a	6048b	6048c	6048d
CAO	56.85	59.03	54.77	54.48	55.98	55.82	49.17	55.66	57.11	54.71
FEO	0.80	0.87	0.27	1.06	0.51	0.22	3.26	0.31	0.49	0.51
MNO	1.13	1.23	0.77	1.39	0.65	0.40	0.79	0.18	0.98	0.21
MGO	0.14	0.16	0.07	0.36	0.23	0.13	1.91	0.04	0.18	0.24
SRO	0.03	0.03	0.00	0.00	0.01	0.00	0.00	0.00	0.04	0.00
BAO	0.01	0.05	0.03	0.00	0.00	0.03	0.00	0.00	0.00	0.01
CO2 *	45.97	47.82	43.71	44.66	44.90	44.34	43.16	44.03	45.94	43.64
TOTAL	104.93	109.19	99.62	101.95	102.28	100.94	98.29	100.22	104.74	99.32
CA2+	1.941	1.937	1.967	1.915	1.957	1.976	1.788	1.984	1.951	1.968
FE2+	0.021	0.022	0.008	0.029	0.014	0.006	0.093	0.009	0.013	0.014
MN2+	0.030	0.032	0.022	0.039	0.018	0.011	0.023	0.005	0.026	0.006
MG2+	0.007	0.007	0.003	0.018	0.011	0.006	0.097	0.002	0.009	0.012
SR2+	0.001	0.001	0.000	0.000	0.000	0.000	0.000	0.000	0.001	0.000
BA2+	0.000	0.001	0.000	0.000	0.000	0.000	0.000	0.000	0.000	0.000
C4+	2.000	2.000	2.000	2.000	2.000	2.000	2.000	2.000	2.000	2.000
CATSUM	4.000	4.000	4.000	4.000	4.000	4.000	4.000	4.000	4.000	4.000
O	6	6	6	6	6	6	6	6	6	6

* Determined by stoichiometry

-Formula contents on a basis of 6 anions

CARBONATES

	6048e	6048f	6048g	6048h	6048i	6048j	6048k	6048l	6048m	6034a
CAO	55.07	54.58	55.87	55.13	56.84	55.49	57.98	57.52	58.12	56.81
FEO	0.52	0.84	1.33	1.40	0.52	1.80	0.92	0.34	1.72	0.54
MNO	0.16	2.36	0.98	1.96	0.96	0.98	1.04	1.00	0.86	0.52
MGO	0.21	0.28	0.24	0.38	0.20	0.33	0.26	0.14	0.30	0.13
SRO	0.00	0.00	0.00	0.00	0.00	0.00	0.02	0.03	0.00	0.00
BAO	0.00	0.02	0.00	0.00	0.00	0.02	0.00	0.00	0.00	0.00
CO2 *	43.86	45.12	45.53	45.75	45.74	45.62	47.00	46.13	47.53	45.38
TOTAL	99.82	103.20	103.95	104.62	104.26	104.24	107.22	105.16	108.53	103.38
CA2+	1.970	1.898	1.926	1.891	1.950	1.909	1.936	1.957	1.919	1.965
FE2+	0.015	0.023	0.036	0.037	0.014	0.048	0.024	0.009	0.044	0.015
MN2+	0.005	0.065	0.027	0.053	0.026	0.027	0.027	0.027	0.022	0.014
MG2+	0.010	0.014	0.012	0.018	0.010	0.016	0.012	0.007	0.014	0.006
SR2+	0.000	0.000	0.000	0.000	0.000	0.000	0.000	0.001	0.000	0.000
BA2+	0.000	0.000	0.000	0.000	0.000	0.000	0.000	0.000	0.000	0.000
C4+	2.000	2.000	2.000	2.000	2.000	2.000	2.000	2.000	2.000	2.000
CATSUM	4.000	4.000	4.000	4.000	4.000	4.000	4.000	4.000	4.000	4.000
O	6	6	6	6	6	6	6	6	6	6

* Determined by stoichiometry

-Formula contents on a basis of 6 anions

CARBONATES

		6034b	6034c	6034d	6034e	6034f	6034g
CAO		34.01	31.92	58.06	29.55	28.16	29.17
FEO		2.88	1.68	0.21	11.33	10.48	8.91
MNO		0.67	0.79	0.25	0.51	1.35	1.16
MGO		16.43	19.00	0.12	13.37	12.26	13.52
SRO		0.00	0.00	0.00	0.03	0.00	0.00
BAO		0.00	0.04	0.06	0.01	0.00	0.00
CO2	*	46.81	47.33	46.00	45.06	42.74	43.83
TOTAL		100.80	100.76	104.70	99.86	94.99	96.59
CA2+		1.140	1.059	1.981	1.029	1.034	1.045
FE2+		0.075	0.043	0.006	0.308	0.300	0.249
MN2+		0.018	0.021	0.007	0.014	0.039	0.033
MG2+		0.767	0.877	0.006	0.648	0.626	0.674
SR2+		0.000	0.000	0.000	0.001	0.000	0.000
BA2+		0.000	0.000	0.001	0.000	0.000	0.000
C4+		2.000	2.000	2.000	2.000	2.000	2.000
CATSUM		4.000	4.000	4.000	4.000	4.000	4.000
O		6	6	6	6	6	6

* Determined by stoichiometry

-Formula contents on a basis of 6 anions

AMPHIBOLE Mafic to intermediate metavolcanic rocks

ALTERED GROUNDMASS

	6046a	6046b	6046c
SIO2	49.40	49.65	47.31
AL2O3	3.19	3.34	5.15
TIO2	.27	.29	.07
CR2O3	.00	.01	.04
FEO	28.68	26.83	24.09
MNO	.98	.87	.48
MGO	4.98	7.43	7.89
K2O	.03	.04	.10
CAO	7.67	6.64	9.58
NA2O	2.39	2.21	1.21
BAO	.00	.00	.00
CL	.16	.12	.10
F	.00	.00	.00
TOTAL	97.75	97.43	96.02
TOT-O	97.71	97.40	96.00
Si	7.70*	7.66*	7.37*
Mg/(Mg+Fe)	0.24*	0.33*	0.37*

*Formula based on 23 oxygens (max. Fe(2+))

AMPHIBOLE Intrusive rocks (Matachewan)

GROUNDMASS

	6030a	6030b
SIO2	53.55	47.13
AL2O3	.77	3.49
TIO2	.04	.51
CR2O3	.03	.06
FEO	19.42	20.87
MNO	.38	.47
MGO	11.60	8.34
K2O	.01	.04
CAO	12.12	11.07
NA2O	.50	4.23
BAO	.00	.00
CL	.03	.15
F	.00	.01
TOTAL	98.45	96.37
TOT-O	98.44	96.33
Si	7.90*	7.35*
Mg/(Mg+Fe)	0.52*	0.42*

*Formula based on 23 oxygens (max. Fe(2+))

PYROXENE Mafic to intermediate metavolcanic rocks

GROUNDMASS

	53a	53b	53c	53d
SIO2	50.50	50.08	52.60	51.63
AL2O3	2.78	2.83	1.47	3.04
TIO2	1.07	.99	.44	.63
CR2O3	.01	.07	.03	.27
FEO	15.78	15.03	13.51	10.89
MNO	.33	.45	.71	.34
MGO	11.92	12.70	11.40	15.22
K2O	.02	.02	.01	.00
CAO	19.01	18.46	19.38	18.83
NA2O	.28	.28	.98	.26
BAO	.00	.00	.00	.00
CL	.01	.01	.02	.00
F	.00	.02	.00	.01
TOTAL	101.71	100.94	100.55	101.12
TOT-O	101.71	100.93	100.55	101.12

	3032a	6032b	6032c
SIO2	53.34	50.70	53.45
AL2O3	2.49	1.83	1.68
TIO2	.30	.26	.26
CR2O3	.43	.02	.06
FEO	7.10	14.83	9.20
MNO	.22	.64	.30
MGO	16.46	10.08	16.69
K2O	.01	.01	.00
CAO	21.05	21.23	19.18
NA2O	.19	.38	.17
BAO	.00	.00	.00
CL	.00	.05	.00
F	.03	.02	.07
TOTAL	101.62	100.05	101.06
TOT-O	101.61	100.03	101.03

PYROXENE Intrusive rocks (Matachewan)

GROUNDMASS

	6030a	6030b
SIO2	48.53	45.95
AL2O3	3.01	3.96
TIO2	.74	.28
CR2O3	.00	.11
FEO	14.69	16.70
MNO	.35	.53
MGO	12.69	10.66
K2O	.01	.02
CAO	18.44	17.44
NA2O	.34	.89
BAO	.00	.00
CL	.01	.07
F	.03	.00
TOTAL	98.84	96.61
TOT-O	98.83	96.59

ALTERED GROUNDMASS

	70a
SIO2	51.37
AL2O3	1.51
TIO2	.14
CR2O3	.04
FEO	14.49
MNO	.45
MGO	9.93
K2O	.00
CAO	21.30
NA2O	.45
BAO	.00
CL	.04
F	.02
TOTAL	99.74
TOT-O	99.72

PYROXENES

	GL53a	GL53B	GL53C	GL53D	6032A	6032B	6032C	6030A	6030B	GL70A
SIO2	50.50	50.08	52.60	51.63	53.34	50.70	53.45	48.53	45.95	51.37
AL2O3	2.78	2.83	1.47	3.04	2.49	1.83	1.68	3.01	3.96	1.51
TIO2	1.07	0.99	0.44	0.63	0.30	0.26	0.26	0.74	0.28	0.14
CR2O3	0.01	0.07	0.03	0.27	0.43	0.02	0.06	0.00	0.11	0.04
FEO	15.78	15.03	13.51	10.89	7.10	14.83	9.20	14.69	16.70	14.49
MNO	0.33	0.45	0.71	0.34	0.22	0.64	0.30	0.35	0.53	0.45
MGO	11.92	12.70	11.40	15.22	16.46	10.08	16.69	12.69	10.66	9.93
K2O	0.02	0.02	0.01	0.00	0.01	0.01	0.00	0.01	0.02	0.00
CAO	19.01	18.46	19.38	18.83	21.05	21.23	19.18	18.44	17.44	21.30
NA2O	0.28	0.28	0.98	0.26	0.19	0.38	0.17	0.34	0.89	0.45
BAO	0.00	0.00	0.00	0.00	0.00	0.00	0.00	0.00	0.00	0.00
CL	0.01	0.01	0.02	0.00	0.00	0.05	0.00	0.01	0.07	0.04
F	0.00	0.02	0.00	0.01	0.03	0.02	0.07	0.03	0.00	0.00
O=CL	-0.00	-0.00	-0.00	0.00	0.00	-0.01	0.00	-0.00	-0.02	-0.01
O=F	0.00	-0.01	0.00	-0.00	-0.01	-0.01	-0.03	-0.01	0.00	0.00
TOTAL	101.71	100.93	100.55	101.12	101.61	100.03	101.03	98.83	96.59	99.71
SI4+	1.267	1.262	1.322	1.271	1.289	1.298	1.304	1.251	1.230	1.315
AL3+	0.082	0.084	0.044	0.088	0.071	0.055	0.048	0.091	0.125	0.046
TI4+	0.020	0.019	0.008	0.012	0.005	0.005	0.005	0.014	0.006	0.003
CR3+	0.000	0.001	0.001	0.005	0.008	0.000	0.001	0.000	0.002	0.001
FE2+	0.331	0.317	0.284	0.224	0.144	0.318	0.188	0.317	0.374	0.310
MN2+	0.007	0.010	0.015	0.007	0.005	0.014	0.006	0.008	0.012	0.010
MG2+	0.446	0.477	0.427	0.559	0.593	0.385	0.607	0.488	0.426	0.379
K+	0.001	0.001	0.000	0.000	0.000	0.000	0.000	0.000	0.001	0.000
CA2+	0.511	0.498	0.522	0.497	0.545	0.582	0.501	0.509	0.500	0.584
NA+	0.014	0.014	0.048	0.012	0.009	0.019	0.008	0.017	0.046	0.022
BA2+	0.000	0.000	0.000	0.000	0.000	0.000	0.000	0.000	0.000	0.000
CL-	0.000	0.000	0.001	0.000	0.000	0.002	0.000	0.000	0.003	0.002
F-	0.000	0.002	0.000	0.001	0.002	0.002	0.005	0.002	0.000	0.000
O2-	4.000	3.998	3.999	3.999	3.998	3.996	3.995	3.997	3.997	3.998
CATSUM	2.679	2.683	2.671	2.676	2.669	2.677	2.668	2.696	2.722	2.669
AN SUM	4	4	4	4	4	4	4	4	4	4

-Formula contents on a basis of 4 anions

garnet

	53A	70A
SIO2	34.74	37.29
AL2O3	3.60	10.20
TIO2	53.70	5.70
CR2O3	1.00	9.00
FEO	21.00	415.00
MNO	40.00	7.00
MGO	17.00	33.00
K2O	0.00	0.00
CAO	0.35	3.34
NA2O	0.01	0.61
BAO	0.00	0.03
CL	0.00	0.00
F	0.01	0.02
O=CL	0.00	0.00
O=F	-0.00	-0.01
TOTAL	171.41	521.18
SI4+	1.774	0.863
AL3+	0.217	0.278
TI4+	2.062	0.099
CR3+	0.040	0.165
FE2+	0.897	8.036
MN2+	1.730	0.137
MG2+	1.294	1.139
K+	0.000	0.000
CA2+	0.019	0.083
NA+	0.001	0.027
BA2+	0.000	0.000
CL-	0.000	0.000
F-	0.002	0.001
O2-	11.998	11.999
CATSUM	8.035	10.829
AN SUM	12	12

-Formula contents on a basis of 12 anions

GRENAT Mafic to intermediate metavolcanic rocks

GROUNDMASS

	53a
SIO2	34.74
AL2O3	3.65
TIO2	3.71
CR2O3	.00
FEO	21.40
MNO	.17
MGO	.00
K2O	.00
CAO	35.01
NA2O	.00
BAO	.00
CL	.01
F	.16
TOTAL	98.85
TOT-O	98.78

GRENAT Intrusive rocks (Matachewan)

ALTERED GROUNDMASS

	70a
SIO2	37.29
AL2O3	10.25
TIO2	.79
CR2O3	.04
FEO	15.07
MNO	.33
MGO	.00
K2O	.03
CAO	34.61
NA2O	.03
BAO	.00
CL	.02
F	.02
---	---
TOTAL	98.48
---	---
TOT-O	98.47

EPIDOTE Mafic to intermadiate metavolcanic rocks

GROUNDMASS

	6032a
SIO2	38.32
AL2O3	23.35
TIO2	.05
CR2O3	.03
FEO	12.92
MNO	.08
MGO	.00
K2O	.01
CAO	24.00
NA2O	.00
BAO	.00
CL	.00
F	.07

TOTAL	98.83

TOT-O	98.80

EPIDOTE Intrusive rocks (Matachewan)

ALTERED GROUNDMASS

	70-1-2	70-3-1
SIO2	38.38	38.50
AL2O3	23.27	23.34
TIO2	.15	.15
CR2O3	.01	.03
FEO	12.97	12.80
MNO	.07	.08
MGO	.00	.00
K2O	.00	.00
CAO	23.61	23.92
NA2O	.00	.02
BAO	.00	.00
CL	.01	.00
F	.05	.00
------	------	------
TOTAL	98.52	98.84
------	------	------
TOT-O	98.50	98.84

VEINS

	70-4-1
SIO2	38.52
AL2O3	23.44
TIO2	.12
CR2O3	.00
FEO	12.76
MNO	.10
MGO	.00
K2O	.03
CAO	24.17
NA2O	.00
BAO	.00
CL	.00
F	.00
-------	-------
TOTAL	99.14
-------	------
TOT-O	99.14

Fe OXIDES Mafic to intermediate metavolcanic rocks

GROUNDMASS

	Titanite	Titanite	TiO2-Magnetite	TiO2-Magnetite
	6046a	**6032a**	**53a**	**53b**
SIO2	33.08	31.09	.21	1.26
AL2O3	4.83	3.98	.76	.93
TIO2	30.76	32.87	20.23	20.34
CR2O3	.00	.09	.02	.07
FEO	2.03	3.00	71.14	70.53
MNO	.03	.05	4.43	1.60
MGO	.00	.38	.03	.10
K2O	.01	.01	.00	.00
CAO	27.41	27.70	.11	1.10
NA2O	.09	.04	.00	.00
BAO	.00	.00	.00	.00
CL	.06	.09	.00	.00
F	.33	.16	.00	.00
TOTAL	98.63	99.46	96.93	95.93
TOT-O	98.48	99.37	96.93	95.93

ALTERED GROUNDMASS

	Magnetite?	Magnetite
	6046b	**6046c**
SIO2	1.78	.20
AL2O3	.78	.03
TIO2	.44	.37
CR2O3	.06	.00
FEO	90.94	93.03
MNO	.05	.04
MGO	.78	.00
K2O	.00	.00
CAO	.17	.16
NA2O	.00	.00
BAO	.00	.00
CL	.00	.00
F	.00	.00
TOTAL	95.00	93.83
TOT-O	95.00	93.83

VEINS

	TiO2-Magnetite	Rutile?
	6024a	**6024b**
SIO2	.48	.24
AL2O3	.13	.09
TIO2	12.63	53.21
CR2O3	.03	.00
FEO	81.07	38.72
MNO	.00	.07
MGO	.08	.00
K2O	.00	.01
CAO	.13	2.77
NA2O	.02	.01
BAO	.00	.00
CL	.00	.01
F	.00	.00
TOTAL	94.57	95.13
TOT-O	94.57	95.13

Fe OXIDES Intrusive rocks (Matachewan)

VEINS

	Titanite
	70a
SIO2	31.67
AL2O3	2.61
TIO2	34.33
CR2O3	.05
FEO	2.32
MNO	.03
MGO	.00
K2O	.01
CAO	28.18
NA2O	.00
BAO	.00
CL	.05
F	.23
TOTAL	99.48
TOT-O	99.37

GROUNDMASS

	TiO2-Magnetite	TiO2-Magnetite
	6030a	**6030b**
SIO2	.25	.81
AL2O3	2.11	.07
TIO2	17.71	3.63
CR2O3	.07	.00
FEO	74.43	89.48
MNO	.01	.00
MGO	.04	.00
K2O	.00	.00
CAO	.28	.48
NA2O	.00	.00
BAO	.00	.00
CL	.00	.00
F	.00	.00
TOTAL	94.90	94.47
TOT-O	94.90	94.47

garnet

	53A	70A
SIO2	34.74	37.29
AL2O3	3.60	10.20
TIO2	53.70	5.70
CR2O3	1.00	9.00
FEO	21.00	415.00
MNO	40.00	7.00
MGO	17.00	33.00
K2O	0.00	0.00
CAO	0.35	3.34
NA2O	0.01	0.61
BAO	0.00	0.03
CL	0.00	0.00
F	0.01	0.02
O=CL	0.00	0.00
O=F	-0.00	-0.01
TOTAL	171.41	521.18

SI4+	1.774	0.863
AL3+	0.217	0.278
TI4+	2.062	0.099
CR3+	0.040	0.165
FE2+	0.897	8.036
MN2+	1.730	0.137
MG2+	1.294	1.139
K+	0.000	0.000
CA2+	0.019	0.083
NA+	0.001	0.027
BA2+	0.000	0.000
CL-	0.000	0.000
F-	0.002	0.001
O2-	11.998	11.999
CATSUM	8.035	10.829
AN SUM	12	12

-Formula contents on a basis of 12 anions